Extended-soft-core Baryon-Baryon Model ESC08
I. Nucleon-Nucleon Scattering

M.M. Nagels and Th.A. Rijken
Institute of Mathematics, Astrophysics, and Particle Physics
University of Nijmegen, Nijmegen, The Netherlands

Y. Yamamoto
Nishina Center for Accelerator-Based Science, Insitute for Physical and Chemical Research (RIKEN). Wako, Saitama, 351-0198, Japan
(Dated: version of: September 27, 2016)

The Nijmegen extended-soft-core ESC08c model for the baryon-baryon (BB) interactions of the SU(3) flavor-octet of baryons (N, Λ, Σ, and Ξ) is presented. In this first of a series of papers, the NN results are reported in detail. In the spirit of the Yukawa-approach to the nuclear force problem, the interactions are studied from the meson-exchange picture viewpoint, using generalized soft-core Yukawa-functions. These interactions are supplemented with (i) multiple-gluon-exchange, and (ii) structural effects due to the quark-core of the baryons. The extended-soft-core (ESC) meson-exchange interactions consist of local- and non-local-potentials due to (i) One-boson-exchanges (OBE), which are the members of nonets of pseudoscalar, vector, scalar, and axial-vector mesons, (ii) diffractive (i.e. multiple-gluon) exchanges, (iii) two pseudo-scalar exchange (PS-PS), and (iv) meson-pair-exchange (MPE). The OBE- and MPE-vertices are regulated by gaussian form factors producing potentials with a soft behavior near the origin. The assignment of the cut-off masses for the BBM-vertices is dependent on the $SU(3)$-classification of the exchanged mesons for OBE, and a similar scheme for MPE.

The ESC-models ESC08, as well as its predecessor ESC04, describe the nucleon-nucleon (NN), hyperon-nucleon (YN), and hyperon-hyperon/nucleon (YY/Ξ N) interactions in a unified way using broken $SU(3)$-symmetry. Important non-standard ingredients in the OBE-sector in the ESC-models are (i) the axial-vector meson potentials, and (ii) a zero in the scalar- and axial-vector meson form factors. These innovations make it possible to keep the meson coupling parameters of the model qualitatively in accordance with the predictions of the $^3P_0$-dominated quark-antiquark pair creation (QPC) model. SU(3)-symmetry serves to connect the NN with the YN and the YY channels. In the fit to NN and YN many parameters are essentially fixed by the NN-data. A few, but severely constrained parameters, e.g. $F/(F+D)$-ratio's, are left for determination of the YN-interactions and the YY experimental indications. In particular, the meson-baryon coupling constants are calculated via $SU(3)$ using the coupling constants of the $NN \oplus YN$-analysis as input. In ESC08 the couplings are kept SU(3)-symmetric.

In establishing the parameters of the model a simultaneous fit to NN- and YN-channels has been performed. Here the information about $\Lambda\Lambda$, ΞN, and hypernuclei played an important role in the form of using constraints. In particular, the experimental indications for the $\Lambda\Lambda$-attraction, the Ξ-nuclear and the Σ-nuclear well-depth were directive. About 25 physical coupling parameters and 8 cut-off and diffractive masses, were searched. The obtained OBE-couplings and the $F/(F+D)$-ratio's can be well understood in the context of the QPC-model.

The simultaneous fit of the ESC-models to the NN- and YN- scattering data with a single set of parameters has achieved excellent results for the NN- and YN-data, and for the YY-data in accordance with the experimental indications for $\Lambda\Lambda$ and ΞN. In the case of ESC08c, the version discussed here, the achievements are: (i) For the selected 4313 pp and np scattering data with energies $0 \leq T_{lab} \leq 350$ MeV, the model reaches a fit having $\chi^2/N_{data} = 1.087$. (ii) The deuteron binding energy and all the NN scattering lengths are fitted very nicely. (iii) The YN-data are described very well with $\chi^2/N_{data} = 1.09$, giving at the same time good descriptions of the Λ, Σ, and Ξ nuclear well-depths. (iv) The model predicts a bound $\Xi N(^3S_1, I = 1)$ state with binding energy 1.36 MeV.

PACS numbers: 13.75.Cs, 12.39.Pn, 21.30.+y

I. INTRODUCTION

In a new series of papers we present the results obtained with the recent ESC08c-version of the Extended-Soft-Core (ESC) model [1] for nucleon-nucleon (NN), hyperon-nucleon (YN), and hyperon-hyperon (YY) interactions with $S = 0, -1, -2$. Moreover, we present predictions for the YY-channels with $S = -3, -4$.

The combined study of all baryon-baryon (BB) interactions, exploiting all experimental information hitherto

available, both on BB-scattering and (hyper-)nuclear systems, might throw light on the basic mechanisms of these interactions. The program, which in its original form was formulated in Refs. [2, 3], pursuits the aims:

- To study the assumption of broken $SU(3)$-symmetry. For example we investigate the properties of the scalar mesons ($\varepsilon(760)$, $f_0(975)$, $a_0(980)$, $\kappa(800)$).
- To determine the $F/(F+D)$-ratio's.
- To study the connection between QCD, the quark-model, and low energy physics.
- To extract, in spite of the scarce experimental YN- and YY-data, information about scattering lengths, effective ranges, the existence of resonances and bound states, etc.
- To provide realistic baryon-baryon potentials, which can be applied in few-body calculations, nuclear- and hyperonic matter studies, neutron-stars;
- To extend the theoretical description to the baryon-baryon channels with strangeness S=-2. This in particular for the $\Lambda\Lambda$ and ΞN channels, where some data already exist, and for which experiments will be realized in the near future.
- Finally, to extend the theoretical description to all baryon-baryon channels with strangeness S=-3,-4. These will be parameter free predictions, and have, like the other BB-channels, relevance for the study of hyperonic matter and compact stars.

With this series of papers this program nears essentially its completion.

As has been amply demonstrated, see Ref.'s [4–8], the ESC-model interactions give excellent simultaneous descriptions of the NN and YN data. Also it turned out that the ESC-approach gives great improvements for the NN description as compared to the One-Boson-Exchange (OBE) models, e.g. [3, 9], and other existing models in the literature. The ESC08c-model presents the culmination in this respect: the NN-model has a quality on equal par with the energy-dependent partial-wave analysis (PWA) [10, 11].

The ESC04-model papers [4–6] contain the first rather extensive exposition of the ESC-approach. As compared to the earlier versions of the ESC-model, we introduced in ESC04-models [4–6] several innovations: Firstly, we introduced a zero in the form factor of the mesons with P-wave quark-antiquark contents, which applies to the scalar and axial-vector mesons. Secondly, we exploited the exchange of the axial-vector mesons with $J^{PC}=1^{++}$ and $J^{PC}=1^{+-}$. Thirdly, we employed some $\Lambda\Lambda, \Xi N$ information.

In the ESC08-models on top of these improvements, we introduce in the ESC-approach for the first time: (i) Odderon-exchange $J^{PC}=1^{--}$. Odderon-exchange represents the exchange of an odd-number of gluons at short-distance. This to complement pomeron-exchange which stands for the exchange of an even-number of gluons. (ii) Quark-core effects. The quark-core effects represent structural effects caused by the occurrence of Pauli-blocked configurations in two-baryon systems. These structural effects depend on the BB-channel and cannot be described by t-channel exchanges.
Furthermore, (iii) the axial-vector ($J^{PC}=1^{++}$) mesons are treated with the most general vertices, and the $(\boldsymbol{\sigma}_1\cdot\mathbf{q})(\boldsymbol{\sigma}_2\cdot\mathbf{q})$-operator is evaluated in a superior mannner compared to ESC04. Not included are the potentials from the tensor ($J^{PC}=2^{++}$) mesons. Attempts including the latter mesons did not lead to substantial potentials from these mesons or qualitative changes in the other contributions to the potentials. The first results with the ESC08-model are reported in [7, 8]. With this simultaneous treatment of the NN, YN, and YY channels we have achieved a high quality description of the baryon-baryon interactions. The results, using a single set of meson and quark-core parameters, include: (a) a description of the NN-data with a $\chi^2_{pdp}=1.087$ and good low energy parameters for the NN-channels including the binding energy E_B of the deuteron, (b) a very good fit to the YN-scattering data. (c) the fitting parameters with a clear physical significance, like e.g. the $NN\pi$-, $NN\rho$-couplings etc. and with realistic values of the $F/(F+D)$-ratio's α_P and α_V^m. The fitting has been done under the constraints of the G-matrix results for the ESC08-interactions. These show (i) satisfactory well-depth values for $U_\Lambda, U_\Sigma > 0$, and $U_\Xi < 0$, (ii) proper spin-spin ($U_{\sigma\sigma}\geq 1$), and small spin-orbit interactions for ΛN. All these features are in agreement with the Hyperball-data [12] and the NAGARA-event [13].

In this first paper of the series, we display and discuss the NN results of the simultaneous fit to the NN- and YN-data, including some $\Lambda\Lambda, \Xi N$ and ΣN information from hypernuclei, using a single set of parameters [14]. In the second paper, henceforth referred to as II [15], we report on the results for strangeness S=-1 YN-channels, using the same simultaneous fit of the NN- and YN-data. This simultaneous fitting procedure was first introduced in [5], and its importance and advantages will be discussed in II. In the third paper, henceforth referred to as III [16], we report on the results and predictions for YY with strangeness $S=-2$. Finally, in the fourth paper (IV), we describe the predictions for YY with strangeness $S=-3,-4$.

The contents of this paper are as follows. In section II a description of the physical background and dynamical contents of the ESC08-model is given. In section III the two-body integral equations in momentum space are discussed. Also, the expansion into Pauli-spinor invariants is reviewed. In section IV the ESC-potentials in momentum and configuration space for non-strange mesons

are discussed in detail. In particular the new potentials are given. Section V contains some brief remarks on the ESC-couplings and the QPC-model. In section VI the simultaneous $NN \oplus YN \oplus YY$ fitting procedure is reviewed. Here, also the results for the coupling constants and $F/(F+D)$-ratios for OBE and MPE are given. In section VII the NN-results for the ESC08c-model are displayed. In section VIII a solution for the the nuclear saturation and neutron star mass is described.

In section IX we discuss the results and draw some conclusions. In appendix A the B-field formalism for vector- and axial-vector mesons is described. The exact treatment of the non-local-tensor operator is explained in appendix B. In appendix D the treatment of the non-local tensor potential is reviewed. In appendix E the basic formulas for the configuration space gaussian-yukawa functions are given.

II. PHYSICAL CONTENT OF THE ESC-MODEL

The general physical basis, within the context of QCD, for the Nijmegen soft-core models has been outlined in the introduction of [4]. The description of baryon-interactions at low energies in terms of baryons and mesons can be reached through the following stages: (i) The strongly interacting sector of the standard-model (SM) contains three families of quarks: (ud), (cs), (tb). (ii) Integrating out the heavy quarks (c,b,t) leads to a QCD-world with effective interactions for the (u,d,s) quarks. (iii) This QCD-world is characterized by a phase transition of the vacuum. Thereby the quarks gets dressed and become the so-called constituent quarks. The emerging picture is that of the constituent-quark-model (CQM) [17]. The phase transition has transformed the effective QCD-world into an complex hadronic-world. (iv) The strong coupling lattice QCD (SCQCD) seems to be a proper model to study the low energy meson-baryon and baryon-baryon physics, see [18] for applications and references. Here the lattice spacing $a \geq 0.11$ fm provides a momentum scale for which the QCD coupling $g \geq 1.1$. Emerging is a picture where the meson-baryon coupling constants get large, and quark-exchange effects are rather small. The latter is due to the suppression due to the gluonic overlaps involved. For a similar reason it has been argued [19] that the pomeron is exchanged between the individual quarks of the baryons. In this picture the Nijmegen soft-core approach to baryon-baryon interactions has a natural motivation. (v) For the mesons we restrict ourselves to mesons with $M \leq 1.5$ GeV/c^2, arriving at a so-called *effective field theory* as the arena for our description of the low energy baryon-baryon scattering.

In view of the success of QCD, pseudo-scalar dominance of the divergence of the axial-vector current (PCAC) leading to small light ("current") quark masses [20, 21], the spectroscopic success of the CQM, where the quarks have definite color charges, in generating the masses of the pseudo-scalar and vector nonets, and the masses and magnetic moments of the baryon octet is rather surprising [22, 23]. The transition from "current" to "constituent" quarks comes from dressing the quark fields in the original QCD Lagrangian, see e.g. Ref. [17, 24, 25].

In all works of the Nijmegen group on the baryon-baryon models, (broken) $SU(3)$ flavor-symmetry is explored to connect the NN, YN, and YY channels, making possible a simultaneous fitting of all the available BB-data using a single set of model-parameters. The dynamical basis is the (approximate) permutation symmetry w.r.t. the constituent (u,d,s)-quarks. This has its roots in the approximate equality of the quark-masses, and more importantly that the gluons have no flavor. This enables the calculation of the baryon-baryon-meson coupling constants using as parameters the nucleon-nucleon-meson couplings and the $F/(F+D)$-ratio's. This provides a strong correlation between the (rich) nucleon-nucleon- and the (scarce) hyperon-nucleon-data.

The obtained coupling constants of the BBM-vertices are interpreted studying the predictions of the constituent quark-model (CQM) in the form of the quark-antiquark pair creation model (QPC). It has been argued that the $^3P_0$-mechanism [26, 27] is dominant over the $^3S_1$-mechanism in lattice QCD [28]. It turned out that the fitted coupling constants in ESC04 and ESC08 indeed follow mainly the pattern of couplings set by the $^3P_0$-model. Also, all $\alpha = F/(F+D)$-ratios are required to deviate no more than 0.1 from the QPC-model predictions for the BBM- and the $BB-Pair$-vertices. Although it is in principle attractive to study the SU(3)-breaking of the BBM-couplings using the QPC-model, as has been explored in ESC04 [5], in ESC08 the couplings are treated as SU(3)-symmetric. In the Nijmegen soft-core OBE- and ESC-models the BBM-vertices are described by coupling constants and gaussian form factors. Given the fact that in the CQM the quark wave functions for the baryons are very much like ground state harmonic oscillator functions, a gaussian behavior of the form factors is most natural. These form factors guarantee a soft behavior of the potentials in configuration space at small distances. The cut-off parameters in the form factors depend only on the type of meson (pseudoscalar, vector, etc.). Within a meson SU(3)-multiplet we distinguish between octet and singlet form factors. Since there is singlet-octet mixing for the I=0 mesons, we attribute the singlet and octet cut-off to the dominant singlet or octet particle respectively. For the considered nonets the singlet and octet cut-off's are the same or close.

In this way we have full predictive power for the $S = -2, -3, -4$ baryon-baryon channels, e.g. $\Lambda\Lambda, \Xi N$-channels which involve the singlet $\{1\}$-irrep that does not occur in the NN and YN channels.

Field theory allows both linear and non-linear realizations of chiral-symmetry (CS) [29–31]. At low-energy phenomenologically the non-linear realization is the most economical and natural. Therefore, we have chosen the

pv-coupling and not the ps-coupling for the pseudoscalar mesons. This choice affects some $1/M^2$-terms in the ps-ps-exchange potential, In ESC04 we tested mixtures of the pv- and ps-coupling, but in ESC08 we use only the pv-coupling. In the non-linear realization chiral-symmetry for the couplings of the scalar-, vector-, axial-vector-, etc. mesons is realized through isospin-symmetry SU(2,I) [30, 31].

A. Potentials ESC-model

The potentials of the ESC-model are generated by (i) One-Boson-Exchange (OBE), (ii) uncorrelated Two-Meson-Exchange (TME), (iii) Meson-Pair-Exchange (MPE), (iv) Diffractive/Multi-gluon Exchange, (v) Quark-Core Effects (QCE).

(i) The OBE-part of the dynamical contents of the ESC08-models is determined by the following meson-exchanges:

  (a) $J^{PC} = 0^{--}$: The pseudoscalar-meson nonet $\pi,\ \eta,\ \eta',\ K$ with the $\eta-\eta'$ mixing angle $\theta_P = -13^0$ [32], close to the Gell-Mann-Okubo quadratic mass formula [33].

  (b) $J^{PC} = 1^{--}$: The vector-meson nonet $\rho,\ \phi,\ K^\star,\ \omega$ with the $\phi-\omega$ mixing angle $\theta_V = 38.70^0$ [32]. This follows from the quadratic GMO mass-formula, and is close to ideal mixing.

  (c) $J^{PC} = 1^{++}$: The axial-vector-meson nonet $a_1, f_1,\ K_{1A}, f_1'$ with the f_1-f_1' mixing angle $\theta_A = 50.0^0$ [34].

  (d) $J^{PC} = 0^{++}$: The scalar-meson nonet $a_0(962)=\delta, f_0(993)=S^\star, \kappa(800), f_0(760)=\varepsilon$ with the ideal $S^\star-\varepsilon$ mixing angle $\theta_S = 35.26^0$.

  (e) $J^{PC} = 1^{+-}$: The axial-vector-meson nonet $b_1, h_1,\ K_{1B}, h_1'$ with the h_1-h_1' ideal mixing angle $\theta_B = 35.26^0$. (Furthermore $K_{1,A}$ and $K_{1,B}$ are completely mixed.)

  The soft-core approach of the OBE has been given originally for NN in [35], and for YN in [3]. With respect to these OBE-interactions the ESC-models contain the modification of the form factor by introducing a zero for the mesons being P-wave quark-antiquark states in the CQM: the scalar- and axial-vector-mesons. Such a zero is natural in the $^3P_0$-quark-pair-creation (QPC) [26, 27] model for the coupling of the mesonic quark-antiquark ($Q\bar{Q}$) system to baryons. A consequence of such a zero is that a bound state in Λp-scattering is less likely to occur.

(ii) The configuration space soft-core uncorrelated two-meson exchange for NN has been derived in [36, 37]. Similarly to ESC04, also in ESC08 we use these potentials for ps-ps exchange with a complete $SU(3)_f$-symmetric treatment in NN, YN and YY. For example, we include double K-exchange in NN-scattering. Since this includes two-pion exchange (TPE) the long-range part of the potentials are represented. Here it is tacitly assumed that other TME potentials, like ps-vc, ps-sc, etc., are either small due to cancellations, or can be described adequately by using effective couplings in the OBE-potentials. When these effective couplings do not deviate from experimentally determined couplings it may be assumed that the corrections from these other SU(3) meson-nonets in the TME potentials are small. This is our working hypothesis for the TME-potentials. From the point of view of SU(3), since OBE contains only {8}- and {1}-exchange, TME can not be represented completely in terms of OBE. This because TME also has $\{27\}-, \{10\}$-, and $\{10^*\}$-exchange components. Therefore, the predictions made by the ESC-models could be sensitive to this incompleteness of TME in the ESC-models. At present the BB-data and the hypernuclear-data do not give information at this point.

(iii) Meson-pair exchanges (MPE) have been introduced in [1] for NN and described in detail in [38]. The two-meson-baryon-baryon vertices are the low energy approximations of (a) the heavy-meson and their two-meson decays, and (b) baryon-resonance contributions Δ_{33} etc [34, 38].

(iv) Diffractive contributions to the soft-core potential have been introduced from the beginning, cfr. [35]. The pomeron is thought of being related to an even number of gluon-exchanges. Here we introduce the odderon-potential, which is related to an odd number of gluon exchanges.

  (a) $J^{PC} = 0^{++}$: The 'diffractive' contribution from the pomeron (P), which is a unitary singlet. These interactions give a repulsive contribution to the potentials in all channels of a gaussian type.

  (b) $J^{PC} = 1^{--}$: The 'diffractive' contribution from the odderon (O). The origin of the odderon is assumed to be purely the exchange of the color-singlets with an odd number of gluons. Similarly to the pomeron, the odderon potential is taken to be an $SU(3)_F$ singlet and of the gaussian form.

  As an explanation of the repulsive character of the pomeron-potential the following: The J^{PC} is identical to that for the scalar-mesons. Naively, one would expect an attractive central potential. However, considering the two-gluon model for the pomeron [39, 40] the two-gluon parallel and crossed diagram contributions to the BB-interaction can be

shown to cancel adiabatically. The remaining non-adiabatic contribution is repulsive [41].

(v) Quark-Core-Effects in the soft-core model can supply extra repulsion, which may be required in some BB-channels. Baryon-baryon studies with the soft-core OBE and ESC-models thus far show that it is difficult to achieve a strongly enough repulsive short-range interactions in (i) the $\Sigma^+p(I = 3/2,^3S_1)$- and (ii) the $\Sigma N(I = 1/2,^1S_0)$-channel. The short-range repulsion in baryon-baryon may in principle come from: (a) meson- and multi-gluon-exchange [4, 5], and/or (b) the occurrence of forbidden six-quark SU(6)-states by the Pauli-principle [42–44]. In view of the mentioned difficulties, we have developed a phenomenological method for the ESC-model, which enables us to incorporate this quark-structural effect. This is an important new ingredient of the here presented ESC08-model. This structural effect we describe phenomenologically by gaussian repulsions, similar to the pomeron. In the ESC08c-model we take the strength of this repulsion proportional to the weights of the SU(6)-forbidden [51]-configuration in the various BB-channels. This in contrast to ESC08a,b [7, 8] where the quark-core effect is only included in the BB-channels with a dominant occurrence of the [51]-configuration.

B. Non-local Potentials, SU(3)-breaking, and Coulomb

As is well known, the non-local potentials are inherent to a relativistic theory, and occur in the central, spin-spin, tensor, spin-orbit etc. potentials. In the ESC-models we include the non-local contributions to the central/spin-spin potentials for scalar, vector, axial, and diffractive exchanges, as in the OBE-models [3, 35]. In addition, for all BB-channels we include for the pseudoscalar-type of potentials, which occur from pseudoscalar-, axial A- and B-mesons, the non-local spin-spin and tensor contributions [45]. This, because it turned out that the non-local pion-exchange spin-spin and tensor force is rather important for achieving a very good fit to the NN-data.

The different sources of $SU(3)$-breaking are discussed in paper II of this series.

As in all Nijmegen models, the Coulomb interaction is included exactly, for which we solve the multichannel Schrödinger equation on the physical particle basis. The nuclear potentials are calculated on the isospin basis. This means that we include only the so-called 'medium strong' SU(3)-breaking and the charge symmetry breaking (CSB) in the potentials.

III. TWO-BODY INTEGRAL EQUATIONS IN MOMENTUM SPACE

A. Three-dimensional Two-Body Equations

We consider the baryon-baryon reactions

$$B(p_a, s_a) + B(p_b, s_b) \to B(p_{a'}, s_{a'}) + B(p_{b'}, s_{b'}) \quad (3.1)$$

In the following we also refer to a and a' as particles 1 and 1' (or 3), and to b and b' as particles 2 and 2' (or 4). The total four-momenta for the initial and the final states are denoted as $P = p_a + p_b, P' = p_{a'} + p_{b'}$, and similarly the relative momenta by $p = \frac{1}{2}(p_a - p_b), p' = \frac{1}{2}(p_{a'} - p_{b'})$. In the center-of-mass system (CM-system) for a and b on-mass-shell one has $P = (W, \mathbf{0})$, $p = (0, \mathbf{p})$, $p' = (0, \mathbf{p}')$. In the following, the on-mass-shell CM-momenta for the initial and final states are denoted respectively by $\mathbf{p}$ and $\mathbf{p}'$. So, $p_a^0 = E_a(\mathbf{p}) = \sqrt{\mathbf{p}^2 + M_a^2}$ and $p_{a'}^0 = E_{a'}(\mathbf{p}') = \sqrt{\mathbf{p}'^2 + M_{a'}^2}$, and similarly for b(2) and b'(4). Because of translation-invariance $P = P'$ and $W = W' = E_a(\mathbf{p}) + E_b(\mathbf{p}) = E_{a'}(\mathbf{p}') + E_{b'}(\mathbf{p}')$. The transition amplitude matrix M is related to the S-matrix via

$$\langle f|S|i\rangle = \langle f|i\rangle - i(2\pi)^4\delta^4(P_f - P_i)\langle f|M|i\rangle. \quad (3.2)$$

The two-particle states we normalize in the following way

$$\langle \mathbf{p}_1', \mathbf{p}_2'|\mathbf{p}_1, \mathbf{p}_2\rangle = (2\pi)^3 2E(\mathbf{p}_1)\delta^3(\mathbf{p}_1' - \mathbf{p}_1)\cdot \times(2\pi)^3 2E(\mathbf{p}_2)\delta^3(\mathbf{p}_2' - \mathbf{p}_2). \quad (3.3)$$

Three-dimensional integral equations for the amplitudes $\langle f|M|i\rangle$ have been derived in various ways, see e.g. [2, 46–49]. Here, we follow Ref. [4] which employs the Macke-Klein procedure [50]. After redefining the CM-amplitude $M(\mathbf{p}', \mathbf{p}|W)$ by

$$M(\mathbf{p}', \mathbf{p}|W) \to \sqrt{\frac{M_a M_b}{E_a(\mathbf{p}')E_b(\mathbf{p}')}}M(\mathbf{p}', \mathbf{p}|W)\sqrt{\frac{M_a M_b}{E_a(\mathbf{p}')E_b(\mathbf{p}')}} \quad (3.4)$$

one arrives, see for details Ref. [4], at the Thompson equation [48]

$$M(\mathbf{p}', \mathbf{p}|W) = K^{irr}(\mathbf{p}', \mathbf{p}|W) + \int \frac{d^3p''}{(2\pi)^3}K^{irr}(\mathbf{p}', \mathbf{p}''|W)\; E_2^{(+)}(\mathbf{p}''; W)\; M(\mathbf{p}'', \mathbf{p}|W), \quad (3.5)$$

where $E_2^{(+)}(\mathbf{p}'';W) = (W - \mathcal{W}(\mathbf{p}'') + i\delta)^{-1}$, and the two-nucleon irreducible kernel is given by

$$\begin{aligned} K^{irr}(\mathbf{p}',\mathbf{p}|W) &= -\frac{1}{(2\pi)^2}\sqrt{\frac{M_aM_b}{E_a(\mathbf{p}')E_b(\mathbf{p}')}}\sqrt{\frac{M_aM_b}{E_a(\mathbf{p})E_b(\mathbf{p})}}\,(W-\mathcal{W}(\mathbf{p}'))\,(W-\mathcal{W}(\mathbf{p})) \\ &\times \int_{-\infty}^{+\infty} dp_0' \int_{-\infty}^{+\infty} dp_0 \left[\left\{ F_W^{(a)}(\mathbf{p}',p_0')F_W^{(b)}(-\mathbf{p}',-p_0') \right\}^{-1} \right. \\ &\times \left. \left[I(p_0',\mathbf{p}';p_0,\mathbf{p})\right]_{++,++} \left\{ F_W^{(a)}(\mathbf{p},p_0)F_W^{(b)}(-\mathbf{p},-p_0) \right\}^{-1} \right], \end{aligned} \tag{3.6}$$

where $F_W(\mathbf{p},p_0) = p_0 - E(\mathbf{p}) + W/2 + i\delta$. This same expression for the kernel was exploited in [36–38].

In case one does not assume the strong pair-suppression, one must study instead of equation (3.5) a more general equation with couplings between the positive and negative energy spinorial amplitudes. Also to this more general case one can apply the described three-dimensional reduction, and we refer the reader to Ref. [51] for a treatment of this case.

The M/E-factors in (3.6) are due to the difference between the relativistic and the non-relativistic normalization of the two-particle states. In the following we simply put $M/E(\mathbf{p}) = 1$ in the kernel K^{irr} Eq. (3.6). The corrections to this approximation would give $(1/M)^2$-corrections to the potentials, which we neglect in this paper. In the same approximation there is no difference between the Thompson [48] and the Lippmann-Schwinger equation, when the connection between these equations is made using multiplication factors. Henceforth, we will not distinguish between the two.

The contributions to the two-particle irreducible kernel K^{irr} up to second order in the meson-exchange are given in detail in [37, 38].

B. Lippmann-Schwinger Equation

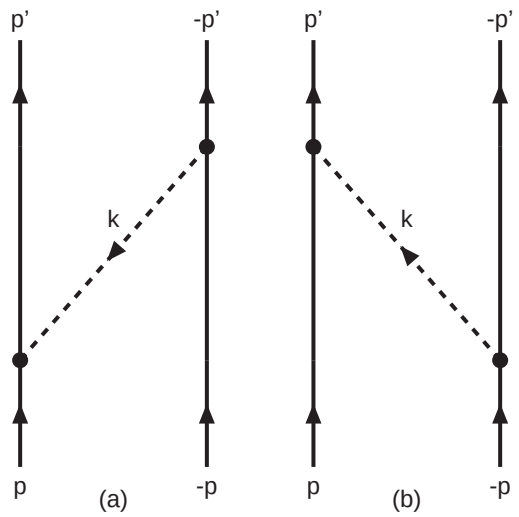

FIG. 1: One-boson-exchange graphs: The dashed lines with momentum $\mathbf{k}$ refers to the bosons: pseudo-scalar, vector, axial-vector, or scalar mesons.

The transformation of (3.5) to the Lippmann-Schwinger equation can be effectuated by defining

$$\begin{aligned} T(\mathbf{p}',\mathbf{p}) &= N(\mathbf{p}')\; M(\mathbf{p}',\mathbf{p}|W)\; N(\mathbf{p}), \\ V(\mathbf{p}',\mathbf{p}) &= N(\mathbf{p}')\; K^{irr}(\mathbf{p}',\mathbf{p}|W)\; N(\mathbf{p}), \end{aligned} \tag{3.7}$$

where the transformation function is

$$N(\mathbf{p}) = \sqrt{\frac{\mathbf{p}_i^2 - \mathbf{p}^2}{2M_N(E(\mathbf{p}_i) - E(\mathbf{p}))}}. \tag{3.8}$$

Application of this transformation, yields the Lippmann-Schwinger equation

$$\begin{aligned} T(\mathbf{p}',\mathbf{p}) &= V(\mathbf{p}',\mathbf{p}) + \int \frac{d^3p''}{(2\pi)^3} \\ &\times V(\mathbf{p}',\mathbf{p}'')\; g(\mathbf{p}'';W)\; T(\mathbf{p}'',\mathbf{p}) \end{aligned} \tag{3.9}$$

with the standard Green function

$$g(\mathbf{p};W) = \frac{M_N}{\mathbf{p}_i^2 - \mathbf{p}^2 + i\delta}. \tag{3.10}$$

The corrections to the approximation $E_2^{(+)} \approx g(\mathbf{p};W)$ are of order $1/M^2$, which we neglect henceforth.

The transition from Dirac-spinors to Pauli-spinors, is given in Appendix C of Ref. [36], where we write for the the Lippmann-Schwinger equation in the 4-dimensional Pauli-spinor space

$$\begin{aligned} \mathcal{T}(\mathbf{p}',\mathbf{p}) &= \mathcal{V}(\mathbf{p}',\mathbf{p}) + \int \frac{d^3p''}{(2\pi)^3} \\ &\times \mathcal{V}(\mathbf{p}',\mathbf{p}'')\; g(\mathbf{p}'';W)\; \mathcal{T}(\mathbf{p}'',\mathbf{p})\;. \end{aligned} \tag{3.11}$$

The $\mathcal{T}$-operator in Pauli spinor-space is defined by

$$\begin{aligned} &\chi_{\sigma_a'}^{(a)\dagger}\chi_{\sigma_b'}^{(b)\dagger}\;\mathcal{T}(\mathbf{p}',\mathbf{p})\;\chi_{\sigma_a}^{(a)}\chi_{\sigma_b}^{(b)} = \\ &\bar{u}_a(\mathbf{p}',\sigma_a')\bar{u}_b(-\mathbf{p}',\sigma_b')\;\tilde{T}(\mathbf{p}',\mathbf{p})\;u_a(\mathbf{p},\sigma_a)u_b(-\mathbf{p},\sigma_b). \end{aligned} \tag{3.12}$$

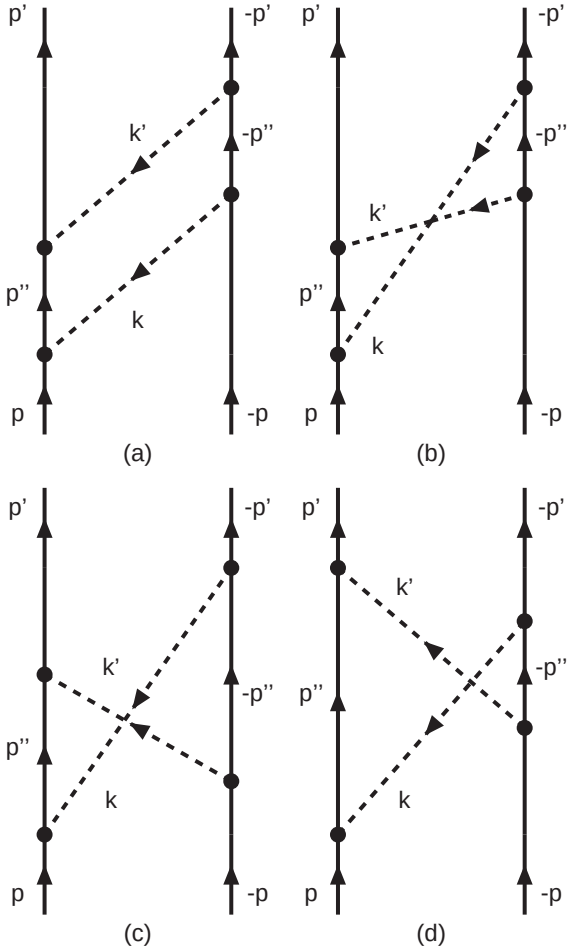

FIG. 2: BW two-meson-exchange graphs: (a) planar and (b)–(d) crossed box. The dashed line with momentum $\mathbf{k}_1$ refers to the pion and the dashed line with momentum $\mathbf{k}_2$ refers to one of the other (vector, scalar, or pseudoscalar) mesons. To these we have to add the "mirror" graphs, and the graphs where we interchange the two meson lines.

and similarly for the $\mathcal{V}$-operator. Like in the derivation of the OBE-potentials [2, 35] we make off-shell and on-shell the approximation, $E(\mathbf{p}) = M + \mathbf{p}^2/2M$ and $W = 2\sqrt{\mathbf{p}_i^2 + M^2} \approx 2M + \mathbf{p}_i^2/M$, everywhere in the interaction kernels, which, of course, is fully justified for low energies only. In contrast to these kinds of approximations, of course the full $\mathbf{k}^2$-dependence of the form factors is kept throughout the derivation of the TME. Notice that the gaussian form factors suppress the high momentum transfers strongly. This means that the contribution to the potentials from intermediate states which are far off-energy-shell can not be very large.

Because of rotational invariance and parity conservation, the $\mathcal{T}$-matrix, which is a 4×4-matrix in Pauli-spinor space, can be expanded into the following set of in general 8 spinor invariants, see for example Ref. [52]. Introducing

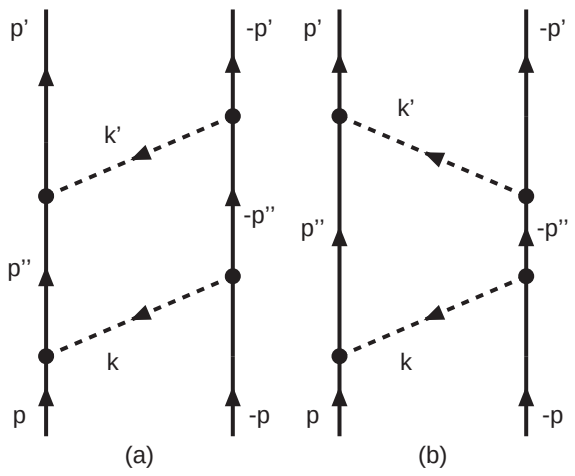

FIG. 3: Planar-box TMO two-meson-exchange graphs. Same notation as in Fig. 2. To these we have to add the "mirror" graphs, and the graphs where we interchange the two meson lines.

[53]

$$\mathbf{q} = \frac{1}{2}(\mathbf{p}' + \mathbf{p}) \ , \ \mathbf{k} = \mathbf{p}' - \mathbf{p} \ , \ \mathbf{n} = \mathbf{p} \times \mathbf{p}', \qquad (3.13)$$

with, of course, $\mathbf{n} = \mathbf{q} \times \mathbf{k}$, we choose for the operators P_j in spin-space

$$\begin{aligned}
&P_1 = 1, \quad P_2 = \boldsymbol{\sigma}_1 \cdot \boldsymbol{\sigma}_2, \\
&P_3 = (\boldsymbol{\sigma}_1 \cdot \mathbf{k})(\boldsymbol{\sigma}_2 \cdot \mathbf{k}) - \frac{1}{3}(\boldsymbol{\sigma}_1 \cdot \boldsymbol{\sigma}_2)\mathbf{k}^2, \\
&P_4 = \frac{i}{2}(\boldsymbol{\sigma}_1 + \boldsymbol{\sigma}_2) \cdot \mathbf{n}, \quad P_5 = (\boldsymbol{\sigma}_1 \cdot \mathbf{n})(\boldsymbol{\sigma}_2 \cdot \mathbf{n}), \\
&P_6 = \frac{i}{2}(\boldsymbol{\sigma}_1 - \boldsymbol{\sigma}_2) \cdot \mathbf{n}, \\
&P_7 = (\boldsymbol{\sigma}_1 \cdot \mathbf{q})(\boldsymbol{\sigma}_2 \cdot \mathbf{k}) + (\boldsymbol{\sigma}_1 \cdot \mathbf{k})(\boldsymbol{\sigma}_2 \cdot \mathbf{q}), \\
&P_8 = (\boldsymbol{\sigma}_1 \cdot \mathbf{q})(\boldsymbol{\sigma}_2 \cdot \mathbf{k}) - (\boldsymbol{\sigma}_1 \cdot \mathbf{k})(\boldsymbol{\sigma}_2 \cdot \mathbf{q}). \qquad (3.14)
\end{aligned}$$

Here we follow Ref. [3], where in contrast to Ref. [35], we have chosen P_3 to be a purely 'tensor-force' operator. The expansion in spinor-invariants reads

$$\mathcal{T}(\mathbf{p}', \mathbf{p}) = \sum_{j=1}^{8} \widetilde{T}_j(\mathbf{p}'^2, \mathbf{p}^2, \mathbf{p}' \cdot \mathbf{p}) \ P_j(\mathbf{p}', \mathbf{p}) \ . \qquad (3.15)$$

Similarly to (3.15) we expand the potentials V. In the case of the axial-vector meson exchange there will occur terms proportional to

$$P_5' = (\boldsymbol{\sigma}_1 \cdot \mathbf{q})(\boldsymbol{\sigma}_2 \cdot \mathbf{q}) - \frac{1}{3}(\boldsymbol{\sigma}_1 \cdot \boldsymbol{\sigma}_2)\mathbf{q}^2. \qquad (3.16)$$

The treatment of such a Pauli-invariant using the Okubo-Marshak identity [54], see also Ref. [52], is not without problems because it involves the division with $\mathbf{k}^2$. Therefore, in the ESC04-models [4, 5] the replacement

$P_5' \to -P_3$ was chosen. For the ESC08-models a satisfactory treatment has been developed, which is described in Appendix B. For the treatment of the potentials with P_8 we use the identity [55]

$$P_8 = -(1 + \boldsymbol{\sigma}_1 \cdot \boldsymbol{\sigma}_2)P_6. \tag{3.17}$$

Under time-reversal $P_7 \to -P_7$ and $P_8 \to -P_8$. Therefore for elastic scattering $V_7 = V_8 = 0$. Anticipating the explicit results for the potentials in section IV we notice the following: (i) For the general BB-reaction we will find no contribution to V_7. The operators P_6 and P_8 give spin singlet-triplet transitions. (ii) In the case of non-strangeness-exchange ($\Delta S = 0$), $V_6 \neq 0$ and V_8=0. The latter follows from our approximation to neglect the mass differences among the nucleons, between the Λ and Σ's, and among the Ξ's. (iii) In the case of strangeness-exchange ($\Delta S = \pm 1$), $V_6, V_8 \neq 0$. The contributions to V_6 come from graphs with both spin- and particle-exchange, i.e. Majorana-type potentials having the $P_f P_\sigma P_6 = -P_x P_6$-operator. Here, $P_f P_\sigma$ reflect our convention for the two-particle wave functions, see [2]. The contributions to V_8 come from graphs with particle-exchange and spin-exchange, because $P_8 = -P_\sigma P_6$. Therefore, we only have to apply P_f in order to map the wave functions after such exchange onto our two-particle wave-functions. So, we have the $P_f P_8 = +P_x P_6$-operator. Here, we used that for BB-systems the allowed physical states satisfy $P_f P_\sigma P_x = -1$.

IV. EXTENDED-SOFT-CORE POTENTIALS IN MOMENTUM SPACE

The potential of the ESC-model contains the contributions from (i) One-boson-exchanges, Fig. 1, (ii) Uncorrelated Two-Pseudo-scalar exchange, Fig. 2 and Fig. 3, and (iii) Meson-Pair-exchange, Fig 4. In this section we review the potentials and indicate the changes with respect to earlier papers on the OBE- and ESC-models. The spin-1 meson-exchange is an important ingredient for the baryon-baryon force. In the ESC08-model we treat the vector-mesons and the axial-vector mesons according to the Proca- [56] and the B-field [57, 58] formalism respectively. For details, we refer to Appendix A.

A. One-Boson-Exchange Interactions in Momentum Space

The OBE-potentials are the same as given in [3, 35], with the exception of (i) the zero in the scalar form factor, and (ii) the axial-vector-meson potentials. Here, we review the OBE-potentials briefly, and give those potentials which are not included in the above references.

Interaction Hamiltonians: The local interaction Hamilton densities for the different couplings are [59]

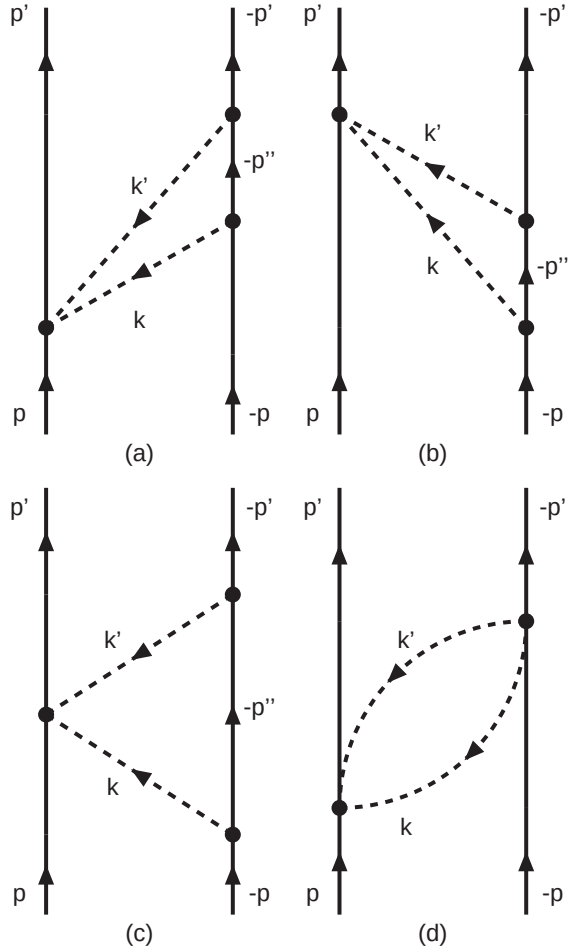

FIG. 4: One- and Two-Pair exchange graphs. To these we have to add the "mirror" graphs, and the graphs where we interchange the two meson lines.

a) Pseudoscalar-meson exchange ($J^{PC} = 0^{-+}$)

$$\mathcal{H}_{PV} = \frac{f_P}{m_{\pi^+}} \bar{\psi}\gamma_\mu\gamma_5\psi\partial^\mu\phi_P. \tag{4.1}$$

This is the pseudovector coupling, and the relation with the pseudoscalar coupling is $g_P = 2M_B/m_{\pi^+}$, where M_B is the nucleon or hyperon mass.

b) Vector-meson exchange ($J^{PC} = 1^{--}$)

$$\mathcal{H}_V = g_V\bar{\psi}\gamma_\mu\psi\phi_V^\mu + \frac{f_V}{4\mathcal{M}}\bar{\psi}\sigma_{\mu\nu}\psi(\partial^\mu\phi_V^\nu - \partial^\nu\phi_V^\mu), \tag{4.2}$$

where $\sigma_{\mu\nu} = i[\gamma_\mu, \gamma_\nu]/2$, and the scaling mass $\mathcal{M}$, will be taken to be the proton mass.

c) Axial-vector-meson exchange ($J^{PC} = 1^{++}$, 1^{st} kind):

$$\mathcal{H}_A = g_A[\bar{\psi}\gamma_\mu\gamma_5\psi]\phi_A^\mu + \frac{if_A}{\mathcal{M}}[\bar{\psi}\gamma_5\psi]\ \partial_\mu\phi_A^\mu. \tag{4.3}$$

In ESC04 the g_A-coupling was included, but not the derivative f_A-coupling [61]. Also, in ESC04 we used a local-tensor approximation (LTA) for the $(\boldsymbol{\sigma}_1 \cdot \mathbf{q})(\boldsymbol{\sigma}_2 \cdot \mathbf{q})$ operator. Here, we improve on that considerably by avoiding such rather crude approximation. The details of our new treatment are given in Appendix B.

d) Axial-vector-meson exchange ($J^{PC} = 1^{+-}$, 2^{nd} kind):

$$\mathcal{H}_B = \frac{if_B}{m_B}[\bar{\psi}\sigma_{\mu\nu}\gamma_5\psi]\ \partial_\nu \phi_B^\mu, \tag{4.4}$$

where m_B is the $b_1(1235)$-mass. In ESC04 this coupling was not included. Like for the axial-vector mesons of the 1^{st}-kind we include an SU(3)-nonet with members $b_1(1235), h_1(1170), h_1(1380)$. In the quark-model they are $Q\bar{Q}(^1P_1)$-states.

e) Scalar-meson exchange ($J^{PC} = 0^{++}$):

$$\mathcal{H}_S = g_S[\bar{\psi}\psi]\phi_S + \frac{f_S}{\mathcal{M}}[\bar{\psi}\gamma_\mu\psi]\ \partial^\mu \phi_S, \tag{4.5}$$

which is the most general interaction up to the first derivative. However, charge conjugation gives $\mathcal{C}[\bar{\psi}\gamma_\mu\psi]\mathcal{C}^{-1} = -[\bar{\psi}\gamma_\mu\psi]$, and therefore $f_S = 0$.

f) Pomeron-exchange ($J^{PC} = 0^{++}$): The vertices for this 'diffractive'-exchange have the same Lorentz structure as those for scalar-meson-exchange.

g) Odderon-exchange ($J^{PC} = 1^{--}$):

$$\mathcal{H}_O = g_O[\bar{\psi}\gamma_\mu\psi]\phi_O^\mu + \frac{f_O}{4\mathcal{M}}[\bar{\psi}\sigma_{\mu\nu}\psi](\partial^\mu\phi_O^\nu - \partial^\nu\phi_O^\mu). \tag{4.6}$$

Since the gluons are flavorless, odderon-exchange is treated as an SU(3)-singlet. Furthermore, since the odderon represents a Regge-trajectory with an intercept equal to that of the pomeron, and is supposed not to contribute for small $\mathbf{k}^2$, we include a factor $\mathbf{k}^2/\mathcal{M}^2$ in the coupling.

Form Factors: Including form factors $f(\mathbf{x}' - \mathbf{x})$, the interaction hamiltonian densities are modified to

$$H_X(\mathbf{x}) = \int d^3x'\, f(\mathbf{x}' - \mathbf{x})\mathcal{H}_X(\mathbf{x}'), \tag{4.7}$$

for $X = P,\ V,\ A$, and S (P = pseudo-scalar, V = vector, A = axial-vector, and S = scalar). The potentials in momentum space are the same as for point interactions, except that the coupling constants are multiplied by the Fourier transform of the form factors.

In the derivation of the V_i we employ the same approximations as in [3, 35], i.e.

1. We expand in $1/M$: $E(p) = \left[\mathbf{k}^2/4 + \mathbf{q}^2 + M^2\right]^{\frac{1}{2}}$ $\approx M + \mathbf{k}^2/8M + \mathbf{q}^2/2M$ and keep only terms up to first order in $\mathbf{k}^2/M$ and $\mathbf{q}^2/M$. This except for the form factors where the full $\mathbf{k}^2$-dependence is kept throughout the calculations. Notice that the gaussian form factors suppress the high $\mathbf{k}^2$-contributions strongly.
2. In the meson propagators $(-(p_1 - p_3)^2 + m^2) \approx (\mathbf{k}^2 + m^2)$, except for the strangeness carrying mesons, see below.
3. When two different baryons are involved at a BBM-vertex their average mass is used in the potentials and the non-zero component of the momentum transfer is accounted for by using an effective mass in the meson propagator (for details see [3]).

Due to the approximations we get only a linear dependence on $\mathbf{q}^2$ for V_1. In the following, separating the local and the non-local parts, we write

$$V_i(\mathbf{k}^2, \mathbf{q}^2) = V_{ia}(\mathbf{k}^2) + V_{ib}(\mathbf{k}^2)(\mathbf{q}^2 + \frac{1}{4}\mathbf{k}^2), \tag{4.8}$$

where in principle $i = 1, 8$.

The OBE-potentials are now obtained in the standard way (see e.g. [3, 35]) by evaluating the BB-interaction in Born-approximation. We write the potentials V_i of Eqs. (3.15) and (4.8) in the form

$$V_i(\mathbf{k}^2, \mathbf{q}^2) = \sum_X \Omega_i^{(X)}(\mathbf{k}^2) \cdot \Delta^{(X)}(\mathbf{k}^2, m^2, \Lambda^2). \tag{4.9}$$

Furthermore for $X = P, V$

$$\Delta^{(X)}(\mathbf{k}^2, m^2, \Lambda^2) = e^{-\mathbf{k}^2/\Lambda^2} / \left(\mathbf{k}^2 + m^2\right), \tag{4.10}$$

and for $X = S, A$ a zero in the form factor

$$\Delta^{(S)}(\mathbf{k}^2, m^2, \Lambda^2) = \left(1 - \mathbf{k}^2/U^2\right)\ e^{-\mathbf{k}^2/\Lambda^2} / \left(\mathbf{k}^2 + m^2\right), \tag{4.11}$$

and for $X = D, O$

$$\Delta^{(D)}(\mathbf{k}^2, m^2, \Lambda^2) = \frac{1}{\mathcal{M}^2} e^{-\mathbf{k}^2/(4m_{P,O}^2)}. \tag{4.12}$$

In the last expression $\mathcal{M}$ is a universal scaling mass, which is again taken to be the proton mass. The mass parameter m_P controls the $\mathbf{k}^2$-dependence of the pomeron. Similarly, m_O controls the $\mathbf{k}^2$-dependence of the odderon.

In the following we give the OBE-potentials in momentum-space for the nucleon/hyperon-nucleon systems for the non-strange mesons. From these those for NN and YY can be deduced easily. We assign the particles 1 and 3 to be hyperons, and particles 2 and 4 to be nucleons. Mass differences among the hyperons and among the nucleons will be neglected.

For pseudo-scalar mesons, the graph's of Fig. 1 give for the potential $V(\mathbf{k},\mathbf{q}) \approx K_{PS}^{(2)}(\mathbf{p}',\mathbf{p}|W)$

$$\begin{aligned} V_{PS}(\mathbf{k},\mathbf{q}) &= -\frac{f_{13}f_{24}}{m_\pi^2}\left(1-\frac{(\mathbf{q}^2+\mathbf{k}^2/4)}{2M_YM_N}\right)\cdot\left[\frac{1}{2\omega}\left\{\frac{1}{\omega+a}+\frac{1}{\omega-a}\right\}(\boldsymbol{\sigma}_1\cdot\mathbf{k})(\boldsymbol{\sigma}_2\cdot\mathbf{k})\right. \\ &\left.+\frac{1}{M_Y+M_N}\left\{\frac{1}{\omega+a}-\frac{1}{\omega-a}\right\}(\boldsymbol{\sigma}_1\cdot\mathbf{q}\;\boldsymbol{\sigma}_2\cdot\mathbf{k}-\boldsymbol{\sigma}_1\cdot\mathbf{k}\;\boldsymbol{\sigma}_2\cdot\mathbf{q})\right]\exp\left(-\mathbf{k}^2/\Lambda^2\right). \end{aligned} \tag{4.13}$$

Here, $\omega=\sqrt{\mathbf{k}^2+m^2}$, and using the on-energy-shell approximation $E_1+E_2=E_3+E_4$, we have

$$\begin{aligned} a &= E_1+E_4-W=\frac{1}{2}\left(E_1+E_4-E_2-E_3\right) \\ &\approx \Delta M+\frac{1}{4}\Delta M\left(\frac{1}{M_1M_3}+\frac{1}{M_2M_4}\right)\left(\mathbf{q}^2+\mathbf{k}^2/4\right), \end{aligned}$$

where $\Delta M=(M_1+M_4-M_3-M_2)/2$, and we neglected the $\mathbf{q}\cdot\mathbf{k}$-term which is of order $(M_Y-M_N)/2M_YM_N$. Henceforth we neglect the non-adiabatic effects, i.e. $a\approx\Delta M$, in the OBE-potentials, except for the P_8-terms, where the leading term is proportional to a. One notices that the P_8-term in (4.13) is only non-zero for K-exchange.

B. Non-strange Meson-exchange

For the non-strange mesons the mass differences at the vertices are neglected, we take at the YYM- and the NNM-vertex the average hyperon and the average nucleon mass respectively. This implies that we do not include contributions to the Pauli-invariants P_7 and P_8. Below the contributions to the different $\Omega_i^{(X)}$'s for baryon-baryon scattering are given in detail.

(a) Pseudoscalar-meson exchange:

$$\Omega_{2a}^{(P)} = -f_{13}^{PV}f_{24}^{PV}\left(\frac{\mathbf{k}^2}{3m_{\pi^+}^2}\right) \quad , \quad \Omega_{3a}^{(P)}=-f_{13}^{PV}f_{24}^{PV}\left(\frac{1}{m_{\pi^+}^2}\right), \tag{4.14a}$$

$$\Omega_{2b}^{(P)} = +f_{13}^{PV}f_{24}^{PV}\left(\frac{\mathbf{k}^2}{6m_{\pi^+}^2M_YM_N}\right) \quad , \quad \Omega_{3b}^{(P)}=+f_{13}^{PV}f_{24}^{PV}\left(\frac{1}{2m_{\pi^+}^2M_YM_N}\right),. \tag{4.14b}$$

(b) Vector-meson exchange:

$$\begin{aligned} \Omega_{1a}^{(V)} &= \left\{g_{13}^Vg_{24}^V\left(1-\frac{\mathbf{k}^2}{2M_YM_N}\right)-g_{13}^Vf_{24}^V\frac{\mathbf{k}^2}{4\mathcal{M}M_N}-f_{13}^Vg_{24}^V\frac{\mathbf{k}^2}{4\mathcal{M}M_Y}\right. \\ &\left.+f_{13}^Vf_{24}^V\frac{\mathbf{k}^4}{16\mathcal{M}^2M_YM_N}\right\}, \quad \Omega_{1b}^{(V)}=g_{13}^Vg_{24}^V\left(\frac{3}{2M_YM_N}\right), \\ \Omega_{2a}^{(V)} &= -\frac{2}{3}\mathbf{k}^2\,\Omega_{3a}^{(V)}, \quad \Omega_{2b}^{(V)}=-\frac{2}{3}\mathbf{k}^2\,\Omega_{3b}^{(V)}, \\ \Omega_{3a}^{(V)} &= \left\{(g_{13}^V+f_{13}^V\frac{M_Y}{\mathcal{M}})(g_{24}^V+f_{24}^V\frac{M_N}{\mathcal{M}})-f_{13}^Vf_{24}^V\frac{\mathbf{k}^2}{8\mathcal{M}^2}\right\}/(4M_YM_N), \\ \Omega_{3b}^{(V)} &= -(g_{13}^V+f_{13}^V\frac{M_Y}{\mathcal{M}})(g_{24}^V+f_{24}^V\frac{M_N}{\mathcal{M}})/(8M_Y^2M_N^2), \\ \Omega_4^{(V)} &= -\left\{12g_{13}^Vg_{24}^V+8(g_{13}^Vf_{24}^V+f_{13}^Vg_{24}^V)\frac{\sqrt{M_YM_N}}{\mathcal{M}}-f_{13}^Vf_{24}^V\frac{3\mathbf{k}^2}{\mathcal{M}^2}\right\}/(8M_YM_N) \\ \Omega_5^{(V)} &= -\left\{g_{13}^Vg_{24}^V+4(g_{13}^Vf_{24}^V+f_{13}^Vg_{24}^V)\frac{\sqrt{M_YM_N}}{\mathcal{M}}+8f_{13}^Vf_{24}^V\frac{M_YM_N}{\mathcal{M}^2}\right\}/(16M_Y^2M_N^2) \\ \Omega_6^{(V)} &= -\left\{(g_{13}^Vg_{24}^V+f_{13}^Vf_{24}^V\frac{\mathbf{k}^2}{4\mathcal{M}^2})\frac{(M_N^2-M_Y^2)}{4M_Y^2M_N^2}-(g_{13}^Vf_{24}^V-f_{13}^Vg_{24}^V)\frac{1}{\sqrt{\mathcal{M}^2M_YM_N}}\right\}. \end{aligned} \tag{4.15}$$

(c) Scalar-meson exchange:

$$\Omega_{1a}^{(S)} = -g_{13}^S g_{24}^S \left(1 + \frac{\mathbf{k}^2}{4M_Y M_N}\right), \quad \Omega_{1b}^{(S)} = +g_{13}^S g_{24}^S \frac{1}{2M_Y M_N}$$

$$\Omega_4^{(S)} = -g_{13}^S g_{24}^S \frac{1}{2M_Y M_N}, \quad \Omega_5^{(S)} = g_{13}^S g_{24}^S \frac{1}{16 M_Y^2 M_N^2}$$

$$\Omega_6^{(S)} = -g_{13}^S g_{24}^S \frac{(M_N^2 - M_Y^2)}{4M_Y M_N}. \tag{4.16}$$

(d) Axial-vector-exchange $J^{PC} = 1^{++}$:

$$\Omega_{2a}^{(A)} = -g_{13}^A g_{24}^A \left[1 - \frac{2\mathbf{k}^2}{3M_Y M_N}\right] + \left[\left(g_{13}^A f_{24}^A \frac{M_N}{\mathcal{M}} + f_{13}^A g_{24}^A \frac{M_Y}{\mathcal{M}}\right) - f_{13}^A f_{24}^A \frac{\mathbf{k}^2}{2\mathcal{M}^2}\right] \frac{\mathbf{k}^2}{6M_Y M_N}$$

$$\Omega_{2b}^{(A)} = -g_{13}^A g_{24}^A \left(\frac{3}{2M_Y M_N}\right)$$

$$\Omega_3^{(A)} = -g_{13}^A g_{24}^A \left[\frac{1}{4M_Y M_N}\right] + \left[\left(g_{13}^A f_{24}^A \frac{M_N}{\mathcal{M}} + f_{13}^A g_{24}^A \frac{M_Y}{\mathcal{M}}\right) - f_{13}^A f_{24}^A \frac{\mathbf{k}^2}{2\mathcal{M}^2}\right] \frac{1}{2M_Y M_N}$$

$$\Omega_4^{(A)} = -g_{13}^A g_{24}^A \left[\frac{1}{2M_Y M_N}\right], \quad \Omega_5^{(A)'} = -g_{13}^A g_{24}^A \left[\frac{2}{M_Y M_N}\right]$$

$$\Omega_6^{(A)} = -g_{13}^A g_{24}^A \left[\frac{(M_N^2 - M_Y^2)}{4M_Y^2 M_N^2}\right] \tag{4.17}$$

Here, we used the B-field description with $\alpha_r = 1$, see Appendix A. The detailed treatment of the potential proportional to P_5', i.e. with $\Omega_5^{(A)'}$, is given in Appendix B.

(e) Axial-vector mesons with $J^{PC} = 1^{+-}$:

$$\Omega_{2a}^{(B)} = +f_{13}^B f_{24}^B \frac{(M_N + M_Y)^2}{m_B^2} \left(1 - \frac{\mathbf{k}^2}{4M_Y M_N}\right) \left(\frac{\mathbf{k}^2}{12 M_Y M_N}\right), \quad \Omega_{2b}^{(B)} = +f_{13}^B f_{24}^B \frac{(M_N + M_Y)^2}{m_B^2} \left(\frac{\mathbf{k}^2}{8M_Y^2 M_N^2}\right)$$

$$\Omega_{3a}^{(B)} = +f_{13}^B f_{24}^B \frac{(M_N + M_Y)^2}{m_B^2} \left(1 - \frac{\mathbf{k}^2}{4M_Y M_N}\right) \left(\frac{1}{4M_Y M_N}\right), \quad \Omega_{3b}^{(B)} = +f_{13}^B f_{24}^B \frac{(M_N + M_Y)^2}{m_B^2} \left(\frac{3}{8M_Y^2 M_N^2}\right). \tag{4.18}$$

(f) Diffractive-exchange (pomeron):
The Ω_i^D are the same as for scalar-meson-exchange Eq.(4.16), but with $\pm g_{13}^S g_{24}^S$ replaced by $\mp g_{13}^D g_{24}^D$, and except for the zero in the form factor.

(g) Odderon-exchange: The Ω_i^O are the same as for vector-meson-exchange Eq. (4.15), but with $g_{13}^V \to g_{13}^O$, $f_{13}^V \to f_{13}^O$ and similarly for the couplings with the 24-subscript.

As in Ref. [3] in the derivation of the expressions for $\Omega_i^{(X)}$, given above, M_Y and M_N denote the mean hyperon and nucleon mass, respectively $M_Y = (M_1 + M_3)/2$ and $M_N = (M_2 + M_4)/2$, and m denotes the mass of the exchanged meson. Moreover, the approximation $1/M_N^2 + 1/M_Y^2 \approx 2/(M_N M_Y)$, is used, which is rather good since the mass differences between the baryons are not large.

C. One-Boson-Exchange Interactions in Configuration Space I

In configuration space the BB-interactions are described by potentials of the general form [60]

$$\begin{aligned} V &= V_C(r) + V_\sigma(r)\boldsymbol{\sigma}_1\cdot\boldsymbol{\sigma}_2 + V_T(r)S_{12} + V_{SO}(r)\mathbf{L}\cdot\mathbf{S} + V_Q(r)Q_{12} \\ &\quad + V_{ASO}(r)\ \frac{1}{2}(\boldsymbol{\sigma}_1-\boldsymbol{\sigma}_2)\cdot\mathbf{L} - \frac{1}{2M_YM_N}\left(\boldsymbol{\nabla}^2V^{n.l.}(r) + V^{n.l.}(r)\boldsymbol{\nabla}^2\right), \qquad (4.19a) \\ V^{n.l.} &= \left\{\varphi_C(r) + \varphi_\sigma(r)\boldsymbol{\sigma}_1\cdot\boldsymbol{\sigma}_2 + \varphi_T(r)S_{12}\right\}, \qquad (4.19b) \end{aligned}$$

where

$$\begin{aligned} S_{12} &= 3(\boldsymbol{\sigma}_1\cdot\hat{r})(\boldsymbol{\sigma}_2\cdot\hat{r}) - (\boldsymbol{\sigma}_1\cdot\boldsymbol{\sigma}_2), \qquad (4.20a) \\ Q_{12} &= \frac{1}{2}\left[(\boldsymbol{\sigma}_1\cdot\mathbf{L})(\boldsymbol{\sigma}_2\cdot\mathbf{L}) + (\boldsymbol{\sigma}_2\cdot\mathbf{L})(\boldsymbol{\sigma}_1\cdot\mathbf{L})\right]. \qquad (4.20b) \end{aligned}$$

For the basic functions for the Fourier transforms with gaussian form factors, we refer to Refs. [3, 35]. For the details of the Fourier transform for the potentials with P_5', which occur in the case of the axial-vector mesons with $J^{PC}=1^{++}$, we refer to Appendix B.

(a) Pseudoscalar-meson-exchange:

$$\begin{aligned} V_{PS}(r) &= \frac{m}{4\pi}\left[f_{13}^Pf_{24}^P\left(\frac{m}{m_{\pi^+}}\right)^2\left(\frac{1}{3}(\boldsymbol{\sigma}_1\cdot\boldsymbol{\sigma}_2)\ \phi_C^1 + S_{12}\phi_T^0\right)\right], \qquad (4.21a) \\ V_{PS}^{n.l.}(r) &= -\frac{m}{4\pi}\left[f_{13}^Pf_{24}^P\left(\frac{m^2}{2m_{\pi^+}^2}\right)\left(\frac{1}{3}(\boldsymbol{\sigma}_1\cdot\boldsymbol{\sigma}_2)\ \phi_C^1 + S_{12}\phi_T^0\right)\right]. \qquad (4.21b) \end{aligned}$$

(b) Vector-meson-exchange:

$$\begin{aligned} V_V(r) &= \frac{m}{4\pi}\left[\left\{g_{13}^Vg_{24}^V\left[\phi_C^0 + \frac{m^2}{2M_YM_N}\phi_C^1\right]\right.\right. \\ &\left.\left. + \left[g_{13}^Vf_{24}^V\frac{m^2}{4\mathcal{M}M_N} + f_{13}^Vg_{24}^V\frac{m^2}{4\mathcal{M}M_Y}\right]\phi_C^1 + f_{13}^Vf_{24}^V\frac{m^4}{16\mathcal{M}^2M_YM_N}\phi_C^2\right\}\right. \\ &+ \frac{m^2}{6M_YM_N}\left\{\left[\left(g_{13}^V + f_{13}^V\frac{M_Y}{\mathcal{M}}\right)\cdot\left(g_{24}^V + f_{24}^V\frac{M_N}{\mathcal{M}}\right)\right]\phi_C^1 + f_{13}^Vf_{24}^V\frac{m^2}{8\mathcal{M}^2}\phi_C^2\right\}(\boldsymbol{\sigma}_1\cdot\boldsymbol{\sigma}_2) \\ &- \frac{m^2}{4M_YM_N}\left\{\left[\left(g_{13}^V + f_{13}^V\frac{M_Y}{\mathcal{M}}\right)\cdot\left(g_{24}^V + f_{24}^V\frac{M_N}{\mathcal{M}}\right)\right]\phi_T^0 + f_{13}^Vf_{24}^V\frac{m^2}{8\mathcal{M}^2}\phi_T^1\right\}S_{12} \\ &- \frac{m^2}{M_YM_N}\left\{\left[\frac{3}{2}g_{13}^Vg_{24}^V + \left(g_{13}^Vf_{24}^V + f_{13}^Vg_{24}^V\right)\frac{\sqrt{M_YM_N}}{\mathcal{M}}\right]\phi_{SO}^0 + \frac{3}{8}f_{13}^Vf_{24}^V\frac{m^2}{\mathcal{M}^2}\phi_{SO}^1\right\}\mathbf{L}\cdot\mathbf{S} \\ &+ \frac{m^4}{16M_Y^2M_N^2}\left\{\left[g_{13}^Vg_{24}^V + 4\left(g_{13}^Vf_{24}^V + f_{13}^Vg_{24}^V\right)\frac{\sqrt{M_YM_N}}{\mathcal{M}} + 8f_{13}^Vf_{24}^V\frac{M_YM_N}{\mathcal{M}^2}\right]\right\}\cdot \\ &\times\frac{3}{(mr)^2}\phi_T^0Q_{12} - \frac{m^2}{M_YM_N}\left\{\left[\left(g_{13}^Vg_{24}^V - f_{13}^Vf_{24}^V\frac{m^2}{\mathcal{M}^2}\right)\frac{(M_N^2-M_Y^2)}{4M_YM_N}\right.\right. \\ &\left.\left. - \left(g_{13}^Vf_{24}^V - f_{13}^Vg_{24}^V\right)\frac{\sqrt{M_YM_N}}{\mathcal{M}}\right]\phi_{SO}^0\right\}\cdot\frac{1}{2}(\boldsymbol{\sigma}_1-\boldsymbol{\sigma}_2)\cdot\mathbf{L}\Bigg], \qquad (4.22a) \\ V_V^{n.l.}(r) &= \frac{m}{4\pi}\left[\frac{3}{2}g_{13}^Vg_{24}^V\ \phi_C^0\right. \\ &+ \frac{m^2}{6M_YM_N}\left\{\left[\left(g_{13}^V + f_{13}^V\frac{M_Y}{\mathcal{M}}\right)\cdot\left(g_{24}^V + f_{24}^V\frac{M_N}{\mathcal{M}}\right)\right]\phi_C^1\right\}(\boldsymbol{\sigma}_1\cdot\boldsymbol{\sigma}_2) \\ &\left. - \frac{m^2}{4M_YM_N}\left\{\left[\left(g_{13}^V + f_{13}^V\frac{M_Y}{\mathcal{M}}\right)\cdot\left(g_{24}^V + f_{24}^V\frac{M_N}{\mathcal{M}}\right)\right]\phi_T^0\right\}S_{12}\right]. \qquad (4.22b) \end{aligned}$$

Note: the spin-spin and tensor non-local terms are not included in ESC08c.

(c) Scalar-meson-exchange:

$$V_S(r) = -\frac{m}{4\pi}\left[g_{13}^S g_{24}^S \left\{\left[\phi_C^0 - \frac{m^2}{4M_Y M_N}\phi_C^1\right] + \frac{m^2}{2M_Y M_N}\phi_{SO}^0\ \mathbf{L}\cdot\mathbf{S} + \frac{m^4}{16M_Y^2 M_N^2}\cdot \right.\right.$$
$$\left.\left. \times\frac{3}{(mr)^2}\phi_T^0 Q_{12} + \frac{m^2}{M_Y M_N}\left[\frac{(M_N^2 - M_Y^2)}{4M_Y M_N}\right]\phi_{SO}^0 \cdot \frac{1}{2}(\boldsymbol{\sigma}_1 - \boldsymbol{\sigma}_2)\cdot\mathbf{L}\right\}\right], \tag{4.23a}$$

$$V_S^{n.l.}(r) = \frac{m}{4\pi}\left[\frac{1}{2}g_{13}^S g_{24}^S\ \phi_C^0\right]. \tag{4.23b}$$

(d) Axial-vector-meson exchange $J^{PC} = 1^{++}$:

$$V_A(r) = -\frac{m}{4\pi}\left[\left\{g_{13}^A g_{24}^A\left(\phi_C^0 + \frac{2m^2}{3M_Y M_N}\phi_C^1\right) + \frac{m^2}{6M_Y M_N}\left(g_{13}^A f_{24}^A\frac{M_N}{\mathcal{M}} + f_{13}^A g_{24}^A\frac{M_Y}{\mathcal{M}}\right)\phi_C^1\right.\right.$$
$$\left. + f_{13}^A f_{24}^A\frac{m^4}{12M_Y M_N\mathcal{M}^2}\phi_C^2\right\}(\boldsymbol{\sigma}_1\cdot\boldsymbol{\sigma}_2) - \frac{m^2}{4M_Y M_N}\left\{\left[g_{13}^A g_{24}^A\right.\right.$$
$$\left.\left. -2\left(g_{13}^A f_{24}^A\frac{M_N}{\mathcal{M}} + f_{13}^A g_{24}^A\frac{M_Y}{\mathcal{M}}\right)\right]\phi_T^0 - f_{13}^A f_{24}^A\frac{m^2}{\mathcal{M}^2}\phi_T^1\right\}S_{12}$$
$$\left. + \frac{m^2}{2M_Y M_N}g_{13}^A g_{24}^A\left\{\phi_{SO}^0\ \mathbf{L}\cdot\mathbf{S} + \frac{m^2}{M_Y M_N}\left[\frac{(M_N^2 - M_Y^2)}{4M_Y M_N}\right]\phi_{SO}^0\cdot\frac{1}{2}(\boldsymbol{\sigma}_1 - \boldsymbol{\sigma}_2)\cdot\mathbf{L}\right\}\right], \tag{4.24a}$$

$$V_A^{n.l.}(r) = -\frac{m}{4\pi}\left[\frac{3}{2}g_{13}^A g_{24}^A\ \phi_C^0(\boldsymbol{\sigma}_1\cdot\boldsymbol{\sigma}_2)\right]. \tag{4.24b}$$

(e) Axial-vector-meson exchange $J^{PC} = 1^{+-}$:

$$V_B(r) = -\frac{m}{4\pi}\frac{(M_N + M_Y)^2}{m^2}\left[f_{13}^B f_{24}^B\left\{\frac{m^2}{12M_Y M_N}\left(\phi_C^1 + \frac{m^2}{4M_Y M_N}\phi_C^2\right)(\boldsymbol{\sigma}_1\cdot\boldsymbol{\sigma}_2)\right.\right.$$
$$\left.\left. + \frac{m^2}{4M_Y M_N}\left(\phi_T^0 + \frac{m^2}{4M_Y M_N}\phi_T^1\right)S_{12}\right\}\right], \tag{4.25a}$$

$$V_B^{n.l.}(r) = -\frac{m}{4\pi}\frac{3(M_N + M_Y)^2}{8m^2}\left[f_{13}^B f_{24}^B\left\{\left(\frac{1}{3}\boldsymbol{\sigma}_1\cdot\boldsymbol{\sigma}_2\ \phi_C^1 + S_{12}\ \phi_T^0\right)\right\}\right]. \tag{4.25b}$$

(f) Pomeron exchange:

$$V_P(r) = \frac{m_P}{4\pi}\left[g_{13}^P g_{24}^P\frac{4}{\sqrt{\pi}}\frac{m_P^2}{\mathcal{M}^2}\cdot\left[\left\{1 + \frac{m_P^2}{2M_Y M_N}(3 - 2m_P^2 r^2) + \frac{m_P^2}{M_Y M_N}\mathbf{L}\cdot\mathbf{S}\right.\right.\right.$$
$$\left.\left.\left. + \left(\frac{m_P^2}{2M_Y M_N}\right)^2 Q_{12} + \frac{m_P^2}{M_Y M_N}\left[\frac{(M_N^2 - M_Y^2)}{4M_Y M_N}\right]\cdot\frac{1}{2}(\boldsymbol{\sigma}_1 - \boldsymbol{\sigma}_2)\cdot\mathbf{L}\right\}\ e^{-m_P^2 r^2}\right]\right], \tag{4.26a}$$

$$V_D^{n.l.}(r) = -\frac{m}{4\pi}\left[\frac{1}{2}e^{-m_P^2 r^2}\right]. \tag{4.26b}$$

(g) Odderon-exchange:

$$
\begin{aligned}
V_{O,C}(r) &= +\frac{g^O_{13}g^O_{24}}{4\pi}\frac{8}{\sqrt{\pi}}\frac{m_O^5}{\mathcal{M}^4}\left[(3-2m_O^2r^2)\right. \\
&\quad \left.-\frac{m_O^2}{M_YM_N}\left(15-20m_O^2r^2+4m_O^4r^4\right)\right]\exp(-m_O^2r^2)\ , \qquad (4.27a)\\
V_O^{n.l.}(r) &= -\frac{g^O_{13}g^O_{24}}{4\pi}\frac{8}{\sqrt{\pi}}\frac{m_O^5}{\mathcal{M}^4}\frac{3}{4M_YM_N}\left\{\boldsymbol{\nabla}^2\left[(3-2m_O^2r^2)\exp(-m_O^2r^2)\right]+\right. \\
&\quad \left.+\left[(3-2m_O^2r^2)\exp(-m_O^2r^2)\right]\boldsymbol{\nabla}^2\right\}\ , \qquad (4.27b)\\
V_{O,\sigma}(r) &= -\frac{g^O_{13}g^O_{24}}{4\pi}\frac{8}{3\sqrt{\pi}}\frac{m_O^5}{\mathcal{M}^4}\frac{m_O^2}{M_YM_N}\left[15-20m_O^2r^2+4m_O^4r^4\right]\exp(-m_O^2r^2)\cdot \\
&\quad \times\left(1+\kappa^O_{13}\frac{M_Y}{\mathcal{M}}\right)\left(1+\kappa^O_{24}\frac{M_N}{\mathcal{M}}\right), \qquad (4.27c)\\
V_{O,T}(r) &= -\frac{g^O_{13}g^O_{24}}{4\pi}\frac{8}{3\sqrt{\pi}}\frac{m_O^5}{\mathcal{M}^4}\frac{m_O^2}{M_YM_N}\cdot m_O^2r^2\left[7-2m_O^2r^2\right]\exp(-m_O^2r^2)\cdot \\
&\quad \times\left(1+\kappa^O_{13}\frac{M_Y}{\mathcal{M}}\right)\left(1+\kappa^O_{24}\frac{M_N}{\mathcal{M}}\right), \qquad (4.27d)\\
V_{O,SO}(r) &= -\frac{g^O_{13}g^O_{24}}{4\pi}\frac{8}{\sqrt{\pi}}\frac{m_O^5}{\mathcal{M}^4}\frac{m_O^2}{M_YM_N}\left[5-2m_O^2r^2\right]\exp(-m_O^2r^2)\cdot \\
&\quad \times\left\{3+\left(\kappa^O_{13}+\kappa^O_{24}\right)\frac{\sqrt{M_YM_N}}{\mathcal{M}}\right\}, \qquad (4.27e)\\
V_{O,Q}(r) &= +\frac{g^O_{13}g^O_{24}}{4\pi}\frac{2}{\sqrt{\pi}}\frac{m_O^5}{\mathcal{M}^4}\frac{m_O^4}{M_Y^2M_N^2}\left[7-2m_O^2r^2\right]\exp(-m_O^2r^2)\cdot \\
&\quad \times\left\{1+4\left(\kappa^O_{13}+\kappa^O_{24}\right)\frac{\sqrt{M_YM_N}}{\mathcal{M}}+8\kappa_{13}\kappa_{24}\frac{M_YM_N}{\mathcal{M}^2}\right\}, \qquad (4.27f)\\
V_{O,ASO}(r) &= -\frac{g^O_{13}g^O_{24}}{4\pi}\frac{4}{\sqrt{\pi}}\frac{m_O^5}{\mathcal{M}^4}\frac{m_O^2}{M_YM_N}\left[5-2m_O^2r^2\right]\exp(-m_O^2r^2)\cdot \\
&\quad \times\left\{\frac{M_N^2-M_Y^2}{M_YM_N}-4\left(\kappa^O_{24}-\kappa^O_{13}\right)\frac{\sqrt{M_YM_N}}{\mathcal{M}}\right\}\ . \qquad (4.27g)
\end{aligned}
$$

Here, $\kappa^O_{13}=g^O_{13}/f^O_{13}$ and $\kappa^O_{24}=g^O_{24}/f^O_{24}$.

D. One-Boson-Exchange Interactions in Configuration Space II

Here we give the extra potentials due to the zero's in the scalar and axial-A vector form factors:

a) Scalar-mesons:

$$
\begin{aligned}
\Delta V_S(r) = -\frac{m}{4\pi}\,\frac{m^2}{U^2}\ &\left[g^S_{13}g^S_{24}\left\{\left[\phi^1_C-\frac{m^2}{4M_YM_N}\phi^2_C\right]+\frac{m^2}{2M_YM_N}\phi^1_{SO}\ \mathbf{L}\cdot\mathbf{S}\right.\right. \\
&\left.\left.+\frac{m^4}{16M_Y^2M_N^2}\phi^1_T\ Q_{12}+\frac{m^2}{4M_YM_N}\frac{M_N^2-M_Y^2}{M_YM_N}\ \phi^{(1)}_{SO}\cdot\frac{1}{2}(\boldsymbol{\sigma}_1-\boldsymbol{\sigma}_2)\cdot\mathbf{L}\right\}\right]\ . \qquad (4.28)
\end{aligned}
$$

b) Axial-mesons: The extra contribution to the potentials coming from the zero in the axial-vector meson form factor are obtained from the expression (4.17) by making substitutions as follows

$$
\Delta V_A^{(1)}(r) \ = \ V_A^{(1)}\left(\phi^0_C\to\phi^1_C,\phi^0_T\to\phi^1_T,\phi^0_{SO}\to\phi^1_{SO}\right)\cdot\frac{m^2}{U^2}\ . \qquad (4.29)
$$

Note that we do not include the similar $\Delta V_A^{(2)}(r)$ since they involve $\mathbf{k}^4$-terms in momentum-space. Then,

$$V_A^{(1)}(r) = -\frac{g_{13}^A g_{24}^A}{4\pi}\; m\left[\phi_C^0\;(\boldsymbol{\sigma}_1\cdot\boldsymbol{\sigma}_2) - \frac{1}{12M_YM_N}\left(\nabla^2\phi_C^0 + \phi_C^0\nabla^2\right)(\boldsymbol{\sigma}_1\cdot\boldsymbol{\sigma}_2)\right.$$
$$+\frac{3m^2}{4M_YM_N}\;\phi_T^0\;S_{12} + \frac{m^2}{2M_YM_N}\;\phi_{SO}^0\;\mathbf{L}\cdot\mathbf{S}$$
$$\left.+\frac{m^2}{4M_YM_N}\frac{M_N^2-M_Y^2}{M_YM_N}\;\phi_{SO}^{(0)}\cdot\frac{1}{2}(\boldsymbol{\sigma}_1-\boldsymbol{\sigma}_2)\cdot\mathbf{L}\right]\;. \tag{4.30}$$

E. PS-PS-exchange Interactions in Configuration Space

In Fig. 2 and Fig. 3 the included two-meson exchange graphs are shown schematically. Explicit expressions for $K^{irr}(BW)$ and $K^{irr}(TMO)$ were derived [36], where also the terminology BW and TMO is explained. The TPS-potentials for nucleon-nucleon have been given in detail in [37, 38] The generalization to baryon-baryon is similar to that for the OBE-potentials. So, we substitute $M \to \sqrt{M_YM_N}$, and include all PS-PS possibilities with coupling constants as in the OBE-potentials. As compared to nucleon-nucleon in [37, 38] here we have in addition the potentials with double K-exchange. The masses are the physical pseudo-scalar meson masses. For the intermediate two-baryon states we take into account of the different thresholds. We have not included uncorrelated PS-vector, PS-scalar, or PS-diffractive exchange. This because the range of these potentials is similar to that of the vector-,scalar-,and axial-vector-potentials. Moreover, for potentially large potentials, in particular those with scalar mesons involved, there will be very strong cancellations between the planar- and crossed-box contributions.

F. MPE-exchange Interactions

In Fig. 4 both the one-pair graphs and the two-pair graphs are shown. In this work we include only the one-pair graphs. The argument for neglecting the two-pair graph is to avoid some 'double-counting'. Viewing the pair-vertex as containing heavy-meson exchange means that the contributions from $\rho(750)$ and $\epsilon = f_0(760)$ to the two-pair graphs is already accounted for by our treatment of the broad ρ and ϵ OBE-potential. For a more complete discussion of the physics behind MPE we refer to our previous papers [1, 37, 38]. The MPE-potentials for nucleon-nucleon have been given in Ref. [37, 38]. The generalization to baryon-baryon is similar to that for the TPS-potentials. For the intermediate two-baryon states we neglect the different two-baryon thresholds. This because, although in principle possible, it complicates the computation of the potentials considerably. For a proper appreciation of the physics it is useful to scale the phenomenological meson-pair baryon-baryon interaction Hamiltonians different from the originally used scalings [37, 38]. Below we give these Hamiltonians:

$$\mathcal{H}_S = \bar\psi\psi\left[g_{(\pi\pi)_0}\boldsymbol{\pi}\cdot\boldsymbol{\pi} + g_{(\sigma\sigma)}\sigma^2\right]/\mathcal{M}, \tag{4.31a}$$
$$\mathcal{H}_V = g_{(\pi\pi)_1}\left[\bar\psi\gamma_\mu\boldsymbol{\tau}\psi\right]\cdot(\boldsymbol{\pi}\times\partial^\mu\boldsymbol{\pi}/m_\pi)/\mathcal{M}$$
$$-\frac{f_{(\pi\pi)_1}}{2M}\left[\bar\psi\sigma_{\mu\nu}\boldsymbol{\tau}\psi\right]\partial^\nu\cdot(\boldsymbol{\pi}\times\partial^\mu\boldsymbol{\pi}/m_\pi)/\mathcal{M}, \tag{4.31b}$$
$$\mathcal{H}_A = g_{(\pi\rho)_1}\left[\bar\psi\gamma_5\gamma_\mu\boldsymbol{\tau}\psi\right]\cdot\boldsymbol{\pi}\times\boldsymbol{\rho}/\mathcal{M}, \tag{4.31c}$$
$$\mathcal{H}_B = ig_{(\pi\omega)}\left[\bar\psi\gamma_5\sigma_{\mu\nu}\boldsymbol{\tau}\psi\right]\cdot\partial^\nu\left(\boldsymbol{\pi}\phi_\omega^\mu\right)/(m_\pi\mathcal{M}), \tag{4.31d}$$
$$\mathcal{H}_P = g_{(\pi\sigma)}\left[\bar\psi\gamma_5\gamma_\mu\boldsymbol{\tau}\psi\right]\cdot(\boldsymbol{\pi}\partial^\mu\sigma - \sigma\partial^\mu\boldsymbol{\pi})/(m_\pi\mathcal{M}). \tag{4.31e}$$

Here, we systematically scaled the partial derivatives with m_π.
The generalization of the pair-couplings to baryon-baryon is described in Ref. [5], section III. Also here in NN, we have in addition to [37, 38] included the pair-potentials with KK-, KK*-, and Kκ-exchange. The convention for the MPE coupling constants is the same as in Ref. [37, 38].

G. The Schrödinger equation with Non-local potential

The non-local potentials are of the central-, spin-spin, and tensor type. The method of solution of the Schrödinger equation for nucleon-nucleon central (and spin-spin) potentials has been described in Ref. [35]. In [45] the extension

of the method to non-local tensor potentials has been presented. The method is reviewed briefly in Appendix D. Here, the non-local tensor is in momentum space of the form $(\mathbf{q}^2 + \mathbf{k}^2/4)\ \tilde{v}_T(\mathbf{k})$.

V. ESC-COUPLINGS AND THE QPC-MODEL

In the ESC-model for baryon-baryon the meson-baryon couplings are in principle only restricted by the requirements of relativistic covariance, time-reversal and parity. However, dynamical input based on e.g. QCD, the QM, chiral-symmetry, and flavor SU(3), is essential in order to be able to link the NN-, YN-, and YY-systems. It appeared that in the ESC-model the $^3P_0$ quark-antiquark pair-creation model [26, 27] leads to a scheme for the meson-baryon-baryon couplings which is very similar to that found in the fits of the ESC-model [4, 5]. The couplings found in the ESC08-model fit very well in the $(^3P_0 +^3 S_1)$-scheme with a ratio $^3P_0/^3S_1 = 2 : 1$.

A. QPC-model Coupling Non-strange Mesons

According to the Quark-Pair-Creation (QPC) model, in the $^3P_0$-version [26, 27], the baryon-baryon-meson couplings are given in terms of the quark-pair creation constant γ_M, and the radii of the (constituent) gaussian quark wave functions, by [27, 62]

$$g_{BBM}(\pm) = \gamma_{q\bar{q}}\ \frac{3}{\sqrt{2}}\ \pi^{-3/4}\ X_M\left(I_M, L_M, S_M, J_M\right)\ F_M^{(\pm)}\ , \tag{5.1}$$

where $\pm = -(-)^{L_f}$ with L_f is the orbital angular momentum of the final BM-state, $X_M(\ldots)$ is a isospin, spin etc. recoupling coefficient, and

$$\begin{aligned} F^{(+)} &= \frac{3}{2}\ (m_M R_M)^{+1/2}\ (\Lambda_{QPC} R_M)^{-2}, \\ F^{(-)} &= \frac{3}{2}\ (m_M R_M)^{-1/2}\ (\Lambda_{QPC} R_M)^{-2} \cdot 3\sqrt{2}(M_M/M_B). \end{aligned} \tag{5.2}$$

are coming from the overlap integrals, see Appendix F. Here, the superscripts $\mp$ refer to the parity of the mesons M: $(-)$ for $J^{PC} = 0^{+-}, 1^{--}$, and $(+)$ for $J^{PC} = 0^{++}, 1^{++}$. The radii of the baryons, in this case nucleons, and the mesons are respectively denoted by R_B and R_M.

The QPC($^3P_0$)-model gives several interesting relations, such as $g_\omega = 3g_\rho, g_\epsilon = 3g_{a_0}$, and $g_{a_0} \approx g_\rho, g_\epsilon \approx g_\omega$. These relations can be seen most easily by applying the Fierz-transformation to the $^3P_0$-pair-creation Hamiltonian, see Appendix F.

From $\rho \to e^+e^-$, employing the current-field-identities (C.F.I's) one can derive, see for example [63], the following relation with the QPC-model

$$f_\rho = \frac{m_\rho^{3/2}}{\sqrt{2}|\psi_\rho(0)|} \Leftrightarrow \gamma \left(\frac{2}{3\pi}\right)^{1/2} \frac{m_\rho^{3/2}}{|'\psi_\rho(0)'|}\ , \tag{5.3}$$

which, neglecting the difference between the wave functions on the left and right hand side, gives for the pair creation constant $\gamma \to \gamma_0 = \frac{1}{2}\sqrt{3\pi} = 1.535$. However, since in the QPC-model gaussian wave functions are used, the $q\bar{q}$-potential is a harmonic-oscillator one. This does not account for the $1/r$-behavior, due to one-gluon-exchange (OGE), at short distance. This implies a OG-correction [64] to the wave function, which gives for γ [65]

$$\gamma = \gamma_0 \left(1 - \frac{16}{3}\frac{\alpha(m_M)}{\pi}\right)^{-1/2}\ . \tag{5.4}$$

In Table I $\gamma(\mu)$ is shown, Using from [66] the parameterization

$$\alpha_s(\mu) = 4\pi/\left(\beta_0 \ln(\mu^2/\Lambda_{QCD}^2)\right)\ , \tag{5.5}$$

with $\Lambda_{QCD} = 100$ MeV and $\beta_0 = 11 - \frac{2}{3}n_f$ for $n_f = 3$, and taking the typical scale $m_M \approx 1$ GeV, the above formula gives $\gamma = 2.19$. This value we will use later when comparing the QPC-model predictions and the ESC08c-model coupling constants.

The formulas (5.2) are valid for the most simple QPC-model. For a realistic description of the coupling constants of

TABLE I: Pair-creation constant γ as a function of μ.

μ [GeV]	$\alpha_s(\mu)$	$\gamma(\mu)$
∞	0.00	1.535
80.0	0.10	1.685
35.0	0.20	1.889
1.05	0.30	2.191
0.55	0.40	2.710
0.40	0.50	3.94
0.35	0.55	5.96

the ESC08-model we include two sophistocations: (i) inclusion of both the $^3P_0$- and the $^3S_1$-mechanism, (ii) inclusion of SU(6)-breaking. For details, see [67]. For the latter we use the ($\underline{56}$) and ($\underline{70}$) SU(6)-irrep mixing [62], and a short-distance quark-gluon form factor. In Table II we show the $^3P_0$ $-^3S_1$-model results and the values obtained in the ESC08c-fit. In this table we fixed $\gamma_M = 2.19$ for the vector-, scalar-, and axial-vector-mesons. From Table I one sees that at the scale of $m_M \approx 1$ GeV such a value is reasonable. Here, one has to realize that the QPC-predictions are kind of "bare" couplings, which allows vertex corrections from meson-exchange. For the pseudo-scalar, a different value has to be used, showing indeed some 'running'-behavior as expected from QCD. In [65], for the decays $\rho, \epsilon \to 2\pi$ etc. it was found $\gamma = 3.33$, which is close to our $\gamma_\pi = 4.19$. For the mesonic decays of the charmonium states $\gamma = 1.12$. One notices the similarity between the QPC($^3P_0$)-model predictions and the fitted couplings. Here, for $f_1(1420)$ we have to take a larger radius $r_M = 1.10$ fm in order to reduce the couplings in the QPC-model. Of course, these results are sensitive to the r_M values. We found that for all solutions with a very good χ^2_{NN} the r_M values varied by ± 0.2 fm.
The ESC08c-couplings and the QPC-couplings agree very well. In particular, the SU(6)-breaking is improving the agreement significantly. All this strengthens the claim that the ESC08c-couplings are realistic ones.

B. ESC-potentials and the Constituent Quark-model

The calculation of Table II uses the constituent quark model (CQM) in the SU(6)-version of [27]. Since this calculation implicity uses the direct coupling of the mesons to the quarks, it defines the QQM-vertex. Then, OBE-potentials can be derived by folding meson-exchange with the quark wave functions of the baryons. prescribed by the Dirac-structure, at the baryon level the vertices have in Pauli-spinor space the $1/\mathrm{M}_B$-expansion

$$\begin{aligned} \bar{u}(p',s')\Gamma u(p,s) &= \chi'^{\dagger}_{s'} \left\{ \Gamma_{bb} + \Gamma_{bs} \frac{\boldsymbol{\sigma}\cdot\mathbf{p}}{E+M} - \frac{\boldsymbol{\sigma}\cdot\mathbf{p}'}{E'+M'}\Gamma_{sb} - \frac{\boldsymbol{\sigma}\cdot\mathbf{p}}{E+M}\Gamma_{ss}\frac{\boldsymbol{\sigma}\cdot\mathbf{p}'}{E'+M'}\Gamma_{sb} \right\} \chi_s \\ &\equiv \sum_l c^{(l)}_{BB} \left[\chi'^{\dagger}_{s'} O_l(\mathbf{p}',\mathbf{p})\, \chi_s \right] (\sqrt{M'M})^{\alpha_l} \quad (l = bb, bs, sb, ss). \end{aligned} \tag{5.6}$$

This expansion is general and does not depend on the internal structure of the baryon. A similar expansion can be made on the quark-level, but now with quark masses m_Q and coefficients $c^{(l)}_{QQ}$. It appears that in the CQM, i.e. $m_Q = M_B/3$, the QQM-vertices can be chosen such that the ratio's $c^{(l)}_{QQ}/c^{(l)}_{BB}$ are constant for each type of meson [68]. Then, by scaling the couplings these coefficients can be made equal. (Ipso facto this defines a meson-exchange quark-quark interaction.) This shows that the use of the QPC-model is consistent with the 1/M-expansion.

TABLE II: SU(6)-breaking in coupling constants, using (56) and (70)-irrep mixing with angle $\varphi = -22^o$ for the $^3P_0$- and $^3S_1$-model. Gaussian Quark-gluon cut-off $\Lambda_{QQG} = 986.6$ MeV. Ideal mixing for vector and scalar meson nonets. For pseudoscalar- and axial-nonets the mixing angles are -13^0 and $+50.0^o$ respectively, imposing the OZI-rule. Here, $\Lambda_{QPC} = 259.6$ MeV, $\gamma(\alpha_s = 0.30) = 2.19$ etc. The weights are A=0.702 and B=0.298 for the $^3P_0$ and $^3S_1$ respectively. The values in parentheses in the column QPC denote the results for $\varphi = 0^o$.

Meson	$r_M[fm]$	γ_M	$^3S_1$	$^3P_0$	QPC	ESC08c
$\pi(140)$	0.30	5.51	$g = -2.60$	$g = +6.14$	3.54 (3.74)	3.65
$\eta'(957)$	0.70	2.22	$g = -2.36$	$g = +5.56$	3.21 (3.90)	3.42
$\rho(770)$	0.80	2.37	$g = -0.17$	$g = +0.78$	0.62 (0.76)	0.63
$\omega(783)$	0.70	2.35	$g = -0.91$	$g = +4.31$	3.40 (3.36)	3.37
$a_0(962)$	0.90	2.22	$g = +0.18$	$g = +0.42$	0.59 (0.61)	0.64
$\epsilon(760)$	0.70	2.37	$g = +1.19$	$g = +2.82$	4.01 (4.01)	4.04
$a_1(1270)$	0.70	2.09	$g = -0.12$	$g = -0.56$	-0.68 (-0.68)	-0.82
$f_1(1420)$	1.10	2.09	$g = -0.14$	$g = -0.64$	-0.78 (-0.79)	-0.77

VI. ESC08-MODEL: FITTING $NN \oplus YN \oplus YY$-DATA

In the simultaneous χ^2-fit of the NN-, YN-, and YY-data a *single set of parameters* was used, which means the same parameters for all BB-channels. The input NN-data are the same as in Ref. [4], and we refer the reader to this paper for a description of the employed phase shift analysis [10, 11]. Note that in addition to the NN-phases, including their correlations, in the ESC08-models also the NN-low energy parameters and the deuteron binding energy are fitted. The YN-data are those used in Ref. [5] with the addition of higher energy data, see paper II. Of course, it is to be expected that the accurate and very numerous NN-data essentially fix most of the parameters. Only some of the parameters, for example certain $F/(F+D)$-ratios, are quite influenced by the YN-data. In the fitting procedure the following constraints are applied: (i) A strong restriction imposed on YN-models is the absence of S=-1 bound states. (ii) During the fitting process sometimes constraints are imposed in the form of 'pseudo-data' for some YN scattering lengths. These constraints are based on experiences with Nijmegen YN-models in the past or to impose constraints from the G-matrix results. In some cases it is necessary to add some extra weight of the YN-scattering data w.r.t. the NN-data in the fitting process. (iii) After obtaining a solution for the scattering data the corresponding model is tested by checking the corresponding G-matrix results for the well-depths for $U_\Sigma > 0$ and $U_\Xi < 0$, and sufficient s-wave spin splitting in the U_Λ. If not satisfactory we refit the scattering data etc. This iterative process implements the constraints from the G-matrix well-depth's results, and plays a vital role in obtaining the final results of the combined fit. (For the G-matrix approach to hyperon-nucleus systems, see e.g. Ref. [69].) The fitting process is discussed more elaborately in paper II.

The χ^2 is a very shallow function of the quark-core parameter, which influences only the YN- and YY-channels. Accordingly solutions have been obtained using different assumptions about the quark-core-effects, all with a strength of about 25% of the total diffractive contribution. In previous work [8], models ESC08a and ESC08a", the solutions were obtained by assuming quark-core effects only for the channels where the [51]-component is dominant: $\Sigma^+p(^3S_1, I = 3/2), \Sigma N(^1S_0, I = 1/2)$, and $\Xi N(^1S_0, I = 1)$. The solution ESC08c is obtained by application of the quark-core effects according to equation (8.4) in [8], see paper II for a full description of the Pauli-blocking scheme.

Like in the NN-fit, described in Ref. [4], also in the simultaneous χ^2-fit of the NN- and YN-data, it appeared

again that the OBE-couplings could be constrained successfully by the 'naive' predictions of the QPC-model [26, 27]. Although these predictions, see section V, are 'bare' ones, we tried to keep during the searches many OBE-couplings in the neighborhood of the QPC-values. Also, it appeared that we could either fix the $F/(F+D)$-ratios to those as suggested by the QPC-model, or apply the same restraining strategy as for the OBE-couplings.

A. Fitted BB-parameters

The treatment of the broad mesons ρ and ϵ is similar to that in the OBE-models [3, 35]. For the ρ-meson the same parameters are used as in these references. However, for the $\epsilon = f_0(760)$ assuming $m_\epsilon = 760$ MeV and $\Gamma_\epsilon = 640$ MeV the Bryan-Gersten parameters [70] are used. For the chosen mass and width they are: $m_1 = 496.39796$ MeV, $m_2 = 1365.59411$ MeV, and $\beta_1 = 0.21781, \beta_2 = 0.78219$. Other meson masses are given in Table III. The sensitivity for the values of the cut-off masses of the η and η' is very weak. Therefore we have set the $\{1\}$-cut-off imass for the pseudoscalar nonet equal to that for the $\{8\}$. Likewise, for the two nonets of the axial-vector mesons, see table III. Furthermore we experience a rather shallow dependence on the value of α_P in the range 0.33-0.40. Therefore, we put it at the Cabbibbo-theory value 0.365.

Summarizing the parameters we have for baryon-baryon (BB): (i) NN Meson-couplings: $f_{NN\pi}, f_{NN\eta'}, g_{NN\rho}, g_{NN\omega}$, $f_{NN\rho}, f_{NN\omega}, g_{NNa_0}, g_{NN\epsilon}, g_{NNa_1}, f_{NNa_1}, g_{NNf_1'}, f_{NNf_1'}, f_{NNb_1}, f_{NNh_1'}$, (ii) $F/(F+D)$-ratios: α_V^m, α_A, (iii) NN Pair couplings: $g_{NN(\pi\pi)_1}, f_{NN(\pi\pi)_1}, g_{NN(\pi\rho)_1}, g_{NN\pi\omega}, g_{NN\pi\eta}, g_{NN\pi\epsilon}$, (iv) Diffractive couplings and masslike parameters g_{NNP}, g_{NNO}, f_{NNO}, m_P, m_O, (v) Cut-off masses: $\Lambda_8^P = \Lambda_1^P$, Λ_8^V, Λ_1^V, Λ_8^S, Λ_1^S, and $\Lambda_8^A = \Lambda_1^A$.

The pair coupling $g_{NN(\pi\pi)_0}$ was kept fixed at zero. Note that in the interaction Hamiltonians of the pair-couplings (4.31b)-(4.31e) the partial derivatives are scaled by m_π, and there is a scaling mass M_N.

The ESC-model described here, is fully consistent with $SU(3)$-symmetry using a straightforward extension of the NN-model to YN and YY. This the case for the OBE- and TPS-potentials, as well as for the Pair-potentials. For example $g_{(\pi\rho)_1} = g_{A_8VP}$, and besides $(\pi\rho)$-pairs one sees also that $KK^*(I=1)$- and $KK^*(I=0)$-pairs contribute to the NN potentials. All $F/(F+D)$-ratio's are taken as fixed with heavy-meson saturation in mind. The approximation we have made in this paper is to neglect the baryon mass differencesi in the TPS-potentials, i.e. we put $m_\Lambda = m_\Sigma = m_N$. This because we have not yet worked out the formulas for the inclusion of these mass differences, which is straightforward in principle.

B. Coupling Constants, $F/(F+D)$ Ratios, and Mixing Angles

In Table III we give the ESC08c meson masses, and the fitted couplings and cut-off parameters. Note that the axial-vector couplings for the B-mesons are scaled with m_{B_1}. The mixing for the pseudo-scalar, vector, and scalar mesons, as well as the handling of the diffractive potentials, has been described elsewhere, see e.g. Refs. [3, 9]. The mixing scheme of the axial-vector mesons is completely similar as for the vector etc. mesons, except for the mixing angle. In the paper II [15] the $SU(3)$ singlet and octet couplings are listed, and also the $F/(F+D)$-ratios and mixing angles. Also the Pauli-blocking effect parameter a_{PB}, described in [8], section 8, for ESC08c is given. As mentioned above, we searched for solutions where all OBE-couplings are compatible with the QPC-predictions. This time the QPC-model contains a mixture of the $^3P_0$ and $^3S_1$ mechanism, whereas in Ref. [4] only the $^3P_0$-mechanism was considered. For the pair-couplings all $F/(F+D)$-ratios were fixed to the predictions of the QPC-model.

One notices that all the BBM α's have values rather close to that which are expected from the QPC-model. In the ESC08c solution $\alpha_A \approx 0.33$, which is not too far from $\alpha_A \sim 0.4$. As in previous works, e.g. Ref. [35], $\alpha_V^e = 1$ is kept fixed. Above, we remarked that the axial-nonet parameters may be sensitive to whether or not the heavy pseudoscalar nonet with the $\pi(1300)$ are included.

In Table IV we listed the fitted Pair-couplings for the MPE-potentials. We recall that only One-pair graphs are included, in order to avoid double counting, see Ref. [4]. The $F/(F+D)$-ratios are all fixed, assuming heavy-boson domination of the pair-vertices. The ratios are taken from the QPC-model for $Q\bar{Q}$-systems with the same quantum numbers as the dominating boson. For example, the α-parameter for the axial $(\pi\rho)_1$-pair could fixed at the quark-model prediction 0.40, see Table IV. The BB-Pair couplings are calculated, assuming unbroken $SU(3)$-symmetry, from the NN-Pair coupling and the $F/(F+D)$-ratio using $SU(3)$. Unlike in Ref. [37, 38], we did not fix pair couplings using a theoretical model, e.g. based on heavy-meson saturation and chiral-symmetry. So, in addition to the 14 parameters used in Ref. [37, 38] we now have 6 pair-coupling fit parameters. In Table IV the fitted pair-couplings are given. Note that the $(\pi\pi)_0$-coupling gets a non-zero contribution from the $\{8_s\}$-pairs, giving $g_{(\pi\pi)_0} - 1.1816/2 \approx -0.59$, which is opposite in sign compared to the result in [37, 38]. The $f_{(\pi\pi)_1}$-pair coupling has opposite sign as compared to Ref. [37, 38]. In a model with a more complex and realistic meson-dynamics [34] this coupling is predicted as found

TABLE III: Meson couplings and parameters employed in the ESC08c-potentials. Coupling constants are at $\mathbf{k}^2 = 0$. An asterisk denotes that the coupling constant is constrained via SU(3). The masses and Λ's are given in MeV.

meson	mass	$g/\sqrt{4\pi}$	$f/\sqrt{4\pi}$	Λ
π	138.04		0.2687	1029.42
η	547.45		0.1314^*	,,
η'	957.75		0.2519	,,
ρ	768.10	0.6343	3.8307	688.40
ϕ	1019.41	-1.2915^*	3.1377^*	,,
ω	781.95	3.3691	–0.7683	771.32
a_1	1270.00	–0.8168	2.5849	1076.56
f_1	1420.00	0.6826^*	1.3884^*	,,
f_1'	1285.00	–0.7687	–0.5448	,,
b_1	1235.00		–1.7670	1029.42
h_1	1380.00		-0.2684^*	,,
h_1'	1170.00		–0.6768	,,
a_0	962.00	0.6351		893.53
f_0	993.00	-1.5129^*		,,
ε	760.00	4.0454		1136.10
Pomeron	223.12	3.3267		
Odderon	270.48	4.3575	–4.1556	

TABLE IV: Pair-meson coupling constants employed in the ESC08c MPE-potentials. Coupling constants are at $\mathbf{k}^2 = 0$. The F/(F+D)-ratio are QPC-predictions, except that $\alpha_{(\pi\omega)} = \alpha_P$, which is very close to QPC.

J^{PC}	$SU(3)$-irrep	$(\alpha\beta)$	$g/4\pi$	$F/(F+D)$
0^{++}	$\{1\}$	$g(\pi\pi)_0$	—	—
0^{++}	,,	$g(\sigma\sigma)$	—	—
0^{++}	$\{8\}_s$	$g(\pi\eta)$	-1.1816	1.000
1^{--}	$\{8\}_a$	$g(\pi\pi)_1$	0.2324	1.000
		$f(\pi\pi)_1$	–1.6979	0.400
1^{++}	,,	$g(\pi\rho)_1$	5.0652	0.400
1^{++}	,,	$g(\pi\sigma)$	–0.2985	0.400
1^{++}	,,	$g(\pi P)$	—	—
1^{+-}	$\{8\}_s$	$g(\pi\omega)$	–0.0557	0.365

in the present ESC-fit. The $(\pi\rho)_1$-coupling is large as expected from A_1-saturation, see Ref. [37, 38]. We conclude that the pair-couplings are in general not well understood quantitatively, and deserve more study.

In Table III we show the OBE-coupling constants and the gaussian cut-off's Λ. The used $\alpha =: F/(F+D)$-ratio's for the OBE-couplings are: pseudo-scalar mesons $\alpha_P = 0.365$, vector mesons $\alpha_V^e = 1.0, \alpha_V^m = 0.472$, and scalar-mesons $\alpha_S = 1.00$, which is calculated using the physical $S^* =: f_0(993)$ coupling etc.. In Table IV we show the MPE-coupling constants. The used $\alpha =: F/(F+D)$-ratio's for the MPE-couplings are: $(\pi\eta)$ pairs $\alpha(\{8_s\}) = 1.0$, $(\pi\pi)_1$ pairs $\alpha_V^e(\{8\}_a) = 1.0, \alpha_V^m(\{8\}_a) = 0.400$, and the $(\pi\rho)_1$ pairs $\alpha_A(\{8\}_a) = 0.400$. The $(\pi\omega)$ pairs $\alpha(\{8_s\})$ has been set equal to $\alpha_P = 0.365$.

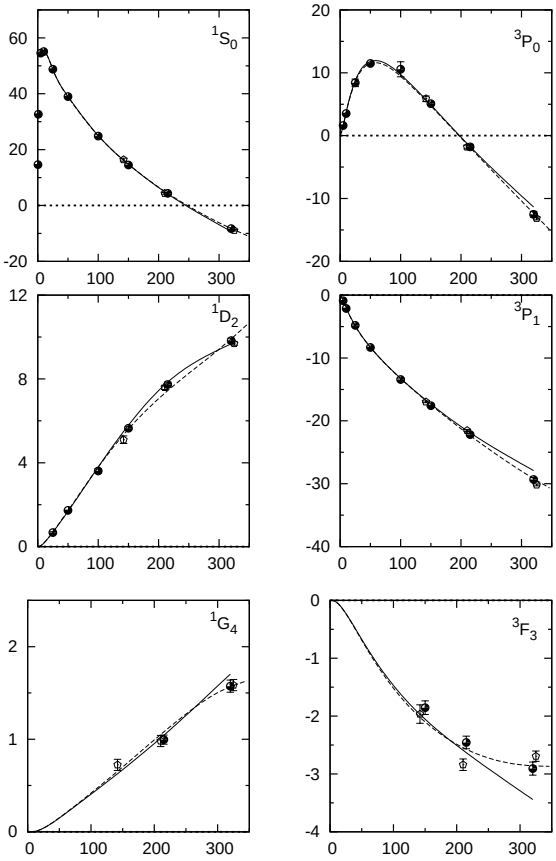

FIG. 5: Solid line: proton-proton $I = 1$ phase shifts for the ESC08c-model. The dashed line: the m.e. phases of the Nijmegen93 PW-analysis [10]. The black dots: the s.e. phases of the Nijmegen93 PW-analysis. The diamonds: Bugg s.e. [71].

VII. ESC08-MODEL , *NN*-RESULTS

A. Nucleon-nucleon Fit, Low-energy and Phase Parameters

For a more detailed discussion on the NN-fitting we refer to Ref. [4]. Here, we fit to the 1993 Nijmegen representation of the χ^2-hypersurface of the NN scattering data below $T_{lab} = 350$ MeV [10, 11], and also the low-energy parameters are fitted for pp, np and nn. In this simultaneous fit of NN and YN, we obtained for ESC08c for the phase shifts $\chi^2/Ndata = 1.087$. For a comparison with Ref. [4], and for use of this model for the description of NN, we give in Table V the nuclear-bar phases for pp in case $I = 1$, and for np in the case of ${}^1S_0(I = 1)$ and the $I = 0$-phases. Here, $\Delta\chi^2$ denotes the accrescence in χ^2 of the ESC-model w.r.t. the phase shift analysis [10, 11].

The deuteron has been included in the fitting procedure, as well as the low-energy parameters. The fitted binding energy $E_B = 2.224611$ MeV, which is very close to $E_B(experiment) = 2.224644$ MeV. The charge-symmetry breaking is described phenomenologically by having next to $g_{\rho nn}$ free couplings for $g_{\rho np}$, and $g_{\rho pp}$. This phenomenological treatment is successful for the various NN-channels, especially for the $np({}^1S_0, I = 1)$-phases, which were included in the NN-fit.

We emphasize that we use the single-energy (s.e.) phases and χ^2-surface [11] as a means to fit the NN-data. The multi-energy (m.e.) phases of the PW-analysis [10] in Fig. 5-Fig. 7 are the dashed lines in these figures. One notices that the central value of the s.e. phases do not correspond to the m.e. phases in general, illustrating that there has been a certain amount of noise fitting in the s.e. PW-analysis, see e.g. ϵ_1 and ${}^1P_1$ at $T_{lab} = 100$ MeV. The m.e. PW-analysis reaches $\chi^2/N_{data} = 0.99$, using 39 phenomenological parameters plus normalization parameters. The related phenomenological PW-potentials NijmI,II and Reid93 [72], with respectively 41, 47, and 50 parameters, turn out all with $\chi^2/Ndata = 1.03$. This should be compared to the ESC-model, which has $\chi^2/N_{data} = 1.087$ using for NN 32 parameters. These are 14 QPC-constrained meson-nucleon-nucleon couplings, 6 meson-pair-nucleon-nucleon couplings, 6 gaussian cut-off parameters, 3 diffractive couplings, and 2 diffractive mass parameters. The 3 remaining fitting parameters (2 F/(F+D) ratios and the Pauli blocking fraction) are mainly or totally determined by the YN-fit.

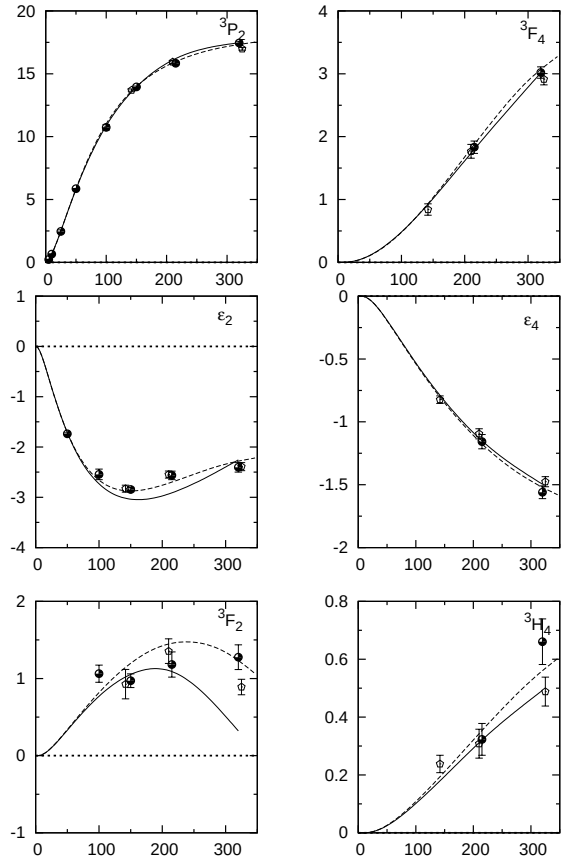

FIG. 6: Solid line: proton-proton $I = 1$ phase shifts for the ESC08c-model. The dashed line: the m.e. phases of the Nijmegen93 PW-analysis [10]. The black dots: the s.e. phases of the Nijmegen93 PW-analysis. The diamonds: Bugg s.e. [71].

From the figures it is obvious that the ESC-model deviates from the m.e. PW-analysis in particular at the highest energy.

In Table VI the results for the low energy parameters are given. In order to discriminate between the $^1S_0$-wave for pp, np, and nn, we introduced some charge independence breaking by taking $g_{pp\rho} \neq g_{np\rho} \neq g_{nn\rho}$. With this device we fitted the difference between the $^1S_0(pp)$ and $^1S_0(np)$ phases, and the different scattering lengths and effective ranges as well. We found $g_{np\rho} = 0.5841,\ g_{pp\rho} = 0.6330$, which are not far from $g_{nn\rho} = 0.6343$, see Table III. The NN low-energy parameters are fitted very well, see Table VI. For a discussion of the theoretical and experimental situation w.r.t. these low energy parameters, see [94].

The binding energy of the deuteron is fitted excellently. The electric quadrupole moment result is typical for models without meson-exchange current effects. Further properties of the deuteron in this model are: $P_D = 6.11\%, D/S = 0.0257, N_G^2 = 0.7718$, and $\rho_{-\epsilon,-\epsilon} = 1.7265$.

B. Nucleon-nucleon Potentials

The hyperon-nucleon OBE-, TPS-, and Pair-potentials for ESC04 model are shown in Ref. [5]. These potentials are rather similar to those of ESC08c, and therefore we refer the reader the cited YN-paper. Also, these NN-potentials are qualitatively rather similar in character. The odderon and the derivative axial-vector coupling, and the non-local pseudoscalar type spin-spin and tensor potentials are added.

The odderon potential is a novel feature of ESC08-model. In Fig. 9 the central and spin-orbit potentials are shown. The spin-spin, tensor, and quadratic spin-orbit potentials are very small. One notices from this figure that the pomeron potential is like an 'anti-scalar' potential whereas the odderon is a normal vector-exchange potential. Note the strong cancellation in the spin-orbit giving a negligible summed contribution. The upshot is a universal central repulsion from the pomeron+odderon.

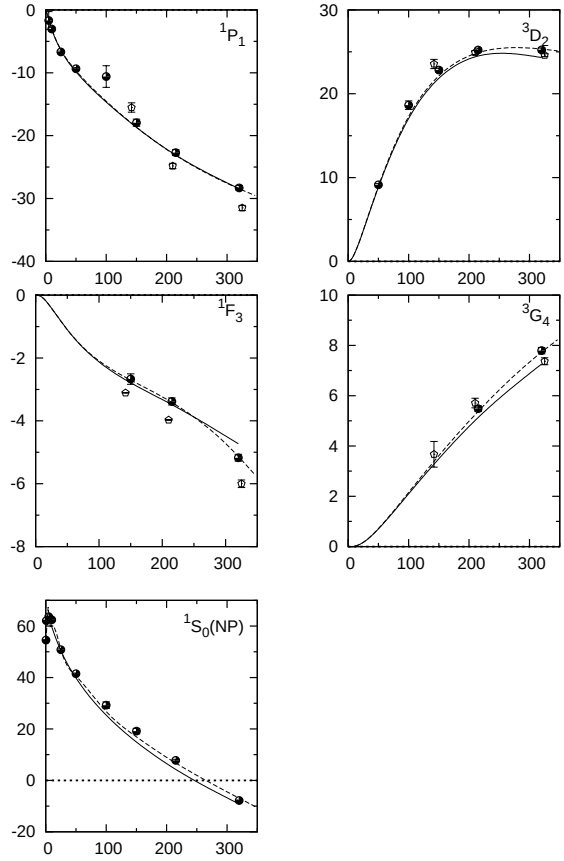

FIG. 7: Solid line: neutron-proton $I = 0$, and the I=1 $^1S_0(NP)$ phase shifts for the ESC08c-model. The dashed line: the m.e. phases of the Nijmegen93 PW-analysis [10]. The black dots: the s.e. phases of the Nijmegen93 PW-analysis. The diamonds: Bugg s.e. [71].

VIII. NUCLEAR SATURATION AND MANY-BODY REPULSION

The lowest-order Bruckner G-matrix calculations with the continuous (CON) choice for intermediate single particle potentials were shown to simulate well the results including higher hole-line contributions up to $3 \sim 4$ ρ_0 [73, 74]. Here, the Bruckner G-matrix theory is considered a good starting point for studies of many-body systems on the basis of free-space baryon-baryon interaction models. We study the properties of high-density nuclear matter on the basis of the lowest-order G-matrix theory with the CON choice.

As is well known, the experimental nuclear saturation properties, the density ρ_N, the binding energy per nucleon E/A, the compression modulus K, cannot be reproduced quantitatively with nuclear two-body interactions only, see e.g. [75]. The inclusion of many-nucleon interactions is essential for giving the correct energy curve $E(\rho_N)$. Here, the three-nucleon interaction (TNI), composed of an attractive (TNA) and a repulsive (TNR) part, seems to be the most important. Integrating over the third particle results in a dependence on the nuclear-matter density ρ_N of the 'effective' two-nucleon potential (see below). Since TNA contributes only moderately as a function of ρ_N, the saturation curve is not so remarkably changed by the TNA [75]. Its inclusion is nevertheless important for obtaining the right nuclear saturation point. On the other hand, it turns out that the TNR contribution increases rapidly in the high-density region, giving high values for the incompressibility. Maximum masses of neutron stars can be reproduced with use of the stiff equation of state (EoS) realized by including the TNR contributions. Soft-core two-baryon potentials give too soft EoS's. In particular, ESC08 gives for the mass of the neutron star $1.35M_\odot$ [76], implying for this model the necessity for a TNR contribution. Therefore, we incorporate the TNR contribution in the ESC-model together with an additional TNA one, giving it a key role in stiffening the EoS for symmetric and neutron-star matter. As will be shown below, this enables to satisfy both the nuclear saturation point and the observed maximum mass of neutron stars.

At high densities hyperon-mixing occurs in neutron-star matter, which brings about a significant softening of the EoS canceling the TNR effect for the maximum mass [77–79]. To compensate this adverse effect Nishizaki, Takatsuka

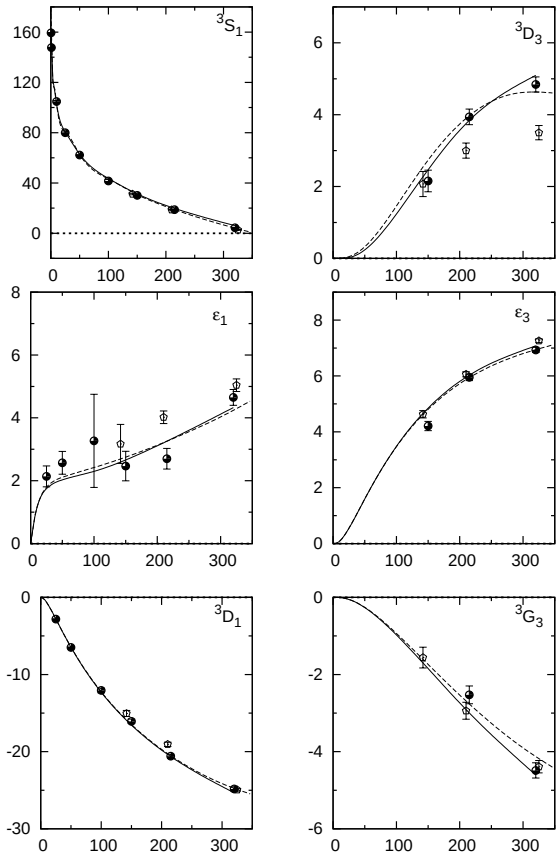

FIG. 8: Solid line: neutron-proton $I = 0$ phase shifts for the ESC08c-model. The dashed line: the m.e. phases of the Nijmegen93 PW-analysis [10]. The black dots: the s.e. phases of the Nijmegen93 PW-analysis. The diamonds: Bugg s.e. [71].

and one of the authors (Y.Y.) [77] made the conjecture that the TNR-type repulsion works universally for *YNN* and *YYN* as well as for *NNN*. They demonstrated that the TNR-stiffening of the EoS can be recovered clearly by this assumption. Universal repulsions among three baryons were called the three-baryon repulsion (TBR). It is our aim to realize the TBR assumption consistently with the ESC modeling of the baryon-baryon systems. The presence of three-body forces (3BF) is a natural possibility in nuclei and hypernuclei, generating effective two-body forces, which very likely improve the binding energies and well-depth's. The latter will appear indeed the case for the ESC-model as shown in the YN-paper [15] of this series.

Since in QCD the gluons are flavor blind it is natural to relate the universality of the TBR repulsion to multi-gluon exchange, see Fig. 10. In the Nijmegen soft-core OBE and ESC models pomeron-exchange can be viewed as due to an even number of gluon-exchange contributing a universal repulsion in BB-systems. Like for the two-baryon systems, in ESC we introduce the multi-gluon three-body forces with the multi-pomeron exchange potential (MPP) [8, 80, 81]. In Fig. 11 the triple- and quartic-pomeron vertices are illustrated. We convert the three-body potential into an effective two-body potential by integrating out third nucleon. As demonstrated in [82], the MPP gives the stiff EoS of neutron matter enough to assure the large observed values of two massive neutron stars with mass $1.97 \pm 0.04 M_\odot$ for PSR J1614-2230 [85] and $2.01 \pm 0.04 M_\odot$ for PSR J0348+0432 [86].

In [5] the medium effect on the vector masses was assumed as the dominant mechanism for generating extra repulsion at higher densities. However, the mass shift of the vector meson masses due to the nuclear medium has been put in doubt [87]. Therefore, in the ESC08-model, in contrast to [5], we assume that the dominant mechanism is triple and quartic pomeron exchange [88, 89].

For the triple pomeron vertex we take the Lagrangian [80, 81]

$$\mathcal{L}_3 = g_P^{(3)} \mathcal{M} \sigma_P^3(x)/3! \; . \tag{8.1}$$

TABLE V: ESC08c nuclear-bar pp and np phases in degrees.

$T_{\rm lab}$	0.38	1	5	10	25	50	100	150	215	320
$^1S_0(np)$	54.56	62.01	63.47	59.72	50.46	39.76	25.31	14.89	4.31	–8.94
$^1S_0$	14.62	32.62	54.75	55.16	48.66	38.92	24.94	14.66	4.14	–9.08
$^3S_1$	159.39	147.78	118.27	102.75	80.86	63.10	43.75	31.45	19.79	6.01
ϵ_1	0.03	0.11	0.68	1.17	1.81	2.12	2.45	2.84	3.47	4.62
$^3P_0$	0.02	0.14	1.61	3.82	8.82	11.83	9.79	5.01	–1.55	–11.12
$^3P_1$	–0.01	–0.08	–0.90	–2.04	–4.89	–8.28	–13.24	–17.33	–21.94	–28.18
$^1P_1$	–0.05	–0.19	–1.50	–3.08	–6.42	–9.84	–14.68	–18.77	–23.40	–29.40
$^3P_2$	0.00	0.01	0.22	0.66	2.49	5.77	10.87	14.03	16.27	17.23
ϵ_2	–0.00	–0.00	–0.05	–0.20	–0.81	–1.71	–2.70	–2.97	–2.82	–2.18
$^3D_1$	–0.00	–0.01	–0.19	–0.69	–2.84	–6.53	–12.43	–16.71	–20.75	–25.16
$^3D_2$	0.00	0.01	0.22	0.85	3.70	8.94	17.22	22.10	24.82	24.64
$^1D_2$	0.00	0.00	0.04	0.17	0.69	1.69	3.78	5.72	7.69	9.24
$^3D_3$	0.00	0.00	0.00	0.00	0.03	0.23	1.19	2.37	3.72	5.06
ϵ_3	0.00	0.00	0.01	0.08	0.55	1.60	3.47	4.83	6.00	7.04
$^3F_2$	0.00	0.00	0.00	0.01	0.11	0.34	0.80	1.10	1.17	0.45
$^3F_3$	–0.00	–0.00	–0.01	–0.03	–0.23	–0.68	–1.47	–2.06	–2.64	–3.44
$^1F_3$	–0.00	–0.00	–0.01	–0.06	–0.42	–1.11	–2.13	–2.79	–3.47	–4.68
$^3F_4$	0.00	0.00	0.00	0.00	0.02	0.12	0.50	1.03	1.79	2.96
ϵ_4	–0.00	–0.00	–0.00	–0.00	–0.05	–0.19	–0.53	–0.83	–1.13	–1.45
$^3G_3$	–0.00	–0.00	–0.00	–0.00	–0.05	–0.26	–0.93	–1.74	–2.78	–4.17
$^3G_4$	0.00	0.00	0.00	0.01	0.17	0.71	2.12	3.53	5.18	7.33
$^1G_4$	0.00	0.00	0.00	0.00	0.04	0.15	0.41	0.68	1.06	1.72
$^3G_5$	–0.00	–0.00	–0.00	–0.00	–0.01	–0.05	–0.17	–0.26	–0.29	–0.18
ϵ_5	0.00	0.00	0.00	0.00	0.04	0.20	0.70	1.22	1.83	2.62

Then, the three-body local potential by pomeron exchange is given by

$$V(\mathbf{x}_1,\mathbf{x}_2,\mathbf{x}_3) = g_P^{(3)}(g_P)^3\Pi_{i=1}^3 \int \frac{d^3k_i}{(2\pi)^3}\Pi_{i=1}^3 e^{-i\mathbf{p}_i\cdot\mathbf{x}}\cdot(2\pi)^3\delta(\mathbf{k}_1+\mathbf{k}_2+\mathbf{k}_3)$$
$$\times \exp(-\mathbf{k}_1^2/4m_P^2)\exp(-\mathbf{k}_2^2/4m_P^2)\exp(-\mathbf{k}_3^2/4m_P^2)\cdot\mathcal{M}^{-5}. \quad (8.2)$$

Here, the (low-energy) pomeron propagator is the same as used in the two-body pomeron potential used in all Nijmegen soft-core OBE and ESC models.

The effective two-body potential in a baryonic medium is obtained by integrating over the coordinate $\mathbf{x}_3$.

$$V_{eff}(\mathbf{x}_1,\mathbf{x}_2) = \rho_{NM}\int d^3x_3 V(\mathbf{x}_1,\mathbf{x}_3,\mathbf{x}_3)$$
$$= g_P^{(3)}(g_P)^3\frac{\rho_{NM}}{\mathcal{M}}\cdot\frac{1}{4\pi}\frac{4}{\sqrt{\pi}}\left(\frac{m_P}{\sqrt{2}}\right)^3\exp\left(-\frac{1}{2}m_P^2r_{12}^2\right). \quad (8.3)$$

In a similar way, one can obtain a four-body interaction $V(\mathbf{x}_1,\mathbf{x}_2,\mathbf{x}_3,\mathbf{x}_4)$ and a corresponding effective two-body potential with a quartic pomeron coupling $g_P^{(4)}$ [81]. The expressions for the N-body interaction and the effective two-body potential by multiple-pomeron exchange are given in Ref. [80–82]. Here, we restrict ourselves to the triple and quartic pomeron couplings where there is information from the ISR pp-data [88]. Since the pomeron is an SU(3)-singlet, the MPP in nuclear medium leads to the density-dependent universal repulsion, which can be associated with the proposal in [77]. Estimates for $g_P^{(3)}$ and $g_P^{(4)}$ can be obtained from [88, 89], which shows that $g_P^{(4)} >> g_P^{(3)}$. The pomeron coupling g_P is fitted to the NN-data etc., see Table III. In [82], the MPP strengths ($g_P^{(3)}$ and $g_P^{(4)}$) were determined by analyzing the ^{16}O+^{16}O elastic scattering at $E/A = 70$ MeV with use of G-matrix folding potentials,

TABLE VI: ESC08c Low energy parameters: S-wave scattering lengths and effective ranges, deuteron binding energy E_B, and electric quadrupole Q_e. The asterisk denotes that the low-energy parameters were not searched.

	experimental data			ESC08c
$a_{pp}(^1S_0)$	–7.823	±	0.010	–7.7719
$r_{pp}(^1S_0)$	2.794	±	0.015	2.7691*
$a_{np}(^1S_0)$	–23.715	±	0.015	–23.7275
$r_{np}(^1S_0)$	2.760	±	0.030	2.6994*
$a_{nn}(^1S_0)$	–18.63	±	0.48	–17.304
$r_{nn}(^1S_0)$	2.860	±	0.15	2.8401*
$a_{np}(^3S_1)$	5.423	±	0.005	5.4409*
$r_{np}(^3S_1)$	1.761	±	0.005	1.7471*
E_B	–2.224644	±	0.000046	–2.224611
Q_e	0.286	±	0.002	0.2731

TABLE VII: ESC08c χ^2 and χ^2 per datum at the ten energy bins for the Nijmegen93 Partial-Wave-Analysis. N_{data} lists the number of data within each energy bin. The bottom line gives the results for the total $0-350$ MeV interval. The χ^2-accrescence for the ESC model is denoted by $\Delta\chi^2$ and $\Delta\hat{\chi}^2$, respectively.

$T_{\rm lab}$	♯ data	χ^2_0	$\Delta\chi^2$	$\hat{\chi}^2_0$	$\Delta\hat{\chi}^2_0$
0.383	144	137.555	21.6	0.960	0.150
1	68	38.019	57.7	0.560	0.848
5	103	82.226	8.3	0.800	0.081
10	290	257.995	29.2	1.234	0.101
25	352	272.197	40.5	0.773	0.115
50	571	538.522	50.2	0.957	0.088
100	399	382.499	19.7	0.959	0.049
150	676	673.055	76.5	0.996	0.113
215	756	754.525	110.9	0.998	0.147
320	954	945.379	192.3	0.991	0.202
Total	4313	4081.971	607.0	0.948	0.139

where the TNR effect appear clearly in the angular distribution. As shown in [90], in such a high scattering energy the frozen-density approximation gives a good prescription, where G-matrices including TNR at about two times of normal density contribute to nucleus-nucleus folding potentials.

In addition to MPP, in order to assure the nuclear saturation property precisely, we introduce also a TNA part phenomenologically as a density-dependent two-body interaction

$$V_{TNA}(r;\rho_N) = V^0_{TNA}\,\exp(-(r/2.0)^2)\,\rho_N\,\exp(-\eta\rho_N)\,(1+P_r)/2\ ,$$

whose form is similar to the TNA part given in [75]. P_r is a space-exchange operator. By a $(1+P_r)$ factor, the TNA part works only in even states, which is needed to reproduce nucleus-nucleus angular distributions precisely. Then, V^0_{TNA} and η are treated as adjustable parameters to reproduce the saturation propety. Strengths of the MPP part ($g^{(3)}_P$ and $g^{(4)}_P$) and the TNA part (V_{TNA} and η) are determined so as to reproduce the ^{16}O+^{16}O angular distribution $E/A = 70$ MeV by use of the G-matrix folding potentials derived from the (ESC08c+MPP+TBA) sets. The ratio of $g^{(3)}_P$ and $g^{(4)}_P$ unsettled in our analysis was taken adequately in reference to the results in Ref. [88, 89]. Quantitatively,

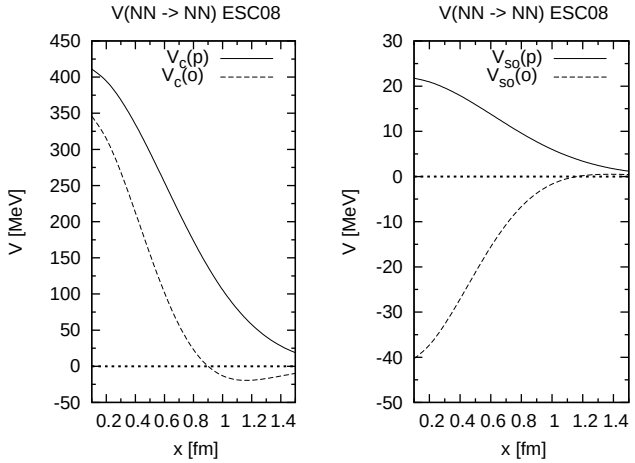

FIG. 9: Pomeron and Odderon central- and spin-orbit potentials.

however, it is quite uncertain. Then, we can find various combinations of $g_P^{(3)}$ and $g_P^{(4)}$ reproducing the data equally well.

In Table VIII, we give the three parameter sets of ($g_P^{(3)}$, $g_P^{(4)}$, V_{TNA}^0, η) named as MPa, MPa$^+$ and MPb, respectively, which reproduce equally well the saturation property. Here, the parameters V_{TNA}^0 and η are taken to reproduce the E/A value -16 MeV at the saturation density 0.155 fm^{-3} in respective cases. Here, MPa and MPb sets were used also in [83]. As stated in [82], the analyses of the experimental cross sections of the process $pp \to pX$ gives rise to rough estimations $g_P^{(3)} = 1.95 \sim 2.6$ and $g_P^{(4)} = 33 \sim 228$ [88, 89]. In the case of MPa, the $g_P^{(3)}$ value is within the estimated range, and the $g_P^{(4)}$ is of a permissible minimum value. MPa$^+$ is specified by having a fairly larger value of $g_P^{(4)}$ than MPa. On the other hand, MPb has no quartic component ($g_P^{(4)} = 0$). As found in Eq.(8.3), the contributions from triple and quartic components are proportional to ρ and ρ^2, respectively. Therefore, the latter contribution play a remarkable role to stiffen the EoS in high density region.

In Fig. 12 and Fig. 13 we show the energy curves of symmetric nuclear matter and neutron matter, respectively, namely binding energy per nucleon (E/A) as a function of ρ_N. Thick solid, dashed and dotted curves are obtained from G-matrix calculations with MPa, MPa$^+$ and MPb, respectively. Thin solid curves are with ESC08c only. The box in the figure shows the area where nuclear saturation is expected to occur empirically. The inset in Fig. 12 shows a zoom of the region around the saturation point. The dotted curve from ESC08c only is found to deviate substantially from the box. As is clearly seen, saturation densities and minimum values of E/A in the cases of MPa, MPa$^+$ and

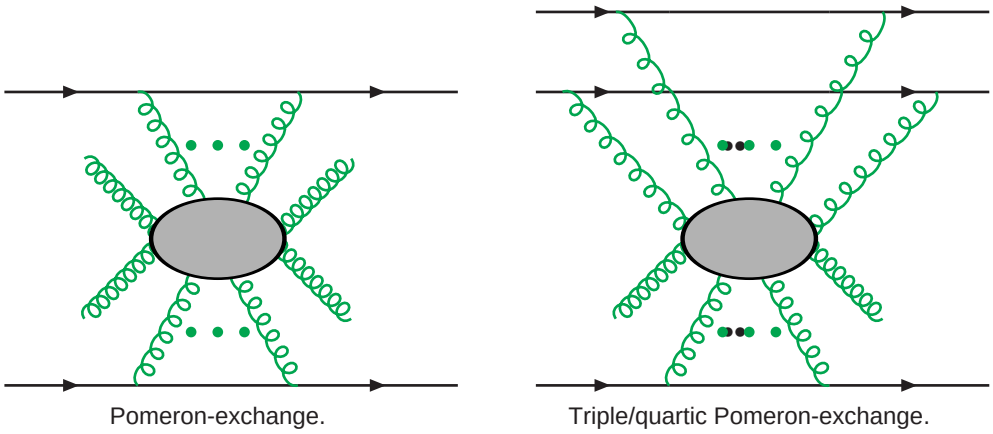

FIG. 10: Multi-gluon exchange processes.

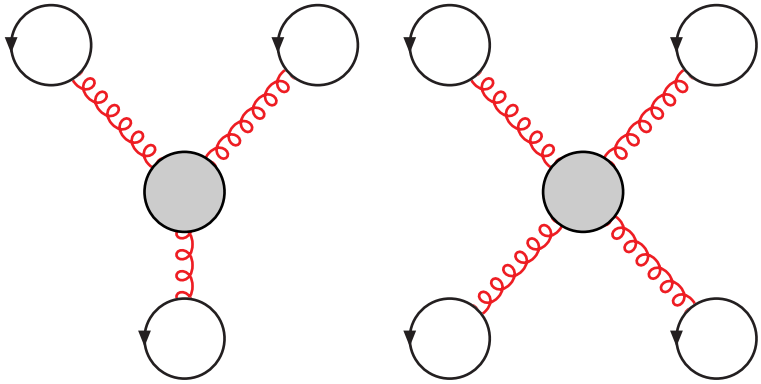

FIG. 11: Triple- and quartic-pomeron 3- and 4-body interaction.

MPb are nicely close to the empirical value shown by the box.

The EoS is specified by the following quantities: The difference between the E/A curves for neutron matter and symmetric matter gives the symmetry energy $E_{sym}(\rho)$, and its slope parameter is defined by $L = 3\rho_0 \left[\frac{\partial E_{sym}(\rho)}{\partial \rho}\right]_{\rho_0}$. The incompressibility is defined by $K = 9\rho_0^2 \left[\frac{\partial^2}{\partial \rho^2} E/A(\rho)\right]_{\rho_0}$, $E/A(\rho)$ being for symmetric matter. In Table IX, the values of these quantities are given at the saturation density $\rho_0 = 0.155$ fm^{-3}. The minimum values of E/A curves for three sets turn out to be nicely close to the empirical value -16 MeV. The symmetric energies and their slope parameters are similar to each other and consistent with the empirical indications. The values of E_{sym} and L in Table IX are in nice agreement to the values $E_{sym} = 32.5 \pm 0.5$ MeV and $L = 70 \pm 15$ MeV determined recently on the basis of experimental data [91]. It should be noted the values of E_{sym} and L for the three sets are similar to the values for ESC08c only, owing to the isospin-independent nature of the present three-body interaction. The difference among these sets appears clearly in values of compressibility K: When the saturation curves are fitted by a function

TABLE VIII: Parameters of MPP+TNA parts. V^0_{TNA} and η are in MeV and fm^{-3}, respectively.

	$g_P^{(3)}$	$g_P^{(4)}$	V^0_{TNA}	η
MPa	2.34	30.0	-54.0	10.0
MPa$^+$	1.31	80.0	-36.0	8.0
MPb	2.94	0.0	-68.0	11.2

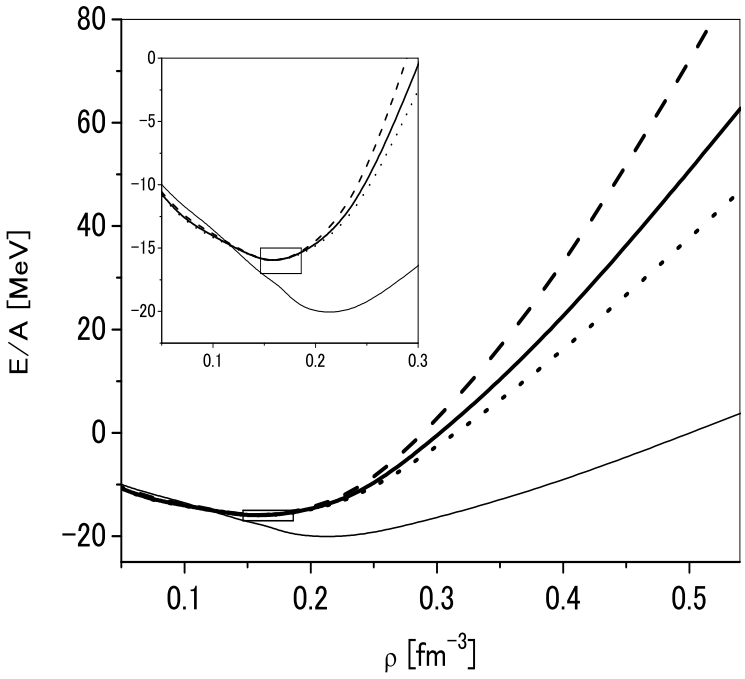

FIG. 12: Energies per nucleon drawn as a function of ρ_N in symmetric nuclear matter. Thick solid, dashed and dotted curves are for MPa, MPa$^+$ and MPb, respectively. Thin solid curve is for ESC08c only. The box shows the empirical value.

TABLE IX: Calculated values of saturation parameters.

	ρ_0 (fm^{-3})	E/A (MeV)	E_{sym} (MeV)	L (MeV)	K (MeV)
MPa	0.155	−16.0	31.3	72.6	270
MPa$^+$	0.155	−16.1	31.2	74.1	317
MPb	0.155	−16.0	31.3	72.5	254

$E/A = a\rho + b\rho^\gamma$ at $0.09 < \rho < 0.33$ fm^{-3}, the obtained values of K are 270, 317 and 254 MeV for MPa, MPa$^+$ and MPb at the same saturation density 0.155 fm^{-3}.

In the case of pure neutron-matter EoS, the mass-radius relations of neutron stars can be derived from the ESC08c+MPP+TNA models. In [82], these models lead to the result that calculated values of maximum masses of neutron stars were larger than $2M_\odot$. Here, they used the previous version of ESC08c, which is similar to the present version. Furthermore, their MPP+TNA parts MP1a and MP2a are similar to MPa and MPb, respectively, in this work. The strong four-body repulsive part included in MPa$^+$ leads to larger masses than MPa and MPb. Because the TNA parts contribute very slightly to maximum masses, the inclusion of MPP and additional TNA provide a solution for both the nuclear saturation and the neutron-star mass problem.

Then, it should be noted that our MPP contributions exist universally in every baryonic systems. The relation between the universal MPP repulsions and the softening effect induced by hyperon mixing to neutron-star matter were investigated in [83, 84]. In these references, they introduced MPa, MPa$^+$ and MPb like this work on the basis of the earlier version of ESC08c. The MPP parts in them are the completly same as those in Table VIII, but their TBA parts are different from those in this work.

Another mechanism for generating extra repulsion at higher densities is suggested by the relativistic mean-field theory (RMFT), see e.g.[92]. Here, at higher densities the scalar field becomes suppressed and the vector field becomes dominating. The effect would be similar to that employed in [5]. For the Dirac-Bruckner approach to the EoS see [93].

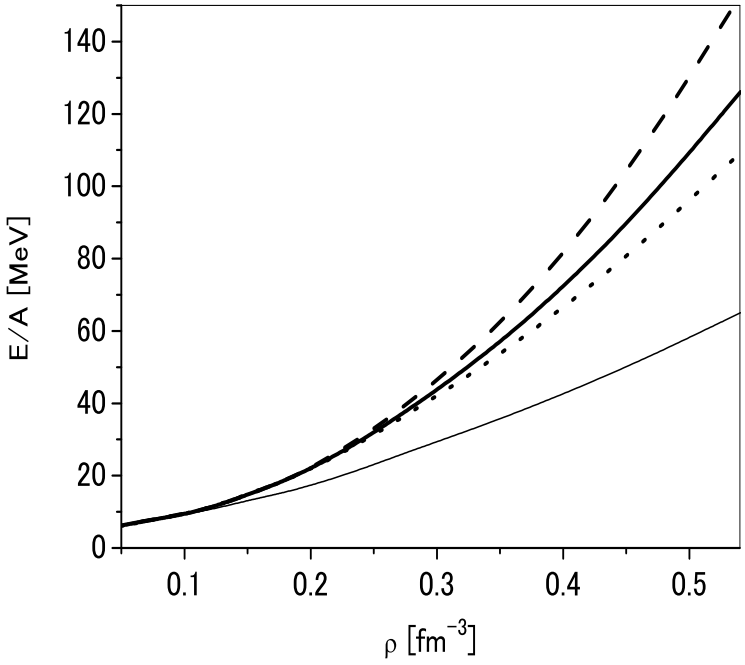

FIG. 13: Energies per nucleon drawn as a function of ρ_N in neutron matter. Thick solid, dashed and dotted curves are for MPa, MPa$^+$ and MPb, respectively. Thin solid curve is for ESC08c only.

IX. DISCUSSION AND CONCLUSIONS

The presentation in this paper reports on the present stage of the ESC-model. Compared to ESC04 [4–6] the model has been developed further. The new version ESC08 has in addition to meson-exchange also incorporated quark-core effects. Furthermore, the multi-gluon sector has been completed by the inclusion of the odderon. Moreover, the treatment of the axial-vector mesons is now in a very satisfactory shape by employing the B-field formalism. The ESC-approach to the nuclear force is a promising one. It opens the possibility to make a connection between the at present available baryon-baryon experimental data on the one hand, and with the underlying quark structure of the baryons and mesons on the other hand. Namely, a successful description of both the NN- and YN-scattering data is obtained with meson-baryon coupling parameters which all comply with the QPC-model. Here, we note that in particular the QPC-model treats the vector and scalar mesons on an equal footing. Apart from its role in $\pi\pi$ and πK scattering, the $f_0(760)$ has been shown to be present in relativistic nuclear scattering as well [95]. We note that by studying the relation between the QPC-processes and the BBM-couplings, we determined the ratio $\gamma(^3P_0)/\gamma(^3S_1) = 2:1$. In the literature, the $^3P_0$-QPC and the $^3S_1$-QPC in the SCQCD [18] has been studied by [96] and [97] respectively. In this paper we give therefore an estimation of the relative importance of the QPC processes. At the same time we comply with the strong constraint of no bound states in the $S = -1$ systems. Therefore, the ESC-models, ESC04 and ESC08, are an important step in the determination of the baryon-baryon interactions for low energy scattering and the description of hypernuclei in the context of broken SU(3)-symmetry. The values for many parameters, which in previous Nijmegen work were considered to be free to a large extent, follow now rather well the pattern shown in quark-model predictions. This is particularly the case for the $F/(F+D)$-ratios of the OBE- and MPE-interactions.

For the nuclear matter description we introduced the multi-pomeron (multi-gluon) exchange three-body force potential, achieving three things (i) right nuclear saturation, (ii) correct neutron star maas, and (iii) better hyperonic well depth's U_Y for $Y = \Lambda, \Sigma, \Xi$ (see the companion papers II,III). The combined fit for NN and YN is extremely good in ESC08. It is for the first time that the quality of the NN-fit does not suffer from the inclusion of the YN-data. The ΛN p-waves seem to be better, which is the result of the truly simultaneous $NN + YN$-fitting. This is also reflected in the better Scheerbaum K_Λ-value [98], making the well-known small spin-orbit splitting smaller, see Ref. [99].

The G-matrix results showed for ESC04 that basic features of hypernuclear data are reproduced nicely, improving

on the soft-core OBE-models NSC89 [3] and NSC97 [9]. In spite of this superiority of ESC04 for hypernuclear data, some problems remained. In particular the well depth U_Σ was attractive, which is very unlikely in view of several other studies e.g. Ref.'s [100–103] Furthermore, it has been shown [77] that the EOS for nuclear matter is too soft for the soft-core models. From this we learn that a good fit to the present scattering data not necessarily means success in the G-matrix results. To explain this one can think of two reasons: (i) the G-matrix results are sensitive to the two-body interactions below 1 fm, whereas the present YN-scattering data are not, (ii) other than two-body forces play an important role. Since the problem with U_Σ hints at a special feature in the $\Sigma^+p(^3S_1)$-channel, it is likely that it is a two-body problem. As we have shown in ESC08 it can be solved by the inclusion of the quark-core effects. For the softness of the EOS a natural possibility is the presence of TBF in nuclear and hyperonic matter, see Ref. [77]. This also solves the nuclear saturation problem [5].

It is important to stress the role of the information on hypernuclei in our analysis. We imposed for the ESC08-solution that $U_\Sigma > 0$ and $U_\Xi < 0$. This induced the occurrence of strong tensor-forces with the consequence of a bound state in the S=-2 systems. Namely, a deuteron-like bound state in the $\Xi N(^3S_1 - ^3D_1, I = 1)$ system.

Summarizing the results of the ESC-approach to baryon-baryon interactions, it can be stated that this is a very successful one. It has been shown that ESC-models are able to give with a single parameter-set extremely satisfactory descriptions of the NN$\oplus$YN-data, and at the same time lead to successful G-matrix results. For the coupling constants (i) flavor SU(3)-symmetry can be maintained, and (ii) they show rather well the pattern as predicted by the QPC-model. The tensor-couplings play an important role, especially in the prediction of a deuteron-like S=-2 bound state. We conclude that these ESC-model predictions, as well as the applications to the S=-3,-4 systems and hyperonic matter, have a rather sound physical basis.

We close by remarking that the determination of the MPE-couplings opens the possibility to compute the TBF-potentials for baryon-systems where all meson-pair vertices are fixed by the ESC-model.

Acknowledgements

We wish to thank E. Hiyama, K. Itonaga, T. Motoba and H.-J. Schulze for stimulating discussions.

APPENDIX A: B-FIELD FORMALISM FOR VECTOR- AND AXIAL-VECTOR MESONS

As an alternative to the usual Proca-formalism for vector mesons, Nakanishi and collaborators [57, 58] introduced the B-field formalism. In the non-abelian theory, e.g. isospin $\mathrm{SU}_I(2)$, one introduces the B-field through the Lagrangian

$$\mathcal{L}_A \;=\; -\frac{1}{4}\mathcal{F}^i_{\mu\nu}\mathcal{F}^{\mu\nu i} + \frac{1}{2}m^2 A^i_\mu A^{\mu i} + B^i\partial_\mu A^{\mu i} + \frac{\alpha}{2}B^i B^i \;, \tag{A1}$$

where the field tensor and the covariant derivative D_μ are given by

$$\mathcal{F}^i_{\mu\nu} \;=\; \partial_\mu A^i_\nu - \partial_\nu A^i_\mu + g_A\epsilon^{ijk}A^j_\mu A^k_\nu, \tag{A2a}$$

$$D_\mu \;=\; \partial_\mu - ig_A t_i\; A^i_\mu \;. \tag{A2b}$$

We assume that the A^i_μ-field is coupled to the conserved, or almost conserved, hadronic 'strong' current $J_{H,\mu}$. The field equations, neglecting the non-abelian term in the axial field tensor, become

$$A^i_\mu \;:\; \partial^\mu\mathcal{F}^i_{\mu\nu} + m^2A^i_\mu = -J^i_{H,\mu} + \partial_\mu B^i \;, \tag{A3a}$$

$$B^i \;:\; \partial^\mu A^i_\mu + \alpha B^i = 0 \;. \tag{A3b}$$

Exploiting now that approximately $\partial^\mu J^i_\mu = 0$, one derives from the field equation for A^i_μ, upon taking the derivative ∂_μ etc., that B^i is a free field, i.e.

$$\left(\Box + \alpha m^2\right) B^i = 0 \;. \tag{A4}$$

This theory can be quantized in a satisfactory way, giving an axial-vector-meson propagator which is covariant, see Nakanishi & Ojima [58] It implies that in the propagator one has for the spectral function of the propagator projection operator

$$\Pi^{\mu\nu}(k) = \left[-\eta^{\mu\nu} + \frac{k^\mu k^\nu}{m^2}\right]\delta(k^2-m^2) - \frac{k^\mu k^\nu}{m^2}\;\delta(k^2-\alpha_r m^2) \;, \tag{A5}$$

where $\alpha_r > 0$ is the renormalized B-field parameter α giving it a mass $\sqrt{\alpha_r}m$ [58]. The propagator becomes

$$\begin{aligned} P^{\mu\nu}(k) &= -\frac{\eta^{\mu\nu}}{k^2 - m^2 + i\epsilon} + (1-\alpha_r)\frac{k^\mu k^\nu}{(k^2 - m^2 + i\epsilon)(k^2 - \alpha_r m^2 + i\epsilon)} \\ &\Rightarrow -\frac{\eta^{\mu\nu}}{k^2 - m^2 + i\epsilon} \quad , \quad \text{for} \quad \alpha_r = 1 \ . \end{aligned} \tag{A6}$$

The case $\alpha_r = 1$ reminds one of the Feynman-gauge in the massless case. Now, in the case of coupling to a conserved current, the potential will be independent of α_r. Therefore, we will use the "Feynman-gauge" in this paper. It implies that the $k^\mu k^\nu$-terms in the vector-meson propagators will not contribute to the potentials in the B-field formalism. This in contrast to the Proca-formalism, see e.g. Ref. [56]. For the axial-vector mesons we will use the B-field formalism, whereas for the vector mesons we continue to use the Proca formalism, like in Refs. [3, 5, 9].

APPENDIX B: EXACT TREATMENT NON-LOCAL-TENSOR (NLT) OPERATOR

From results given in Ref. [104], we derive a new method for the treatment of the non-local-tensor (NLT) $\boldsymbol{\sigma}_1 \cdot \mathbf{q} \boldsymbol{\sigma}_2 \cdot \mathbf{q}$-operator. Starting from

$$\widetilde{V}(\mathbf{k}, \mathbf{q}) = \int d^3r' \int d^3r \ e^{i\mathbf{p}'\cdot\mathbf{r}'} V(\mathbf{r}', \mathbf{r}) e^{-i\mathbf{p}\cdot\mathbf{r}} \ , \tag{B1}$$

where

$$V(\mathbf{r}', \mathbf{r}) = \delta^3(\mathbf{r}' - \mathbf{r}) \ f(r) \ Q_{12} \ , \tag{B2}$$

with the quadratic-spin-orbit operator $Q_{12} = (\boldsymbol{\sigma}_1 \cdot \mathbf{L} \boldsymbol{\sigma}_2 \cdot \mathbf{L} + \boldsymbol{\sigma}_2 \cdot \mathbf{L} \boldsymbol{\sigma}_1 \cdot \mathbf{L})/2$. Introducing the functions $g(r)$ and $h(r)$ by

$$r_i f(r) = -\nabla_i g(r) \quad , \quad r_i r_j f(r) = \left[-\nabla_i \nabla_j + \delta_{ij} \left(\frac{1}{r} \frac{d}{dr} \right) \right] \ h(r) \ , \tag{B3}$$

executing the Fourier transformation in (B1) leads to the identity

$$\begin{aligned} \widetilde{V}(\mathbf{k}, \mathbf{q}) &= [\boldsymbol{\sigma}_1 \cdot \mathbf{q} \times \mathbf{k}] \, [\boldsymbol{\sigma}_2 \cdot \mathbf{q} \times \mathbf{k}] \ \widetilde{h}(\mathbf{k}^2) \\ &\quad - \left[\boldsymbol{\sigma}_1 \cdot \mathbf{q} \boldsymbol{\sigma}_2 \cdot \mathbf{q} - \mathbf{q}^2 \boldsymbol{\sigma}_1 \cdot \boldsymbol{\sigma}_2 \right] \ \widetilde{g}(\mathbf{k}^2) \\ &\quad + \frac{1}{4} \left[\boldsymbol{\sigma}_1 \cdot \mathbf{k} \boldsymbol{\sigma}_2 \cdot \mathbf{k} - \mathbf{k}^2 \boldsymbol{\sigma}_1 \cdot \boldsymbol{\sigma}_2 \right] \ \widetilde{g}(\mathbf{k}^2) \ , \end{aligned} \tag{B4}$$

where $\widetilde{h}(\mathbf{k}^2)$ and $\widetilde{g}(\mathbf{k}^2)$ are the Fourier transforms of respectively $h(r)$ and $g(r)$.

The strategy is now to derive the configuration potentials with the $\boldsymbol{\sigma}_1 \cdot \mathbf{q} \boldsymbol{\sigma}_2 \cdot \mathbf{q}$-operator by utilizing (B4), which we rewrite as

$$\begin{aligned} &\left[\boldsymbol{\sigma}_1 \cdot \mathbf{q} \boldsymbol{\sigma}_2 \cdot \mathbf{q} - \mathbf{q}^2 \boldsymbol{\sigma}_1 \cdot \boldsymbol{\sigma}_2 \right] \ \widetilde{g}(\mathbf{k}^2) = \\ &\left\{ [\boldsymbol{\sigma}_1 \cdot \mathbf{q} \times \mathbf{k}] \, [\boldsymbol{\sigma}_2 \cdot \mathbf{q} \times \mathbf{k}] \ \widetilde{h}(\mathbf{k}^2) - \widetilde{V}(\mathbf{k}, \mathbf{q}) \right\} \\ &+ \frac{1}{4} \left[\boldsymbol{\sigma}_1 \cdot \mathbf{k} \boldsymbol{\sigma}_2 \cdot \mathbf{k} - \mathbf{k}^2 \boldsymbol{\sigma}_1 \cdot \boldsymbol{\sigma}_2 \right] \ \widetilde{g}(\mathbf{k}^2) \ , \end{aligned} \tag{B5}$$

In our application

$$\widetilde{g}(\mathbf{k}^2) = \frac{\exp(-\mathbf{k}^2/\Lambda^2)}{\mathbf{k}^2 + m^2} \quad , \quad g(r) = \frac{m}{4\pi} \phi_C^0(r, m, \Lambda) \ . \tag{B6}$$

Then, from (B3) one derives that

$$f(r) = -\frac{1}{r}\frac{d}{dr} g(r) = -\frac{m}{4\pi}\frac{1}{r}\frac{d}{dr}\phi_C^0(r, m, \Lambda) = \frac{m^3}{4\pi}\phi_{SO}^0(r, m, \Lambda) \ . \tag{B7}$$

In momentum space, one easily derives the relation $d\widetilde{f}(\mathbf{k}^2)/d\mathbf{k}^2 = -\widetilde{g}(\mathbf{k}^2)/2$, which leads to

$$\widetilde{f}(\mathbf{k}^2) = \frac{1}{2}\exp\left(m^2/\Lambda^2\right)\ E_1\left[(\mathbf{k}^2+m^2)/\Lambda^2\right]\ , \tag{B8}$$

where $E_1(x)$ is the standard exponential integral function.

Next, we turn to the determination of $h(r)$. From (B3) one readily derives the momentum space differential equation

$$\boldsymbol{\nabla}_k^2\ \widetilde{g}(\mathbf{k}^2) = (\mathbf{k}\cdot\boldsymbol{\nabla}_k + 3)\ \widetilde{h}(\mathbf{k}^2)\ . \tag{B9}$$

Trying the form

$$\widetilde{h}(\mathbf{k}^2) = \left(A + \frac{B}{\mathbf{k}^2+m^2}\right)\widetilde{g}(\mathbf{k}^2)\ , \tag{B10}$$

one obtains from (B9) the solution $A = -2/\Lambda^2$ and $B = -2$. So,

$$\widetilde{h}(\mathbf{k}^2) = -2\left(\frac{1}{\Lambda^2} + \frac{1}{\mathbf{k}^2+m^2}\right)\widetilde{g}(\mathbf{k}^2) = -2\left(\frac{1}{\Lambda^2} - \frac{d}{dm^2}\right)\widetilde{g}(\mathbf{k}^2) = 2\frac{d\widetilde{g}(\mathbf{k}^2)}{d\mathbf{k}^2} \tag{B11}$$

Using the (approximate) axial-current conservation, and the "Feynman gauge" in the B-field formalism, we have from the $\Omega_i^{(A)}$ in (4.17) the following expression for $\mathcal{V}_A^{(1)}$

$$\begin{aligned}\tilde{\mathcal{V}}_A^{(1)} \ =\ & -g_A^2\left[\left(1 - \frac{1}{3MM'}\mathbf{k}^2 + \frac{3(\mathbf{q}^2+\mathbf{k}^2/4)}{2M'M}\right)\boldsymbol{\sigma}_1\cdot\boldsymbol{\sigma}_2 + \frac{2}{MM'}\left((\boldsymbol{\sigma}_1\cdot\mathbf{q})(\boldsymbol{\sigma}_2\cdot\mathbf{q})\right.\right.\\ & \left.-\mathbf{q}^2\boldsymbol{\sigma}_1\cdot\boldsymbol{\sigma}_2\right) - \frac{1}{4M'M}\left((\boldsymbol{\sigma}_1\cdot\mathbf{k})(\boldsymbol{\sigma}_2\cdot\mathbf{k}) - \frac{1}{3}\mathbf{k}^2\boldsymbol{\sigma}_1\cdot\boldsymbol{\sigma}_2\right)\\ & \left.+\frac{i}{4M'M}(\boldsymbol{\sigma}_1+\boldsymbol{\sigma}_2)\cdot\mathbf{q}\times\mathbf{k}\right]\cdot\widetilde{g}(\mathbf{k}^2)\ ,\end{aligned} \tag{B12}$$

Here, the superscript (1) refers to the circumstance that this comes from the $g_{\mu\nu}$-term in the axial-vector-meson propagator. Then, using the identity (B5) we get from (B12)

$$\begin{aligned}\tilde{\mathcal{V}}_A^{(1)} \ =\ & -g_A^2\left[\left(1 - \frac{2\mathbf{k}^2}{3MM'} + \frac{3(\mathbf{q}^2+\mathbf{k}^2/4)}{2M'M}\right)\boldsymbol{\sigma}_1\cdot\boldsymbol{\sigma}_2\right.\\ & +\frac{1}{4M'M}\left((\boldsymbol{\sigma}_1\cdot\mathbf{k})(\boldsymbol{\sigma}_2\cdot\mathbf{k}) - \frac{1}{3}\mathbf{k}^2\boldsymbol{\sigma}_1\cdot\boldsymbol{\sigma}_2\right)\\ & \left.+\frac{i}{4M'M}(\boldsymbol{\sigma}_1+\boldsymbol{\sigma}_2)\cdot\mathbf{q}\times\mathbf{k}\right]\cdot\widetilde{g}(\mathbf{k}^2)\\ & -g_A^2\left[\frac{2}{MM'}\left\{[\boldsymbol{\sigma}_1\cdot\mathbf{q}\times\mathbf{k}]\,[\boldsymbol{\sigma}_2\cdot\mathbf{q}\times\mathbf{k}]\ \widetilde{h}(\mathbf{k}^2) - \widetilde{V}(\mathbf{k},\mathbf{q})\right\}\right]\ .\end{aligned} \tag{B13}$$

Making now our standard approximation of the Fourier transformation of the $[\boldsymbol{\sigma}_1\cdot\mathbf{q}\times\mathbf{k}]\,[\boldsymbol{\sigma}_2\cdot\mathbf{q}\times\mathbf{k}]$-operator, cfr. Ref. [35], the configuration space potentials corresponding with (B13) read

$$\begin{aligned}\mathcal{V}_A^{(1)} \ =\ & -\frac{g_A^2}{4\pi}\ m\left[\left(\phi_C^0 + \frac{2m^2}{3M'M}\ \phi_C^1\right)(\boldsymbol{\sigma}_1\cdot\boldsymbol{\sigma}_2) - \frac{3}{4M'M}\left(\nabla^2\phi_C^0 + \phi_C^0\nabla^2\right)(\boldsymbol{\sigma}_1\cdot\boldsymbol{\sigma}_2)\right.\\ & \left.-\frac{m^2}{4M'M}\ \phi_T^0\ S_{12} + \frac{m^2}{2M'M}\ \phi_{SO}^0(m,r)\ \mathbf{L}\cdot\mathbf{S}\right]\\ & +\frac{g_A^2}{4\pi}\ \frac{2m^2}{M'M}\left[\phi_{SO}^0(r) + \frac{3}{(mr)^2}\left\{3 - \frac{2m^2}{\Lambda^2} + \left(m\frac{d}{dm}\right)\right\}\ \phi_T^0(r)\right]\ Q_{12}\ .\end{aligned} \tag{B14}$$

Now it happens that the second term in the coefficient of Q_{12} in (B14) becomes by virtue of the properties of the Gaussian Yukawa-functions, see Appendix E,

$$\frac{3}{(mr)^2}\left\{\ldots\right\} = -\frac{3}{(mr)^2}\ \psi_T^0(r) = -\phi_{SO}^0(r)\ , \tag{B15}$$

and so the coefficient of Q_{12} in (B14) vanishes!

APPENDIX C: AXIAL-DERIVATIVE COUPLING AND CAC

In the B-field theory the conservation of the axial-current conservation (CAC) is an important ingredient. Therefore, an analysis of the realization of CAC in the ESC-model is opportune. Isolating the derivative coupling terms in the axial-vector meson-exchange potential we have

$$V_{A,a}(r) = -\frac{m}{4\pi}\frac{m^2}{2M_Y M_N}\left(g^A_{13}f^A_{24}\frac{M_N}{\mathcal{M}} + f^A_{13}g^A_{24}\frac{M_Y}{\mathcal{M}}\right)\left[\frac{1}{3}(\boldsymbol{\sigma}_1\cdot\boldsymbol{\sigma}_2)\ \phi^1_C + S_{12}\ \phi^0_T\right], \tag{C1a}$$

$$V_{A,b}(r) = -\frac{m}{4\pi}\ f^A_{13}f^A_{24}\frac{m^2}{\mathcal{M}^2}\frac{m^2}{4M_Y M_N}\left[\frac{1}{3}(\boldsymbol{\sigma}_1\cdot\boldsymbol{\sigma}_2)\ \phi^2_C + S_{12}\ \phi^1_T\right]. \tag{C1b}$$

Depending on the sign of $g_A f_A$ the first potential $V_{A,a}(r)$ is a B-type ($g_A f_A > 0$) or a P-type ($g_A f_A < 0$) potential, and the second potential $V_{A,b}(r)$ is a B-type potential.
Axial-vector current conservation at the meson-pole requires

$$\partial_\mu J^\mu_A = 0: \ \frac{f^A}{g^A} = -2\frac{M_N\mathcal{M}}{m^2_A}, \tag{C2}$$

For NN the response of the axial potentials upon the change $f^A \to f^A_0 + \Delta f^A$ from (C1b) is

$$\begin{aligned}\Delta V_A(r) \ &= \ \Delta V_{A,a}(r) + \Delta V_{A,b}(r) = -\frac{m}{4\pi}\frac{m^2}{2M^2_N}\left[2\left(g_A + \frac{m^2}{2M^2_N}f_A\right)\Delta f^A\right.\\ &\left. + \frac{m^2}{2M^2_N}(\Delta f^A)^2\right]\cdot\left[\frac{1}{3}(\boldsymbol{\sigma}_1\cdot\boldsymbol{\sigma}_2)\ \phi^1_C + S_{12}\ \phi^0_T\right].\end{aligned} \tag{C3}$$

Now, it turns out that for ESC08c, with the parameters presented in this paper, the expression $[\ldots] > 0$ for the axial mesons $a_1(1270), f_1(1420), f_1(1285)$. The coupling constant for the compensating B-meson potential is

$$f^2_B(A) = \frac{3m^2}{2M^2_N}\left[2\left(g_A + \frac{m^2}{2M^2_N}f_A\right)\Delta f^A + \frac{m^2}{2M^2_N}(\Delta f^A)^2\right] \tag{C4}$$

From the results for the couplings it appears that changes in the derivative couplings can be made in order to satisfy (C2), which can be compensated by changing the B-meson couplings.

APPENDIX D: NON-LOCAL TENSOR-CORRECTION

In this appendix we repeat the treatment of the non-local correction correction to the tensor-potential similar to that for the central non-local potential

$$\Delta\widetilde{V}_T = \left(\mathbf{q}^2 + \frac{1}{4}\mathbf{k}^2\right)\widetilde{v}_T\ S_{12}. \tag{D1}$$

This incorporation of this kind of potential in the solution of the Schrödinger equation is given in [45], see Appendix D. For completeness we repeat here the treatment of this type of potential, which is exact when there is no non-local spin-orbit potential. For definiteness we consider the contribution to the π-exchange potential

$$\widetilde{v}_T = \frac{f^2_P}{2MM'\ m^2_\pi}\left(\mathbf{q}^2 + \frac{1}{4}\mathbf{k}^2\right)/(\mathbf{k}^2 + m^2). \tag{D2}$$

In configuration space this leads to the potential

$$\begin{aligned}V_T(r) \ &= \ \frac{f^2_P}{4\pi}\frac{m}{4MM'}\left[\frac{1}{3}(\boldsymbol{\sigma}_1\cdot\boldsymbol{\sigma}_2)\left(\nabla^2\phi^1_C + \phi^1_C\nabla^2\right) + \left(\nabla^2\phi^0_T S_{12} + \phi^0_T S_{12}\nabla^2\right)\right]\\ &\equiv \ -\left[\left(\nabla^2\phi(r) + \phi(r)\nabla^2\right) + \left(\nabla^2\chi(r)S_{12} + \chi(r)S_{12}\nabla^2\right)\right].\end{aligned} \tag{D3}$$

Here we put $\boldsymbol{\sigma}_1\cdot\boldsymbol{\sigma}_2 = 1$, because this potential contributes for spin-triplet states only. The radial Schrödinger equation reads

$$\begin{aligned}&\left\{(1+2\phi) + 2\chi\ S_12\right\}\ u'' + \left(2\phi' + 2\chi'\ S_{12}\right)\ u' + \left[k^2_{cm} - 2M_{red}V\right.\\ &\left. - \left\{(1+2\phi) + \chi\ S_{12}\right\}\frac{\mathbf{L}^2}{r^2} - \frac{\mathbf{L}^2}{r^2}\chi\ S_{12} + \phi'' + \chi''\ S_{12}\right]\ u = 0.\end{aligned} \tag{D4}$$

Under the substitution $u = A^{-1/2}v$, where

$$A \equiv (1 + 2\phi) + 2\chi\ S_{12}, \tag{D5}$$

over into the radial equation for $v(r)$

$$v''(r) + \left[k_{cm}^2 - \frac{l(l+1)}{r^2} - 2M_{red}W\right]\ v(r) = 0 \tag{D6}$$

with the (pseudo) potential

$$\begin{aligned} 2M_{red}W &= 2M_{red}A^{-1/2}V\ A^{-1/2} - A^{-2}\left(\phi' + \chi'\ S_{12}\right)^2 - \left(A^{-1} - 1\right)\ k_{cm}^2 \\ &+ \left\{A^{1/2}\left[L^2, A^{-1/2}\right] + A^{-1/2}\left[L^2, A^{1/2}\right]\right\}/(2r^2). \end{aligned} \tag{D7}$$

In passing we note that A and S_{12} commute, and therefore

$$A^{-2}\left(\phi' + \chi'\ S_{12}\right)^2 = \left[A^{-1/2}\left(\phi' + \chi'\ S_{12}\right)A^{-1/2}\right]^2 = \frac{1}{4}\left[A^{-1/2}\ A'\ A^{-1/2}\right]^2.$$

Defining

$$X = (1 + 2\phi + 4\chi)^{1/2}\ \ ,\ \ Y = (1 + 2\phi - 8\chi)^{1/2}, \tag{D8}$$

the transformation A is given as

$$\begin{aligned} A^{1/2} &= \frac{1}{3}(2X + Y) + \frac{1}{6}(X - Y)\ S_{12} \\ A^{-1/2} &= \left\{\frac{1}{3}(X + 2Y) + \frac{1}{6}(-X + Y)\ S_{12}\right\}/(XY). \end{aligned} \tag{D9}$$

Using (D10) one readily derives

$$\begin{aligned} &\left\{A^{1/2}\left[L^2, A^{-1/2}\right]_- + A^{-1/2}\left[L^2, A^{1/2}\right]_-\right\} = \\ &-2\frac{(X-Y)^2}{XY}\ \frac{\sqrt{J(J+1)}}{2J+1}\ \begin{pmatrix} 2\sqrt{J(J+1)} & -1 \\ -1 & -2\sqrt{J(J+1)} \end{pmatrix}. \end{aligned} \tag{D10}$$

Writing $A^{-1} = \alpha + \beta\ S_{12}$ one finds

$$\begin{aligned} \alpha &= +(1 + 2\phi - 4\chi)\left[(1 + 2\phi + 4\chi)(1 + 2\phi - 8\chi)\right]^{-1}, \\ \beta &= -2\chi\ \left[(1 + 2\phi + 4\chi)(1 + 2\phi - 8\chi)\right]^{-1}, \end{aligned} \tag{D11}$$

leading to

$$\begin{aligned} -\left(A^{-1} - 1\right) &= \left[\left\{(2\phi - 8\chi)(1 + 2\phi + 4\chi) - 8\chi\right\} + 2\chi\ S_{12}\right]\cdot \\ &\times\left[(1 + 2\phi + 4\chi)(1 + 2\phi - 8\chi)\right]^{-1}. \end{aligned} \tag{D12}$$

APPENDIX E: GAUSSIAN YUKAWA-FUNCTIONS

The basic Fourier transforms for the soft-core potentials is Refs. [3, 35]

$$\int \frac{d^3k}{(2\pi)^3}\frac{e^{i\mathbf{k}\cdot\mathbf{r}}}{\mathbf{k}^2 + m^2}(\mathbf{k}^2)^n \exp\left(-\mathbf{k}^2/\Lambda^2\right) \equiv \frac{m}{4\pi}(-m^2)^n\phi_C^n(r) = (-\boldsymbol{\nabla}^2)^n\frac{m}{4\pi}\phi_C^0(r), \tag{E1}$$

and similar ones for the tensor-, spin-orbit-, and the quadratic-spin-orbit potentials. The basic central, tensor, and spin-orbit functions are

(i) central potentials:

$$\phi_C^0(r) \;=\; \exp(m^2/\Lambda^2)\left[e^{-mr}\mathcal{E}rfc\left(-\frac{\Lambda r}{2}+\frac{m}{\Lambda}\right)-e^{mr}\mathcal{E}rfc\left(\frac{\Lambda r}{2}+\frac{m}{\Lambda}\right)\right]/2mr\ , \tag{E2a}$$

$$\phi_C^1(r) \;=\; \phi_C^0(r)-\frac{1}{2\sqrt{\pi}}\left(\frac{\Lambda}{m}\right)^3\exp\left[-\left(\frac{\Lambda r}{2}\right)^2\right], \tag{E2b}$$

$$\phi_C^2(r) \;=\; \phi_C^1(r)+\frac{1}{2\sqrt{\pi}}\left(\frac{\Lambda}{m}\right)^5\left[\frac{3}{2}-\left(\frac{\Lambda r}{2}\right)^2\right]\exp\left[-\left(\frac{\Lambda r}{2}\right)^2\right], \tag{E2c}$$

(ii) tensor potentials:

$$\begin{aligned}\phi_T^0(r) \;=\; & \frac{1}{3}\frac{1}{m^2}r\frac{\partial}{\partial r}\frac{1}{r}\frac{\partial}{\partial r}\phi_C^0(r)=\Big\{\exp(m^2/\Lambda^2)\left[[1+mr+(mr)^2/3]e^{-mr}\cdot\right.\\ & \times\mathcal{E}rfc\left(-\frac{\Lambda r}{2}+\frac{m}{\Lambda}\right)-[1-mr+(mr)^2/3]e^{mr}\mathcal{E}rfc\left(\frac{\Lambda r}{2}+\frac{m}{\Lambda}\right)\Big]\\ & \left.-\frac{4}{\sqrt{\pi}}\left(\frac{\Lambda r}{2}\right)\left[1+\frac{2}{3}\left(\frac{\Lambda r}{2}\right)^2\right]\exp\left[-\left(\frac{\Lambda r}{2}\right)^2\right]\right\}/2(mr)^3\ ,\end{aligned} \tag{E3a}$$

$$\phi_T^1(r) \;=\; \phi_T^0-\frac{1}{6\sqrt{\pi}}\left(\frac{\Lambda}{m}\right)^5\left(\frac{\Lambda r}{2}\right)^2\exp\left[-\left(\frac{\Lambda r}{2}\right)^2\right]. \tag{E3b}$$

(iii) spin-orbit potentials:

$$\begin{aligned}\phi_{SO}^0(r) \;=\; & -\frac{1}{m^2}\frac{1}{r}\frac{\partial}{\partial r}\phi_C^0(r)=\Big\{\exp(m^2/\Lambda^2)\left[[1+mr]e^{-mr}\cdot\right.\\ & \times\mathcal{E}rfc\left(-\frac{\Lambda r}{2}+\frac{m}{\Lambda}\right)-[1-mr]e^{mr}\mathcal{E}rfc\left(\frac{\Lambda r}{2}+\frac{m}{\Lambda}\right)\Big]\\ & \left.-\frac{4}{\sqrt{\pi}}\left(\frac{\Lambda r}{2}\right)\left(\frac{\Lambda r}{2}\right)\exp\left[-\left(\frac{\Lambda r}{2}\right)^2\right]\right\}/2(mr)^3\ ,\end{aligned} \tag{E4a}$$

$$\phi_{SO}^1(r) \;=\; \phi_{SO}^0-\frac{1}{4\sqrt{\pi}}\left(\frac{\Lambda}{m}\right)^5\left(\frac{\Lambda r}{2}\right)^2\exp\left[-\left(\frac{\Lambda r}{2}\right)^2\right]. \tag{E4b}$$

(iv) quadratic-spin-orbit potentials:

$$\phi_Q^0(r) \;=\; -\frac{m^5}{4\pi}\frac{3}{(mr)^2}\phi_T^0(r). \tag{E5}$$

The Fourier transforms of the Pomeron-type of potentials are gaussian-integrals, which can be obtained from the above formulas by the substitutions

$$\frac{1}{2}\Lambda\equiv m_P,\quad m=0,\quad \phi_i^{P,n}=\phi_i^{n+1}. \tag{E6}$$

For explicit formulas see Refs. [3, 35].

APPENDIX F: NEW VERSION QUARK-PAIR-CREATION MODEL [67]

In this appendix we give a short description of the evaluation of the BBM coupling constants in the QPC-model using the Fierz-transformation technique. For details we refer to Ref. [67]. Here, apart from the Fierz-transformation, the techniques used are those of [27, 62, 65]. In Fig. 14 the two kind of processes, direct (a) and exchange (b), are shown. The derivation of the BBM-couplings starts from the generalized $^3P_0$ (S) and $^3S_1$ (V) Pair-creation

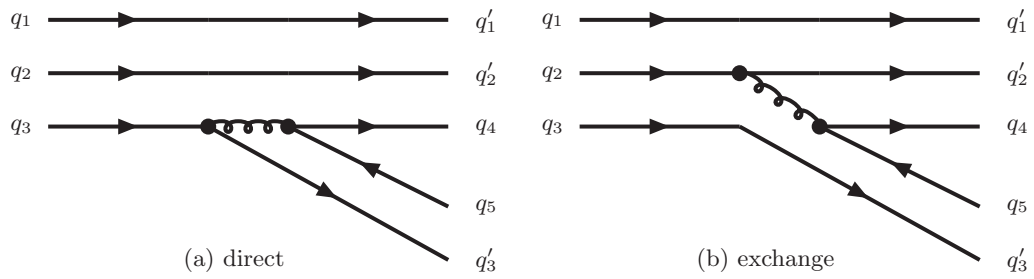

FIG. 14: $^3P_0$- *and* $^3S_1$-*quark-pair-creation (QPC)*

Hamiltonians

$$\begin{aligned}
\mathcal{H}_I^{(S)} &= -4\gamma_{q\bar{q}}^{(S)} \left(\sum_i \bar{q}_i q_i\right) \cdot \left(\sum_j \bar{q}_j q_j\right), \\
\mathcal{H}_I^{(V)} &= -\gamma_{q\bar{q}}^{(V)} \left(\sum_i \bar{q}_{i,\alpha} (\boldsymbol{\lambda})^{\alpha}{}_{\beta} \gamma^{\mu} q_{i,\beta}\right) \otimes \left(\sum_j \bar{q}_{j,\gamma} (\boldsymbol{\lambda})^{\gamma}{}_{\delta} \gamma_{\mu} q_{j,\delta}\right)
\end{aligned} \tag{F1}$$

where $\gamma_{q\bar{q}}^{(V)}$ is a phenomenological constant, and the summations run as $i,j = u,d,s$. In this QPC-model in the fundamental process there is a (confined) scalar or gluon propagator. This implies, assuming a constant propagator, an extra factor depending on a scalar or (massive) gluon exchange $(-i)^2.(\mp i/m_G^2) \sim \pm i/\Lambda_{QPC}^2$. meaning $\sim \pm i H_{int}$. Rearrangement is supposed to take place when a quark-antiquark pair is created by some mechanism in a baryon, where one quark from the baryon combines into a mesonic state with the anti-quark from the pair. The quark from the pair recombines with the two remaining quarks of the baryon to make the baryon in the final state. This rearrangements into mesons of different kind can be understood from a Fierz-transformation applied to (F1). One has the identity [105]

$$\begin{aligned}
\mathcal{H}_I^{(S)} &= \gamma_{q\bar{q}}^{(S)} \sum_{i,j} \Big[+\ \bar{q}_i\ q_j \cdot \bar{q}_i\ q_j + \bar{q}_i \gamma_{\mu} q_j \cdot \bar{q}_j \gamma^{\mu} q_i \\
&-\frac{1}{2}\ \bar{q}_i \sigma_{\mu\nu} q_j \cdot \bar{q}_j \sigma^{\mu\nu} q_i - \bar{q}_i \gamma_{\mu} \gamma_5 q_j \cdot \bar{q}_j \gamma^{\mu} \gamma^5 q_i + \ \bar{q}_i \gamma_5 q_j \cdot \bar{q}_j \gamma^5 q_i \Big], \\
\mathcal{H}_I^{(V)} &= +\gamma_{q\bar{q}}^{(V)} \sum_{i,j} \Big[+\ \bar{q}_i\ q_j \cdot \bar{q}_i\ q_j - \frac{1}{2}\ \bar{q}_i \gamma_{\mu} q_j \cdot \bar{q}_j \gamma^{\mu} q_i \\
&-\frac{1}{2}\ \bar{q}_i \gamma_{\mu} \gamma_5 q_j \cdot \bar{q}_j \gamma^{\mu} \gamma^5 q_i - \ \bar{q}_i \gamma_5 q_j \cdot \bar{q}_j \gamma^5 q_i \Big].
\end{aligned} \tag{F2}$$

Here, we considered only the flavor-spin Fierzing. [1] The appropriate Fierzing of the color structure is different for diagram (a) and diagram (b) in Fig. 14: (i) For diagram (a) we use the identity [105]

$$(\boldsymbol{\lambda})^{\gamma}{}_{\delta} \cdot (\boldsymbol{\lambda})_{\alpha}{}^{\beta} = \frac{16}{9} \delta_{\alpha}^{\gamma} \delta_{\delta}^{\beta} - \frac{1}{3} (\boldsymbol{\lambda})_{\alpha}^{\gamma} \cdot (\boldsymbol{\lambda})_{\delta}^{\beta} \tag{F3}$$

Since the mesons are colorless, the second term in (F3) may be neglected, and color gives the simple factor 16/9. (ii) In diagram (b) there is in fact a sum over q_1 and q_2. Because the baryons are colorless, we have

$$(\boldsymbol{\lambda}_1)_{\alpha}{}^{\beta} + (\boldsymbol{\lambda}_2)_{\alpha}{}^{\beta} = -(\boldsymbol{\lambda}_3)_{\alpha}{}^{\beta}. \tag{F4}$$

---

[1] It should be noted that the terms for the couplings of the B-axial $J^{PC} = 1^{+-}$- and tensor $J^{PC} = 2^{++}$mesons are missing on the r.h.s. of (F2). The same is true for the $^3P_0$-interaction (F1).

Therefore, for this diagram we have, using (F3), the identity

$$(\boldsymbol{\lambda}_5)^{\gamma}{}_{\delta} \cdot \sum_{i=1,2} (\boldsymbol{\lambda}_i)_{\alpha}^{\ \beta} = -\frac{16}{9}\delta_{\alpha}^{\gamma}\delta_{\delta}^{\beta} + \frac{1}{3}(\boldsymbol{\lambda}_5)_{\alpha}^{\gamma} \cdot (\boldsymbol{\lambda}_3)_{\delta}^{\beta} \tag{F5}$$

Again, for colorless mesons the second term in (F5) may be neglected, and color gives the simple factor $-16/9$.
We find that the direct (a) and exchange (b) diagram give different color factors. Such a difference does not occur in the $^3P_0$-model. Now, it appears that the momentum overlap for type (b) is usually much smaller than for type (a), see [67]for details. This can be traced back to our use of a constant propagator for the (confined) gluon. Therefore, in the following we neglect processes described in diagram (b). Then, the difference between the $^3P_0$- and $^3S_1$-model is, apart from an overall constant, exclusively given by the different coefficients in the flavor-spin Fierz-identities (F2).

In the $^3S_1$-model for the interaction Hamiltonian for the pair-creation one uses the one-gluon-exchange (OGE) model [106, 107], see Fig. 14. Considering one-gluon exchange, see Fig. 14, one derives the effective vertex [106, 107] by using a (confined) constant $P_g(ji)$ gluon propagator between quark line i and line j: $P_g(ji) \sim \delta_{ji}/m_g^2$, where the (effective) gluon mass is taken to be $m_g \approx (0.8fm^{-1}) \approx 250$ MeV [107]. We notice that the color factor for the coupling of colorless mesons to colorless baryons is always the same, and we can include this into an effective coupling γ_S, i.e.

$$\frac{\pi\alpha_s(\boldsymbol{\lambda}_i \cdot \boldsymbol{\lambda}_j)}{m_G^2} \Rightarrow \gamma_{q\bar{q}}^{(V)}. \tag{F6}$$

Here we use for the gluon a constant (confined) propagator $P_g = 1/m_G^2$. As is clear from (F1) $\gamma_{q\bar{q}}$ has the dimension $[\mathrm{MeV}]^{-2}$. Also, we notice that $m_G \approx \Lambda_{QPC}$, therefore $\gamma_{q\bar{q}} \longrightarrow \gamma_{q\bar{q}}/\Lambda_{QPC}^2$. From the momentum conservation rules one now gets different dependences between the momenta as compared to the version of the $^3P_0$-model in [27, 65]. Hence, we have different momentum overlap-integrals.

From the results for the couplings of the mesons in the $^3P_0$-model those for the $^3S_1$–model meson-couplings can be read off by comparing the coefficients in the Fierz-identities (F2) and (F1) for the corresponding operators. Here, we assume that the effect of color in the $^3P_0$- and $^3S_1$-model can be absorbed into $\gamma_{q\bar{q}}^{(S,V)}$, see below. For example, the prediction for the scalar-meson couplings will have the ratio $g_\epsilon(^3S_1) = \left[\gamma_{q\bar{q}}^{(V)}/\gamma_{q\bar{q}}^{(S)}\right] g_\epsilon(^3P_0)$. Apart from an overall constant, the couplings for the $^3S_1$-model can be read off from those of the $^3P_0$-model.

1. Meson-states, Meson- and baryon wave-functions

We list the $\langle B, M|H_{int}|A\rangle$ matrix elements for the different type of mesons. Restriction on the quark-level to process (a) in Fig. 14, using the Fierzed form of the interaction Hamiltonians in (F1). So, below we will give the

results for the $^3P_0$-model. Following [108] we write the meson creation operators as

$$
\begin{aligned}
J^{PC}=0^{-+}: \qquad d^\dagger_{M,P}(\mathbf{k}) &= i\sum_{r,s=\pm}\int d^3k_1 d^3k_2\ \delta(\mathbf{k}-\mathbf{k}_1-\mathbf{k}_2)\ \cdot \\
&\times\widetilde{\psi}^{(L=0)}_M(\mathbf{k}_1,\mathbf{k}_2)\ \varphi^{(0)}(r,s)\ b^\dagger(\mathbf{k}_1,r)\ d^\dagger(\mathbf{k}_2,s), \qquad \text{(F7)}\\
J^{PC}=1^{--}:\ d^\dagger_{M,V}(\mathbf{k},m) &= \sum_{r,s=\pm}\int d^3k_1 d^3k_2\ \delta(\mathbf{k}-\mathbf{k}_1-\mathbf{k}_2)\ \cdot \\
&\times\widetilde{\psi}^{(L=0)}_M(\mathbf{k}_1,\mathbf{k}_2)\ \varphi^{(1)}_m(r,s)\ b^\dagger(\mathbf{k}_1,r)\ d^\dagger(\mathbf{k}_2,s), \qquad \text{(F8)}\\
J^{PC}=0^{++}:\ d^\dagger_{M,S}(\mathbf{k},m) &= \sum_{r,s=\pm}\int d^3k_1 d^3k_2\ \delta(\mathbf{k}-\mathbf{k}_1-\mathbf{k}_2)\ (-)^m\cdot \\
&\times\widetilde{\psi}^{(L=1)}_{M,m}(\mathbf{k}_1,\mathbf{k}_2)\ \varphi^{(1)}_{-m}(r,s)\ b^\dagger(\mathbf{k}_1,r)\ d^\dagger(\mathbf{k}_2,s), \qquad \text{(F9)}\\
J^{PC}=1^{++}:\ d^\dagger_{M,A}(\mathbf{k},m) &= \sum_{r,s=\pm}\int d^3k_1 d^3k_2\ \delta(\mathbf{k}-\mathbf{k}_1-\mathbf{k}_2)\ C(1,1,1;m_L,m_\sigma,m)\cdot \\
&\times\widetilde{\psi}^{(L=1)}_{M,m_L}(\mathbf{k}_1,\mathbf{k}_2)\ \varphi^{(1)}_{m_\sigma}(r,s)\ b^\dagger(\mathbf{k}_1,r)\ d^\dagger(\mathbf{k}_2,s), \qquad \text{(F10)}\\
J^{PC}=1^{+-}:\ d^\dagger_{M,B}(\mathbf{k},m) &= \sum_{r,s=\pm}\int d^3k_1 d^3k_2\ \delta(\mathbf{k}-\mathbf{k}_1-\mathbf{k}_2)\ \cdot \\
&\times\widetilde{\psi}^{(L=1)}_{M,m}(\mathbf{k}_1,\mathbf{k}_2)\ \varphi^{(0)}(r,s)\ b^\dagger(\mathbf{k}_1,r)\ d^\dagger(\mathbf{k}_2,s), \qquad \text{(F11)}\\
J^{PC}=2^{++}:\ d^\dagger_{M,T}(\mathbf{k},m) &= \sum_{r,s=\pm}\int d^3k_1 d^3k_2\ \delta(\mathbf{k}-\mathbf{k}_1-\mathbf{k}_2)\ C(1,1,2;m_L,m_\sigma,m)\cdot \\
&\times\widetilde{\psi}^{(L=1)}_{M,m_L}(\mathbf{k}_1,\mathbf{k}_2)\ \varphi^{(1)}_{m_\sigma}(r,s)\ b^\dagger(\mathbf{k}_1,r)\ d^\dagger(\mathbf{k}_2,s), \qquad \text{(F12)}
\end{aligned}
$$

for respectively the pseudoscalar-, vector-, scalar-, axial-vector mesons of the first (A_1 etc.) and second kind (B_1 etc.)[109], and tensor mesons. The baryon and meson wave , harmonic oscillator, functions are

$$
\begin{aligned}
\widetilde{\psi}_N(\mathbf{k}_1,\mathbf{k}_2,\mathbf{k}_3) &= \left(\frac{\sqrt{3}R_A^2}{\pi}\right)^{3/2}\exp\left[-\frac{R_A^2}{6}\sum_{i<j}(\mathbf{k}_i-\mathbf{k}_j)^2\right]\ ,\\
\widetilde{\psi}^{(L=0)}_M(\mathbf{k}_1,\mathbf{k}_2) &= \left(\frac{R_M^2}{\pi}\right)^{3/4}\exp\left[-\frac{R_M^2}{8}(\mathbf{k}_1-\mathbf{k}_2)^2\right]\ ,\\
\widetilde{\psi}^{(L=1)}_{M,m}(\mathbf{k}_1,\mathbf{k}_2) &= \frac{R_M}{\sqrt{2}}\left(\frac{R_M^2}{\pi}\right)^{3/4}[-\boldsymbol{\epsilon}_m\cdot(\mathbf{k}_1-\mathbf{k}_2)]\ .\exp\left[-\frac{R_M^2}{8}(\mathbf{k}_1-\mathbf{k}_2)^2\right].
\end{aligned}
$$

Here we used the spherical unit vectors $\boldsymbol{\epsilon}_{\pm1}=\mp\frac{1}{\sqrt{2}}(\mathbf{e}_1\pm i\mathbf{e}_2)\quad,\quad\boldsymbol{\epsilon}_0=\mathbf{e}_3$.

2. Coupling-constant Formulas

The matrix elements $\langle B-f(\mathbf{p}')\ M(\mathbf{k})|\mathcal{H}_I^{(S),(V)}|B_i(\mathbf{p})\rangle$ involve the momentum space overlap integrals, which can be performed in a straightforward manner [67]. The summary of the derived formulas in [67], in the case of the $^3P_0$-model, for the divers (I=1)-couplings is:

$$
\begin{aligned}
g_P &= +\pi^{-3/4}\ \gamma_{q\bar{q}}\ \frac{(m_PR_P)^{1/2}}{(\Lambda_{QPC}R_P)^2}\cdot(6\sqrt{2})\ ,\\
g_V &= +\pi^{-3/4}\ \gamma_{q\bar{q}}\ \frac{(m_VR_V)^{1/2}}{(\Lambda_{QPC}R_V)^2}\cdot(3/\sqrt{2})\ ,\\
g_S &= +\pi^{-3/4}\ \gamma_{q\bar{q}}\ \frac{(m_SR_S)^{-1/2}}{(\Lambda_{QPC}R_S)^2}\cdot\frac{9m_S}{M_B}\ ,\\
g_A &= -\pi^{-3/4}\ \gamma_{q\bar{q}}\ \frac{(m_AR_A)^{-1/2}}{(\Lambda_{QPC}R_A)^2}\cdot\frac{6m_A}{M_B},
\end{aligned}
$$

with $\Lambda_{QPC} \approx 600$ MeV, and $R_M \approx 0.66$.

---

[1] Th.A. Rijken, in *Proceedings of the XIVth European Conference on Few-Body Problems in Physics*, Amsterdam 1993, edited by B. Bakker and R. van Dantzig, Few-Body Systems, Suppl. **7**, 1 (1994).
[2] M.M. Nagels, T.A. Rijken, and J.J. deSwart, Phys. Rev. D 15 (1977) 2547.
[3] P.M.M. Maessen, Th.A. Rijken, and J.J. de Swart, Phys. Rev. C **40** (1989) 2226.
[4] Th.A. Rijken, Phys. Rev. **C73**, 44007 (2006).
[5] Th.A. Rijken and Y. Yamamoto, Phys. Rev. **C73**, 44008 (2006).
[6] Th.A. Rijken and Y. Yamamoto, *Extended-soft-core Baryon-Baryon Model, III. $S = -2$: $\Lambda\Lambda, \Xi N$ etc. Scattering* , nucl-th/0608074.
[7] Th.A. Rijken, M.M. Nagels, and Y. Yamamoto, Nucl. Phys. **A 835** (2010) 160.
[8] Th.A. Rijken, M.M. Nagels, and Y. Yamamoto, Progres of Theoretical Physics Suppl. No. **185**, 14 (2010).
[9] Th.A. Rijken, V.G.J. Stoks, and Y. Yamamoto, Phys. Rev. C 59 (1999) 21.
[10] V.G.J. Stoks, R.A.M. Klomp, M.C.M. Rentmeester, and J.J. de Swart, Phys. Rev. C 48 (1993) 792.
[11] R.A.M. Klomp, private communication (unpublished).
[12] O. Hashimoto and H. Tamura, *Spectroscopy of* Λ*-hypernuclei*, progress in Particle and nuclear Physics **57** (2006) 564-653.
[13] H. Takahashi et al., Phys. Rev. Lett. 87 (2001) 212502.
[14] The fortran code ESC08C.NN16 is available on the open-access website NN-Online, URL *http://NN-Online.org*.
[15] M.M. Nagels, Th.A. Rijken, and Y. Yamamoto, *Extended-soft-core Baryon-baryon Model ESC08. II. Hyperon-Nucleon Interactions*, to be published (referred to as II).
[16] M.M. Nagels, Th.A. Rijken, and Y. Yamamoto, *Extended-soft-core Baryon-baryon Model ESC08. III. Hyperon-Hyperon Interactions*, to be published (referred to as III).
[17] A. Manohar and H. Georgi, Nucl. Phys. **B234** (1984) 189.
[18] G.A. Miller, Phys. Rev. **C 39** (1989) 1563.
[19] P.V. Landshoff and O. Nachtmann, Z. f. Physik, **C 35** (1987) 405.
[20] F.J. Ynduráin, *Quantum chromodynamics* (Springer, Berlin, 1980), see chapter IV for a description and references original literature.
[21] J. Gasser and H. Leutwyler, Nucl. Phys. **B94** (1975) 269.
[22] S. Gasiorowicz and J.L. Rossner, Am. J. Phys. **49** (1981) 954. Here, one uses the constituent quark masses: $m_u = m_d = 310$ MeV and $m_s = 483$ MeV.
[23] B. Povh et al, *Particles and Nuclei* (Springer, Berlin, 1995).
[24] H.D. Politzer, Nucl. Phys. **B117** (1976) 397.
[25] M. Lavelle and D. McMullan, Physics Reports **279** (1997) 1-65. In this reference an extensive discussion of the dressing-problem can be found.
[26] L. Micu, Nucl. Phys. **B10** (1969) 521; R. Carlitz and M. Kislinger, Phys. Rev. D **2** (1970) 336.
[27] A. Le Yaouanc, L. Oliver, O. Péne, and J.-C. Raynal, Phys. Rev. D **8** (1973) 2223; Phys. Rev. D **11** (1975) 1272.
[28] This pair-creation mechanism has been shown to be dominant in Lattice QCD. See: N. Isgur and J. Paton, Phys. Rev. **D31**, 2910 (1985); R. Kokoski and N. Isgur, Phys. Rev. **D35**, 907 (1987).
[29] J. Schwinger, Phys. Rev. Lett. **18**, 923 (1967); Phys. Rev. **167**, 1432 (1968); *Particles and Sources*, Gordon and breach, Science publishers, Inc., New York, 1969.
[30] S. Weinberg, Phys. Phys. 166 (1968) 1568; Phys. Phys. 177 (1969) 2604.
[31] V. De Alfaro, S. Fubini, G. Furlan, and C. Rosetti, *Currents in Hadron Physics* Ch. 5, North-Holland Pulishing Company, Amsterdam 1973.
[32] F. Ambrosino et al, JHEP 0907 92009 105, arXiv:hep-ph/0906.3819; Jing-Wu Li and Doing-Sheng Du, Phys. Rev. D 78 (2008) 074030.
[33] M. Gell-Mann, Phys. Rev. **125**, 1067 (1962); S. Okubo, Progr. Theor. Phys. **27** 949 (1962); ibid **28** 24 (1962).
[34] V.G.J. Stoks and Th.A. Rijken, Nucl. Phys. **A 613** (1997) 311.
[35] M.M. Nagels, Th.A. Rijken, and J.J. de Swart, Phys. Rev. D **17** (1978) 768.
[36] Th.A. Rijken, Ann. Phys. (N.Y.) **208**, 253 (1991).
[37] Th.A. Rijken and V.G.J. Stoks, Phys. Rev. C 54 (1996) 2851;
[38] Th.A. Rijken and V.G.J. Stoks, Phys. Rev. C 54 (1996) 2869;
[39] F.E. Low, Phys. **D 12**, 163 (1975).
[40] S. Nussinov, Phys. Rev. Lett., **34**, 1286 (1975).
[41] J.J. de Swart, T.A. Rijken, P.M. Maessen, and R.G.E. Timmermans, Nuov. Cim. **102 A**, 203 (1989).
[42] S. Otsuki, R. Tamagaki, and W. Wada, Progr. Theor. Phys. **32** (1964) 320; S. Otsuki, R. Tamagaki, and M. Yasuno, Progr. Theor. Phys. Suppl. Extra number (1965), 578.
[43] M. Oka, K. Shimizu, and K. Yazaki, Progr. Theor. Phys. Suppl. **137**, 1 (2000).
[44] Y. Fujiwara, Y. Suzuki, and C. Nakamoto, Progr. in Part. and Nuclear physics, **58** (2007) 439.
[45] M.M. Nagels, T.A. Rijken, and J.J. de Swart, *N-N Potentials from Regge-Pole Theory*, in Few body Systems and Nuclear Forces I, Proceedings Graz 1978, Edited by H.Zingl, M. Haftel, and H. Zankel. Springer-Verlag, Berlin Heidelberg New

york.
[46] T.A. Rijken, Ann. Phys. (N.Y.), **164** (1985) 1,23.
[47] A.A. Logunov and A.N. Tavkhelidze, Nuovo Cimento **29**, 380 (1963); R. Blankenbecler and R. Sugar, Phys. Rev. **142**, 1051 (1966); M.H. Partovi and E.L. Lomon, Phys. Rev. **D2**, 1999 (1970).
[48] R.H. Thompson, Phys. Rev. **D1**, 110 (1970).
[49] A. Gersten, P.A. Verhoeven, and JJ.J. de Swart, Nuovo Cimento **A26**, 375 (1975).
[50] A. Klein, Phys. Rev. **90**, 1101 (1952); W. Macke, Z. Naturforsch. **89**, 599 (1953); **89**, 615 (1953).
[51] A. Klein and T-S. H. Lee, Phys. Rev. **D12**, 4308 (1974).
[52] J.J. de Swart, M.M. Nagels, T.A. Rijken, and P.A. Verhoeven, Springer tracts in Modern Physics, Vol. **60**, 137 (1971).
[53] At this point it is suitable to change the notation of the initial and final momenta. We use from now on the notations $\mathbf{p}_i \equiv \mathbf{p}$, $\mathbf{p}_f \equiv \mathbf{p}'$ for both on-shell and off-shell momenta.
[54] S. Okubo and R.E. Marshak, Ann. Phys. (N.Y.) **4**, 166 (1968).
[55] J.T. Brown, B.W. Downs, and C.K. Iddings, Ann. Phys. (N.Y.) **60**, 148 (1970).
[56] C. Itzykson and J-B Zuber, 'Quantum Field Theory', McGraw-Hill Inc. 1980.
[57] N. Nakanishi, Suppl. Progr. Theor. Phys. **51** (1972) 1
[58] N. Nakanishi and I. Ojima, 'Covariant Operator Formalism of Gauge Theories and quantum Gravity', section 2.4.2, World Scientific Lecture Notes in Physics, Vol. 27, World Scientific Pub. Co 1990.
[59] We follow the conventions of J.D. Bjorken and S.D. Drell, *Relativistic Quantum Mechanics* and *Relativistic Quantum Fields* (McGraw-Hill Inc., New York, 1965). We note that in [4, 5] in the definition of the interaction Hamiltonians, we used the conventions of [2, 3].
[60] The relation with the non-local $\phi(r)$-function defined in Ref. [35], Eq. (35), and the $V^{n,l.}(r)$ is

$$\phi(r) = [2M_{red}/(2M_Y M_N)]\ V^{n.l.}(r)$$

[61] Note that in this paper we suppose that f_A does not contain the one-pion-pole etc. In momentum space $\widetilde{f}_A(\mathbf{k}^2)$ is a smooth function of $\mathbf{k}^2$.
[62] A. Le Yaouanc, L. Oliver, O. Péne, and J.-C. Raynal, Phys. Rev. D **12** (1975) 2137; ibid **18**, 1591 (1978).
[63] R. van Royen and V.F. Weisskopf, Nuovo Cimento A **50**, 617 (1967).
[64] E. Leader and E. Predazzi, *An introduction to gauge theories and modern particle physics*, Vol. I, chapter 12, Cambridge Monographs on Particle Physics, Nuclear Physics and Cosmology, Editors T. Ericson and P.V. Landshoff, Cambridge University Press 1996.
[65] M. Chaichian and R. Kögerler,Ann. Phys. **124**, 61 (1980).
[66] *Review of Particle Physics*, Particle Data Group, Phys. Rev. **D 66** 010001-1 (2002).
[67] Th. A. Rijken, *Baryon-baryon Couplings in the* $^3P_0$ *and* $^3S_1$ *QPC-models*, Notes University of Nijmegen, Nijmegen, The Netherlands, *NN-online, THEF 12.01.*
[68] Th.A. Rijken, *Nucleon-Nucleon Interactions*, talk at KITPC workshop on Present Status Nuclear Interaction Theory, Beijin August 2014.
[69] Y. Yamamoto, T. Motoba, and Th.A. Rijken, *G-matrix approach to Hyperon-Nucleus systems*, Progr. Theor. Phys. Suppl. **185** (2010) 72.
[70] R.A. Bryan and A. Gersten, Phys. Rev. D **6** (1972) 341.
[71] D.V. Bugg and R.A. Bryan, Nucl. Phys. **A540** (1992) 449.
[72] V.G.J. Stoks, R.A.M. Klomp, C.P.F. Terheggen, and J.J. de Swart, Phys. Rev. C**49** (1994) 2950.
[73] H.Q. Song, M.Baldo , G. Giansiracusa and U. Lombardo, Phys. Rev. Lett. **81** (1998), 1584.
[74] M. Baldo, A. Fiasconaro, H.Q. Song, G. Giansiracusa and U. Lombardo, Phys. Rev. **C65** (2002), 017303.
[75] I.E. Lagaris and V.R. Pandharipande, Nucl. Phys. bf A 359 (1981) 349.
[76] H.-J. Schulze and Th.A. Rijken, Phys. Rev. **C 84** (2011) 035801.
[77] S. Nishizaki, Y. Yamamoto, and T. Takatsuka, Progr. Theor. Phys. **105**, 607 (2001); **108**, 703 (2002).
[78] M. Baldo, G.F. Burgio and H.-J. Schulze, Phys. Rev. **C61** (2000), 055801.
[79] I. Vidaõna, A. Polls, A. Ramos, L. Engvik and M. Hjorth-Jensen, Phys. Rev. **C62** (2000), 035801.
[80] Th.A. Rijken, *Multiple-Pomeron Coupling and the Universal Repulsion in Nuclear/Hyperonic Matter. I. Triple-Pomeron Vertices*, notes Nijmegen 2005 (unpublished).
[81] Th.A. Rijken, *Multi-Pomeron Exchange and the Universal Repulsion in Nuclear/Hyperonic Matter*, NN-online, THEF 08.01.
[82] Y. Yamamoto, T. Furumoto, N. Yasutake, and Th.A. Rijken, Phys. Rev. **C 88**, 022801(R) (2013).
[83] Y. Yamamoto, T. Furumoto, N. Yasutake, and Th.A. Rijken, Phys. Rev. **C 90**, 045805 (2014).
[84] Y. Yamamoto, T. Furumoto, N. Yasutake, and Th.A. Rijken, Eur. Phys. J. **A52** (2016) 19.
[85] P.B. Cemorest, T. Pennucci, S.M. Ransom, M.S.E. Roberts, and J.W. Hessels, Nature(London) **467** (2010), 1081.
[86] J. Antoniadis et al, Science **340** (2013), 6131.
[87] U. Mosel, S. Leupold, and V. Metag, Progr. Theor. Phys. Suppl. **186** (2010) 260.
[88] A.B.Kaidalov and K.A. Ter-Materosyan, Nucl. Phys. B75 (1974), 471.
[89] J.B. Bronzan and R.L. Sugar, Phys. Rev. D16 (1977), 466.
[90] T. Furumoto, Y. Sakuragi, and Y. Yamamoto, Phys. Rev. C**79** (2009), 011601(R); C**80** (2009), 044614.
[91] P. Möller, W.D. Myers, H. Sagawa and S. Yoshida, Phys. Rev. Lett. **108** (2012), 052501.
[92] P.-G. Reinhard, Z.Phys.A - Atomic Nuclei **329**, 257-266 (1988).

[93] B. ter Haar and R. Malfliet, Phys. Reports, **149** (1987) 207.
[94] G.A. Miller, B.M.F. Nefkens, and I. Slaus, Phys. Reports **194**, 1-116 (1990).
[95] A. Andronic, P. Braun-Munzinger, and J. Stachel, Physics Letters B 673 (2009) 142.
[96] R. Kokoski and N. Isgur, Phys. Rev. **D 35** (1987) 907.
[97] S. Kumano and V.R. Pandharipande, Phys. Rev. **D 38** (1988) 146.
[98] R.R. Scheerbaum, Nucl. Phys. A257 (1976) 77.
[99] E. Hiyama, M. Kamimura, T. Motoba, T. Yamada, and Y. Yamamoto, Phys. Rev. Lett. 85 (2000) 270.
[100] C.J. Batty, E. Friedman, and A. Gal, Prog. Theor. Phys. Suppl. No.117 (1994) 227.
[101] J. Dabrowski, Phys. Rev. C 60 (1999) 025205.
[102] H. Noumi et al., Phys. Rev. Lett. 89 (2002) 072301.
[103] M. Kohno, Y. Fujiwara, Y. Watanabe, K. Ogata, and M. Kawai, Prog. Theor. Phys. 112 (2004) 895.
[104] Th. A. Rijken, R.A.M. Klomp, and J.J. de Swart, *A Gift of Prophecy*, Essays in celebration of the life of Robert Marshak. Edited by E.C.G. Sudarshan, World scientific publishing Co., 1994.
[105] L.B. Okun, *Leptons and Quarks*, chapter 29, North-Holland Publishing Company 1984.
[106] A. De Rújula, H. Georgi, and S.L. Glashow, Phys. Rev. **D 12**, 147 (1975).
[107] E.M. Henley and Z.-Y. Zhang, Nucl. Phys. **A472**, 759 (1987). **D 12**, 147 (1975).
[108] R. Van Royen and V.F. Weisskopf, Nuovo Cimento **50 A**, 617 91967).
This representation is the equal-time Bethe-Salpeter wave function [110]:

$$f_{\mathbf{k},\alpha}(x,y) \equiv \langle 0|T\left[q_i(x)q_j(y)\right]|M(\mathbf{k},\alpha\rangle \stackrel{x^0=y^0}{\longrightarrow} (0|q_i(\mathbf{x})q_j(\mathbf{y})|M(\mathbf{k},\alpha)\,,$$

using the definition $\theta[0] = 1/2$.
[109] The factor i is included in the definition of the $d^\dagger_{M,P}(\mathbf{k})$-operator. This in order to have under time-reversal $\mathcal{T}|\pi_0(\mathbf{k})\rangle = |\pi_0(-\mathbf{k})\rangle$. The reason is that under time-reversal the spin-components change sign, which implies for the spin-singlet $\varphi^{(0)}(-r,-s) = -\varphi^{(0)}(r,s)$ etc.
[110] M. Gell-Mann and F. Low, Phys. Rev. **51**, 350 (1951).